# Appendix 5C-1: Evaluation of Phosphorus Sources, Forms, Flux, and Transformation Processes in the Stormwater Treatment Areas

Odi Villapando and Jill King

# INTRODUCTION

The overarching goal of the Evaluation of Phosphorus Sources, Forms, Flux, and Transformation Processes in the Stormwater Treatment Areas (P Flux Study) is to improve the understanding of mechanisms and factors that affect phosphorus (P) treatment performance of stormwater treatment areas (STAs), particularly those that are key performance drivers at the lower reaches of the treatment trains. To gain this understanding, it is critical to evaluate biogeochemical variables and processes along the STA flow-ways (FWs). The information gathered should provide information for the development or enhancement of strategies to improve STA performance toward achievement of the water quality based effluent limits (WQBELs). The study was designed to address two key questions for the Restoration Strategies Science Plan for the Everglades Stormwater Treatment Areas (Science Plan; SFWMD 2013):

- How can internal loading of P to the water column be reduced or controlled, especially in the lower reaches of the treatment trains?
- How can the biogeochemical or physical mechanisms be managed to further reduce soluble reactive phosphorus (SRP), particulate phosphorus (PP), and dissolved organic phosphorus (DOP) concentrations in the outflow of the STAs?

The study consists of several substudies: (1) data mining, (2) organic P speciation, (3) FW water quality assessments at different flow conditions, (4) in situ particle dynamics, (5) internal P loading measurements, (6) soil characterization, (7) assessment of enzyme and microbial activity, (8) vegetation assessments, and (9) quantification of faunal role in P cycling. In addition, limited data are being collected in Water Conservation Area (WCA) 2A for comparison purposes. The substudies are in various stages of implementation. Once completed, using conceptual models as a guide, new and existing STA information will be analyzed, synthesized, and integrated using both top-down and bottom-up approaches as described in the Data Synthesis and Integration Plan The top-down approach will employ data mining techniques to identify master variables in the low P domain (Figure 1). The bottom-up approach will focus on developing and improving mathematical equations to characterize the relationship among the different components (boxes) and drivers (arrows) of the conceptual model (Figure 2).

Preliminary results from the following substudies are presented in this report:

- FW Water Quality Assessments
- Internal P Loading Measurements

- Microbial Patterns and Response to Flow
- Settling and Entrainment of Particulates
- Soil Phosphorus Forms
- Vegetation Dynamics

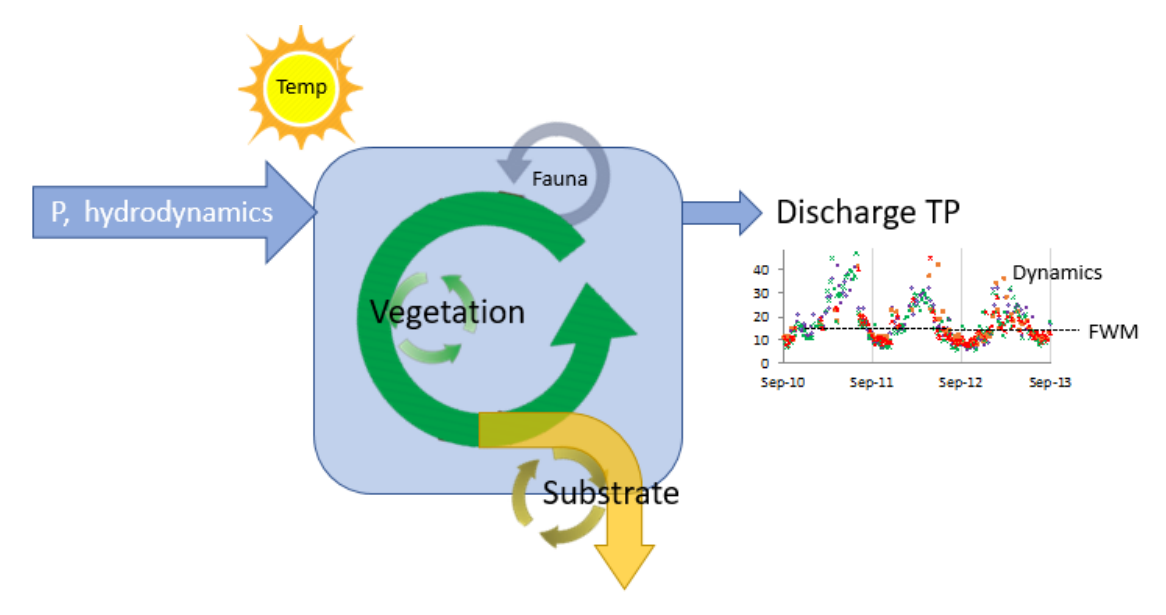


Figure 1. Conceptual model for the top-down integration approach to synthesize and integrate data from the P Flux study. Circular arrows suggest P turnover rates within various compartments, including slow (thick arrows: e.g. aquatic macrophyte growth, soil substrate accumulation) and fast (thin arrows; e.g. epiphyte and phytoplankton growth, etc.) compartments associated with vegetation. The "hydrodynamics" category includes factors such as water velocity, residence time and depth.

(Note: FWM – flow-weighted mean)

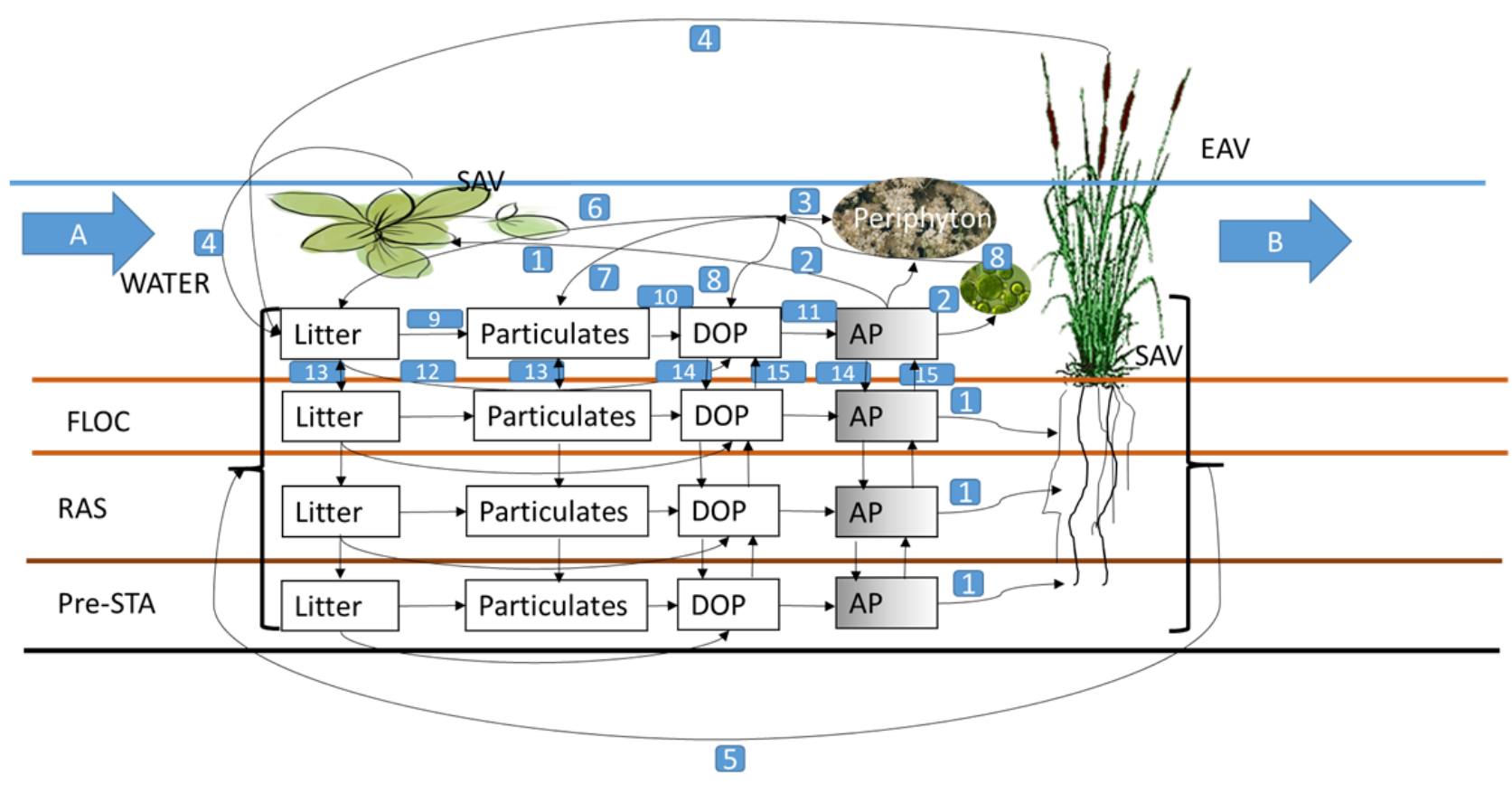


Figure 2. Conceptual model with state variables and fluxes to be incorporated into a numerical framework. The figure depicts a length segment within an STA cell. The state variables are operating in 4 domains: water, floc, recently accreted soil (RAS), and pre-STA soil. Carbon and P are tracked in all the pools containing organic forms of P, including emergent aquatic vegetation (EAV), submerged aquatic vegetation (SAV), periphyton, litter, particulates, and DOP. Thick arrows (A and B) indicate import and export of P into and out from the depicted length segment, respectively. The thin arrows represent P (and to some degree carbon) transformations. The numbers identify the respective fluxes: (1) uptake of available P (AP) by EAV and SAV plants, (2) P uptake by periphyton and algae from the water column, (3) incorporation of plant and other organic materials into periphyton, (4) litterfall and plant mortality, (5) root mortality, (6, 7, and 8) mineralization/mortality of periphyton and algae, (9) litter fragmentation, (10) decomposition of organic matter, (11) mineralization of organic matter, (12) leaching from litter, (13) sedimentation and resuspension of litter and particulate (fragmented) organic matter, (14) integration of AP into floc, RAS, and pre-STA domains via evaporation pumping, and (15) diffusion of AP across domains. The AP gradient fill includes the partitioning of dissolved inorganic P into sorbed and desorbed species where the sorption potential changes across the domain.

# FLOW-WAY WATER QUALITY ASSESSMENTS

Odi Villapando, Jill King, Matt Powers, and Jake Dombrowski

## INTRODUCTION

This field study is an evaluation of the biogeochemical responses of selected STA FWs with different vegetation types to no flow, low flow, and high flow conditions. These flow scenarios were selected to simulate the different hydraulic and hydrologic conditions that the STAs experience during full-scale operations. The objective is to obtain quantitative and qualitative information on nutrient dynamics in the water column during different flow conditions and relate those with other variables, including soil chemistry and vegetation, to determine the factors influencing the measured biogeochemical responses and their relative magnitudes, particularly those related to P cycling and reduction in the STAs.

## **METHODS**

# **Study Sites**

STA-2 FW 1, STA-2 FW 3, and STA-3/4 western FW (Cells 3A and 3B) were chosen as study sites (**Figure 3**). The results presented here were from six controlled flow events conducted in STA-2 FWs 1 and 3. These FWs have been achieving outflow TP concentrations of 20 micrograms per liter (μg/L) or less, and represent different FW configurations, vegetation communities, and soil conditions. STA-2 FW 1 is a single cell FW with predominantly emergent aquatic vegetation (EAV) consisting primarily of cattail (*Typha domingensis*) with patches of sawgrass (*Cladium jamaicense*) and water lily (*Nymphaea odorata*). The top 10 centimeters (cm) of the soil in the FW is highly organic. STA-2 FW 3 is also a single cell FW with predominantly submerged aquatic vegetation (SAV) with a large patch of EAV in the southeastern region of the FW. The pre-STA soil in the FW is highly organic but the current surface substrate is predominantly inorganic floc on top of inorganic recently accreted soil (RAS).

# Hydraulic and Hydrologic Conditions during Flow Events

The controlled flow events differed in timing and duration and consisted of either a low or high flow period preceded and/or followed by a period of stagnation (no flow). Flow periods were categorized into no flow, low flow, and high flow based on average flow (in cubic meters per second [m³/s]) the FW received during the different phases of a flow event. An average flow of > 0 to 4.25 m³/s was considered low flow, moderate if the average flow was between > 4.25 and 8.50 m³/s, and high flow if the FW experienced an average flow greater than 8.50 m³/s. The system was considered stagnant under no flow condition, although wind-driven flows still occur within each cell. Hydraulic loading rate (HLR) and P loading rate (PLR) for all phases of a flow event were calculated from daily flow volumes and daily TP loads, respectively. **Table 1** provides a summary of the hydraulic and hydrologic conditions during the flow events in STA-2 FWs 1 and 3.

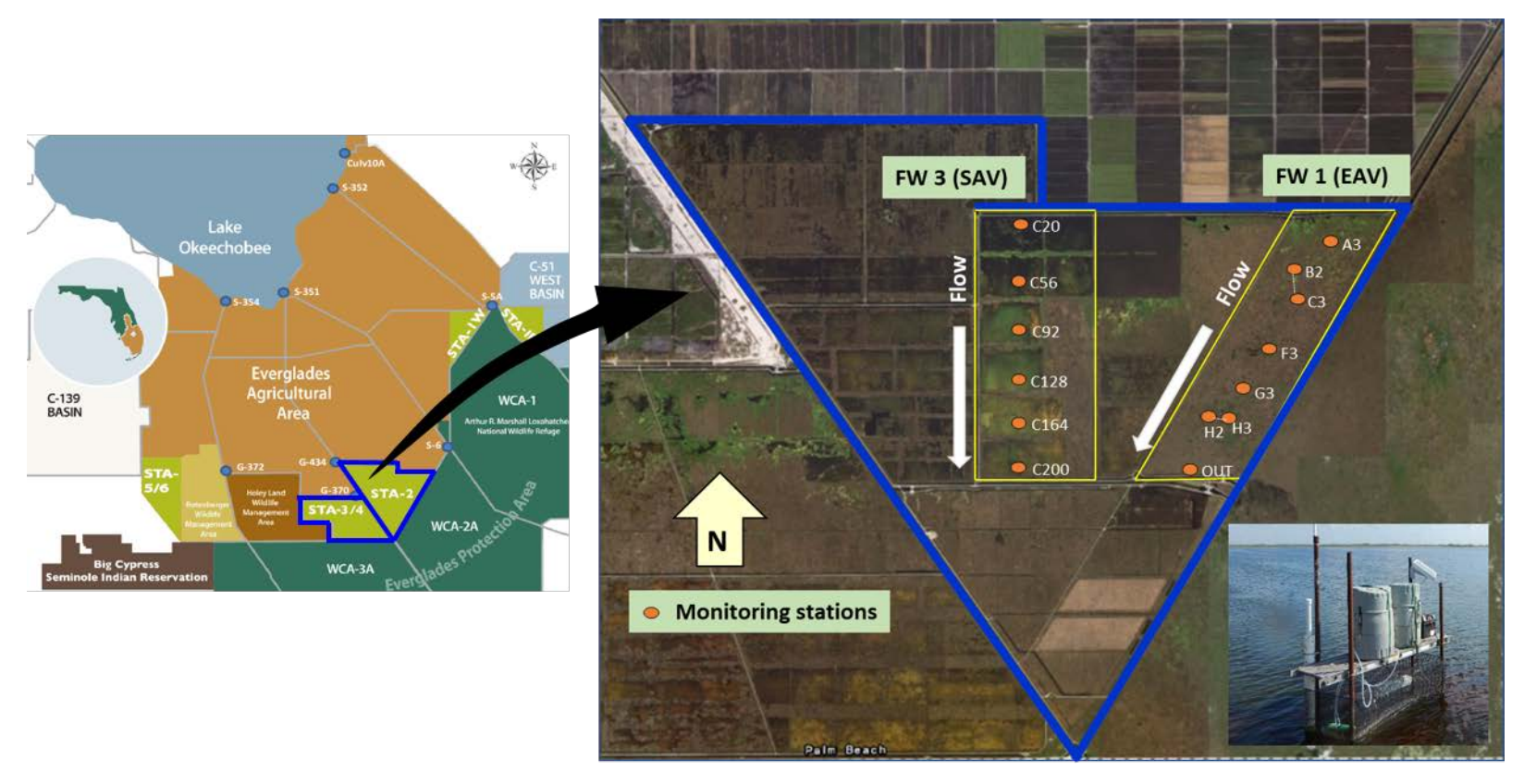


**Figure 3.** Location of STA-2 and STA-3/4 in relation to other STAs and the Everglades Agricultural Area (left) and STA-2 map showing the water quality monitoring stations in FWs 1 and 3 (right). Stations B2 and H2 in FW 1 were relocated and renamed C3 and H3, respectively, at the start of the May–July 2017 flow event. The inset is a monitoring platform deployed at each station for continuous monitoring of water quality and field conditions.

**Table 1.** Hydrologic conditions, HLR, and PLR during the flow events in STA-2 FW 1. Values for water depth, flow, HLR, and PLR are averaged over phase period ± standard deviation. <sup>a</sup>

Phase	Phase Period	Water Depth (m)	Flow (m³/s)	HLR (cm/d)	PLR (mg/m²/d)			
STA-2 FW 1								
1 <sup>st</sup> Flow Event (August 10–September 14, 2015) – 35 days								
Low Flow	8/10–8/16	$0.44 \pm 0.06$	$0.71 \pm 0.93$	$0.80 \pm 1.08$	0.8 ± 1.1			
No Flow	8/17–8/31	$0.45 \pm 0.01$	0	0	0			
Low Flow	9/1–9/14	$0.51 \pm 0.02$	0.91 ± 0.31	$1.05 \pm 0.36$	$0.8 \pm 0.3$			
2 <sup>nd</sup> Flow Event (May 29–July 29, 2017) – 61 days								
No Flow	5/29-6/4	$0.37 \pm 0.01$	0	0	0			
High Flow	6/5-6/26	$0.77 \pm 0.10$	$8.98 \pm 4.16$	10.41 ± 4.82	20.1 ± 10.2			
Low Flow	6/27-7/29	$0.47 \pm 0.03$	$0.20 \pm 0.00$	$0.22 \pm 0.91$	$0.3 \pm 1.3$			
3 <sup>rd</sup> Flow Event (November 12–December 26, 2017) – 47 days								
Low Flow	11/12-11/27	$0.65 \pm 0.02$	$2.89 \pm 1.39$	$3.35 \pm 1.61$	$0.9 \pm 0.4$			
No Flow	11/28–12/26	$0.43 \pm 0.06$	0	0	0			
STA-2 FW 3								
	1 <sup>st</sup> Flo	w Event (February	y 22–April 11, 20	16) – 50 days				
High Flow	2/22-3/7	$0.60 \pm 0.01$	$9.20 \pm 1.70$	8.55 ± 1.58	$3.7 \pm 1.3$			
No Flow	3/8-3/29	$0.58 \pm 0.02$	0	0	0			
Low Flow	3/30-4/11	$0.49 \pm 0.06$	1.56 ± 111	$1.45 \pm 2.91$	$1.0 \pm 2.0$			
	2 <sup>nd</sup> Flo	ow Event (June 27	7–August 29, 20 <sup>,</sup>	16) – 64 days				
No Flow	6/27-7/2	$0.45 \pm 0.02$	0	0	0			
Low Flow	7/3–7/24	$0.62 \pm 0.05$	$3.74 \pm 0.93$	$3.48 \pm 0.87$	$1.6 \pm 0.7$			
No Flow	7/25-8/8	$0.59 \pm 0.02$	0	0	0			
Low Flow	8/9-8/29	$0.61 \pm 0.02$	$3.40 \pm 0.44$	3.15 ± 2.26	2.3 ± 1.6			
3 <sup>rd</sup> Flow Event (October 12–November 22, 2016) – 42 days								
High Flow	10/22-11/3	$0.75 \pm 0.04$	8.52 ± 1.44	7.90 ± 1.34	5.9 ± 2.1			
No Flow	11/4–11/22	$0.71 \pm 0.03$	0	0	0			

a. Key to units: cm/d – centimeters per day; m – meters;  $m^3/s$  – cubic meters per second; and  $mg/m^2/d$  – milligrams per square meter per day.

## **Water Quality Monitoring**

Water quality and field conditions were continuously monitored during the flow events at six water quality monitoring stations along the inflow to outflow transect of the treatment FWs (**Figure 1**). Stations were equipped with autosamplers, EXO-sondes, water level loggers, and HOBO<sup>®</sup> light meters. Autosamplers collected six water samples daily at four-hour intervals (0200, 0600, 1000, 1400, 1800, and 2200 hours). Discrete samples were analyzed for total phosphorus (TP) and daily composite samples were analyzed for total nitrogen (TN) and total organic carbon (TOC). Weekly surface grab samples also were collected from these sites and analyzed for TP, SRP, total dissolved P (TDP), dissolved organic carbon (DOC), TN, calcium (Ca), magnesium (Mg), potassium (K), sodium (Na), ammonium (NH<sub>4</sub><sup>+</sup>), nitrogen oxides nitrate-nitrite (NO<sub>x</sub>-N), iron (Fe), sulfate (SO<sub>4</sub><sup>2-</sup>), chloride (Cl), aluminum (Al), alkalinity, color, total suspended solids (TSS), total dissolved solids (TDS), hardness, chlorophyll, and alkaline phosphatase activity (APA). Deployed EXO-sondes measured pH, temperature, specific conductance, and dissolved oxygen (DO) at 15-minute intervals. PP was calculated as the difference between TP and TDP, and DOP

was calculated as the difference between TDP and SRP. These P species were determined only from weekly grab samples since the autosampler containers were pre-preserved with sulfuric acid and acidic condition results in hydrolysis of organic and condensed inorganic P.

# **Data Management and Statistical Analysis**

Data screening, i.e. detection of outliers, was a necessary step prior to data analysis. Autosampler TP measurements greater than the 99<sup>th</sup> percentile for a given station and flow period were identified as outliers and removed from further statistical analysis (Julian and Hill 2012). The screening removed 176 out of 9,423 data measurements collected during the six flow events. Daily mean TP values for each station were calculated and compared between flow periods using Wilcoxon's test, a non-parametric pairwise multiple comparisons procedure based on rank sums following rejection of a Wilcoxon/Kruskal-Wallis test. The relationship between TP and other key water quality parameters were explored using the predictor screening platform. The screening platform uses a bootstrap forest partitioning to evaluate the contribution of predictors on the response. For each response, a bootstrap forest model using 100 decision trees is built. All statistical analyses were done using JMP® Software 13.1 (SAS Institute Inc. 2016).

#### **RESULTS**

## **Surface Water TP Concentrations**

## STA-2 Flow-Way 1

A distinct TP concentration gradient was observed along the treatment FW for all periods of each flow event (**Figures 4** through **6**). For the first flow event, median inflow to outflow TP concentrations ranged from 98 to 15  $\mu$ g/L during the first low flow period, from 96 to 12  $\mu$ g/L during the no flow period, and from 46 to 10  $\mu$ g/L during the second low flow period (**Figure 4**). Median TP concentrations decreased significantly at all stations as the flow event progressed. Using the mean inflow and outflow TP concentrations observed at all phases of the flow event, TP concentration reductions during the first low flow, no flow, and second low flow periods were 89, 87, and 80%, respectively.

Daily mean TP concentrations measured during the second flow event ranged from 9 to 928 µg/L, with the highest concentrations observed at station C3 during the initial no flow period (Figure 5). TP concentrations observed at station C3 were uncharacteristically elevated due to high amounts of particulates in the samples, likely due to the decreasing water levels during the no flow period, which may have resulted in intake of particulate matter into the collection bottles. The ensuing high flow period resulted in TP concentrations higher than those observed during the other phases of the flow event except for TP concentrations seen at station C3 during the no flow period. During the high flow period from June 5 to June 26, 2017, the area received 17 inches of rainfall, the most for the month of June since 2005 (Zhao 2018). Increased basin runoff and inflow TP concentrations contributed to an extremely high PLR of 20.1 milligrams P per square meter per day (mg P/m<sup>2</sup>/d) or 7.3 grams P per square meter per year (g P/m<sup>2</sup>/yr) during this period. The long-term average PLR for the FW is just under 1.0 g P/m<sup>2</sup>/yr. Despite the high loading during the study period, the FW effectively reduced TP concentrations during all phases of the flow event. TP concentrations during the high flow period were more variable than during the no flow and low flow periods, particularly at stations close to midflow and outflow regions. Median TP concentrations along the FW decreased from 183 to 15 µg/L during the initial no flow period, from 188 to 10 µg/L during the high flow period, and from 135 to 13 µg/L during the low flow period. TP concentrations at all stations except at the outflow station during the high flow period were significantly higher than those seen during the low flow period. Based on mean inflow and outflow TP concentrations, the TP concentration reductions during no flow, high flow, and low flow periods were 93, 95, and 91%, respectively.

Consistent with the first two flow events, a decline in daily mean TP concentrations was observed along the treatment FW during the third flow event (**Figure 6**). TP concentrations at the inflow station, however

were lower than in the previous two flow events. TP concentrations were consistently higher under a no flow condition that followed a period of low flow with significant differences in median TP values observed at stations A3, F3, G3, and H3. Data shows that the greatest TP reduction along the FW occurred between stations C3 and F3. No further treatment was observed until the outflow point of the FW (**Figure 6**). Mean inflow to outflow TP concentration reductions were 79 and 88% under low flow and no flow conditions, respectively.

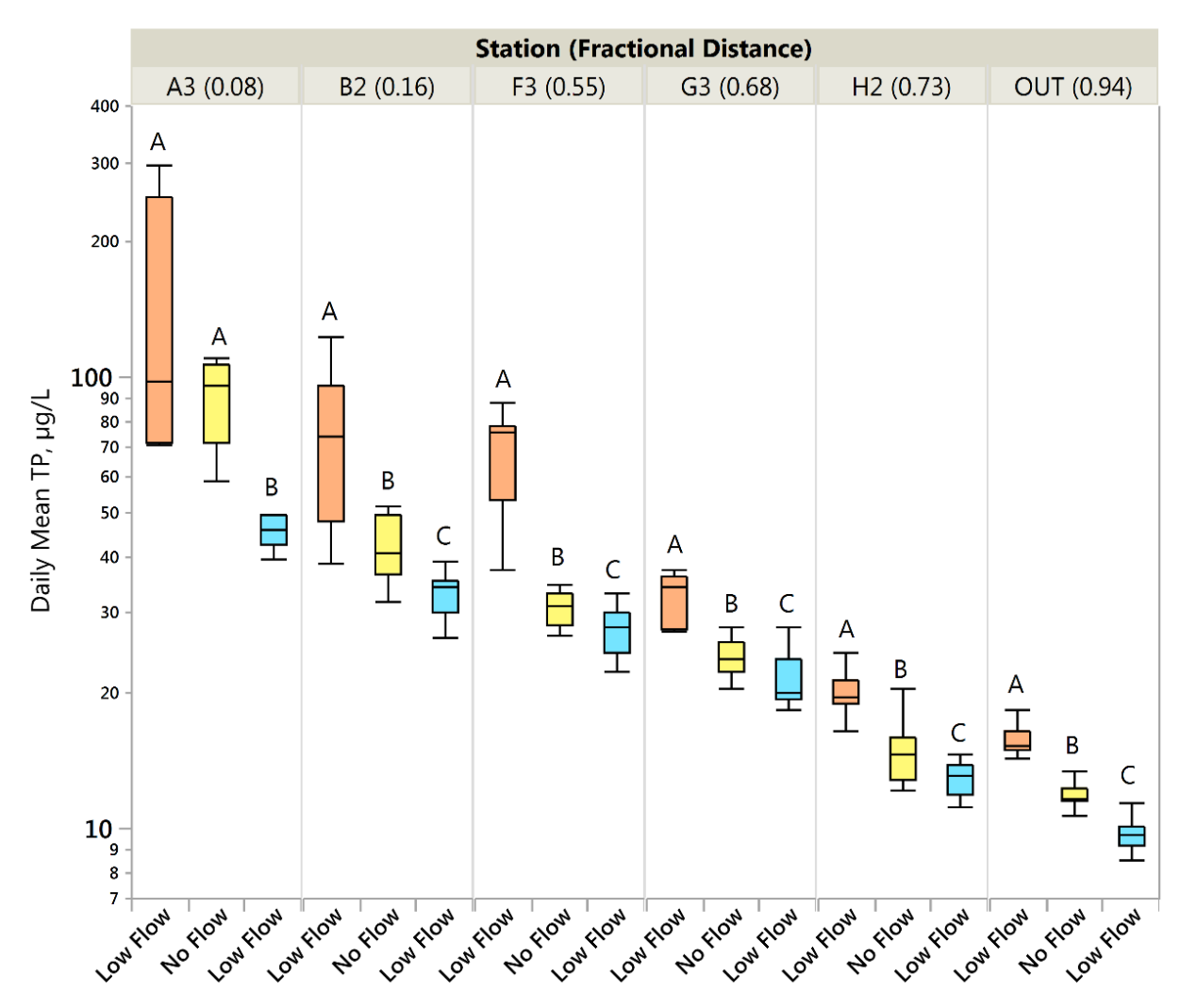


**Figure 4.** Daily mean TP concentrations in the auto samples collected every 4 hours at each monitoring station in STA-2 FW 1 during the first flow event (August 10–September 14, 2015). Fractional distance represents the distance between sampling station and inflow structure. For each station, median TP concentrations with the same letter are not significantly different at significance level (a) of 0.05 using Wilcoxon's multiple pairwise comparisons. Median TP values are indicated by the band inside the box. (Note: Y-axis is on a log-scale.)

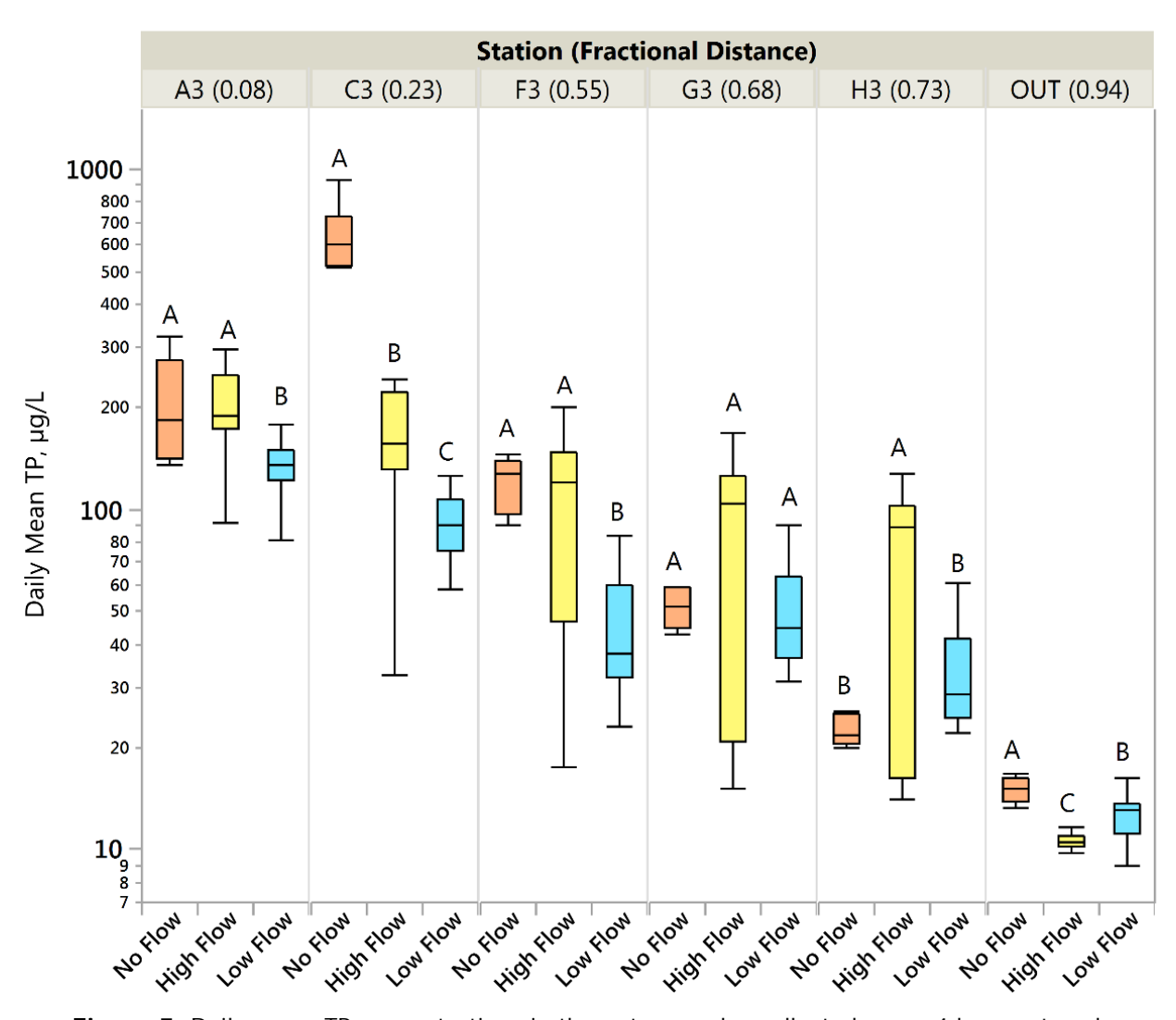


**Figure 5.** Daily mean TP concentrations in the auto samples collected every 4 hours at each monitoring station in STA-2 FW 1 during the second flow event (May 29–July 29, 2017). Fractional distance represents the distance between sampling station and inflow structure. For a given station, median TP concentrations with the same letter are not significantly different at a = 0.05 using Wilcoxon's multiple pairwise comparisons. Median TP values are indicated by the band inside the box. (Note: Y-axis is on a log-scale).

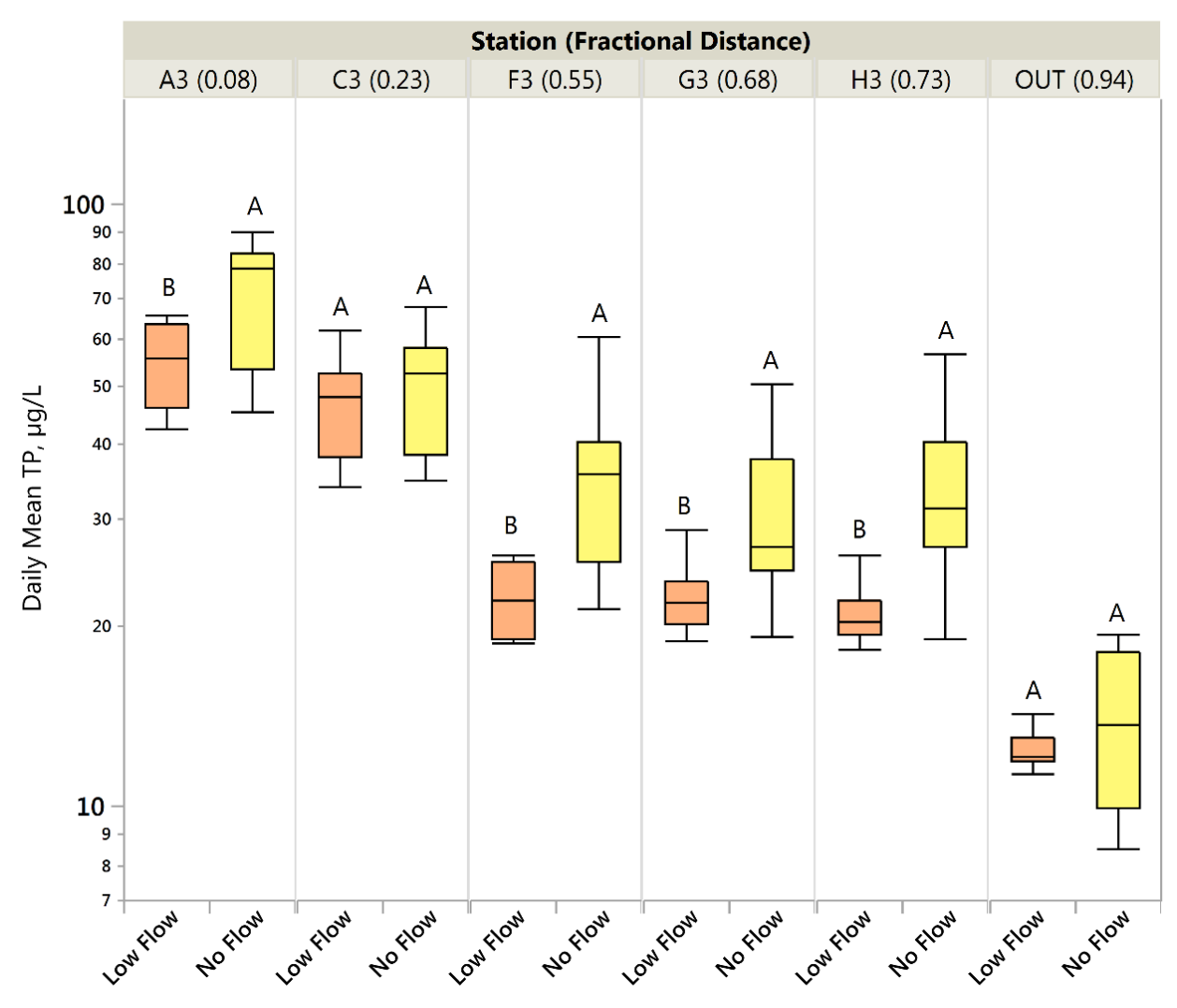


**Figure 6.** Daily mean TP concentrations in the auto samples collected every 4 hours at each monitoring station in STA-2 FW 1 during the third flow event (November 12–December 26, 2017). Fractional distance represents the distance between sampling station and inflow structure. For a given station, median TP concentrations with the same letter are not significantly different at α = 0.05 using Wilcoxon's multiple pairwise comparisons. Median TP values are indicated by the band inside the box. (Note: Y-axis is on a log-scale.)

#### **Surface Water TP Concentrations**

## STA-2 Flow-Way 3

Similar to the flow events conducted in STA-2 FW 1, daily mean TP concentrations significantly declined along the FW at all phases of the three flow events in STA-2 FW 3 (**Figures 7** through **9**). The inflow to outflow pattern of reduction however, was not as distinct as observed in FW 1. For the first flow event, median TP concentrations decreased from 39 to 11 µg/L during the high flow period, from 75 to 22 µg/L during the no flow period, and from 100 to 18 µg/L during the low flow period (**Figure 7**). TP concentrations increased significantly at all stations as the FW transitioned from high flow to no flow period. The spike in TP concentration at station C20 during low flow condition was likely a result of moderate to high flows (average 6.77 m³/s) during the first three days of low flow operation. TP concentrations during the high flow period were significantly lower than during periods of no flow and low flow. The mean TP concentration reductions based on inflow and outflow concentrations under high flow, no flow, and low flow conditions were 75, 63, and 94%, respectively.

The extended period of no flow that preceded the first low flow period during the second flow event resulted in TP concentrations higher than those seen during any other period of the flow event (Figure 8). Median TP concentrations along the treatment FW during the initial no flow period were 171 and 58 µg/L at stations C20 and C200, respectively. There was a significant decrease in TP concentrations at all stations as the FW transitioned from the no flow to the first low flow period. During the second no flow period, TP concentrations increased at the inflow and midflow stations. There was a general decrease in TP concentrations at all stations except at the inflow region (C20) during the second low flow period. At the outflow region (stations C164 and C200), TP concentrations were lowest during the second low flow period. TP concentrations at station C92 remained high and variable across all flow periods, suggesting lack of P treatment. TP concentrations at this station are consistently higher than the surrounding stations suggesting a potential P hotspot. However, an examination of the soil TP data at this station and the surrounding stations suggests that the elevated TP concentration at C92 could be coming from the high TP concentration in both floc and RAS at station C74 (one of our spatial soil sampling locations), which is directly above C92. TP concentrations at C74 were 865 and 896 mg/kg, for floc and RAS, respectively, compared to 538 and 479 mg/kg at station C92. TP concentrations in the surrounding stations were similar to TP concentrations seen at station C92. It is likely that as the water travels from station C74 to C92, the flux of P from soil to water column at C74 is manifested at station C92. An evaluation of the vegetation and microbial data in this region of the flow-way will be conducted to ascertain any influence these factors might have had on the observed TP concentrations at station C92. Based on the mean TP concentrations at the inflow and outflow regions, TP concentration reductions were 64, 45, 73, and 81%, for the initial no flow, first low flow, second no flow, and second low flow conditions, respectively.

Daily mean TP concentrations during the third flow event were the lowest among the three flow events conducted in this FW despite receiving the highest PLR of 5.9 mg  $P/m^2/d$  (2.15 g  $P/m^2/yr$ ) (**Figure 9**). While the spatial pattern in TP concentrations along the FW indicates reduction, elevated TP concentrations were measured at C92 at both periods of the flow event, which suggests localized internal P loading. TP concentrations during the no flow period were significantly higher from C92 to C200 (probability [p] < 0.05) than during the high flow period. TP concentration reductions based on inflow and outflow concentrations were 71 and 52% under high flow and no flow conditions, respectively.

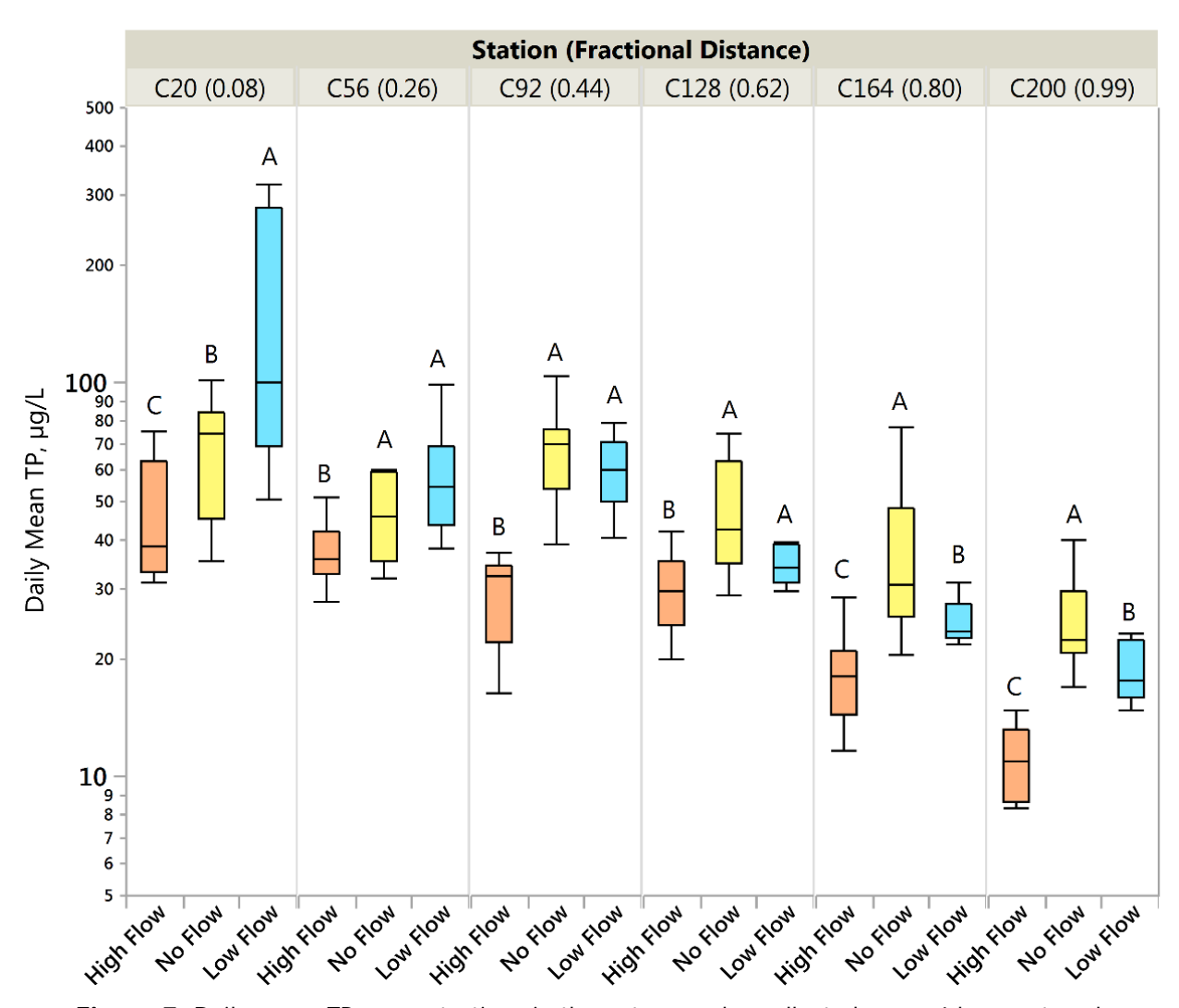


**Figure 7.** Daily mean TP concentrations in the auto samples collected every 4 hours at each monitoring station in STA-2 FW 3 during the first flow event (February 22–April 11, 2016). Fractional distance represents the distance between sampling station and inflow structure. For a given station, median TP concentrations with the same letter are not significantly different at  $\alpha=0.05$  using Wilcoxon's multiple pairwise comparisons. Median TP values are indicated by the band inside the box. (Note: Y-axis is on a log-scale).

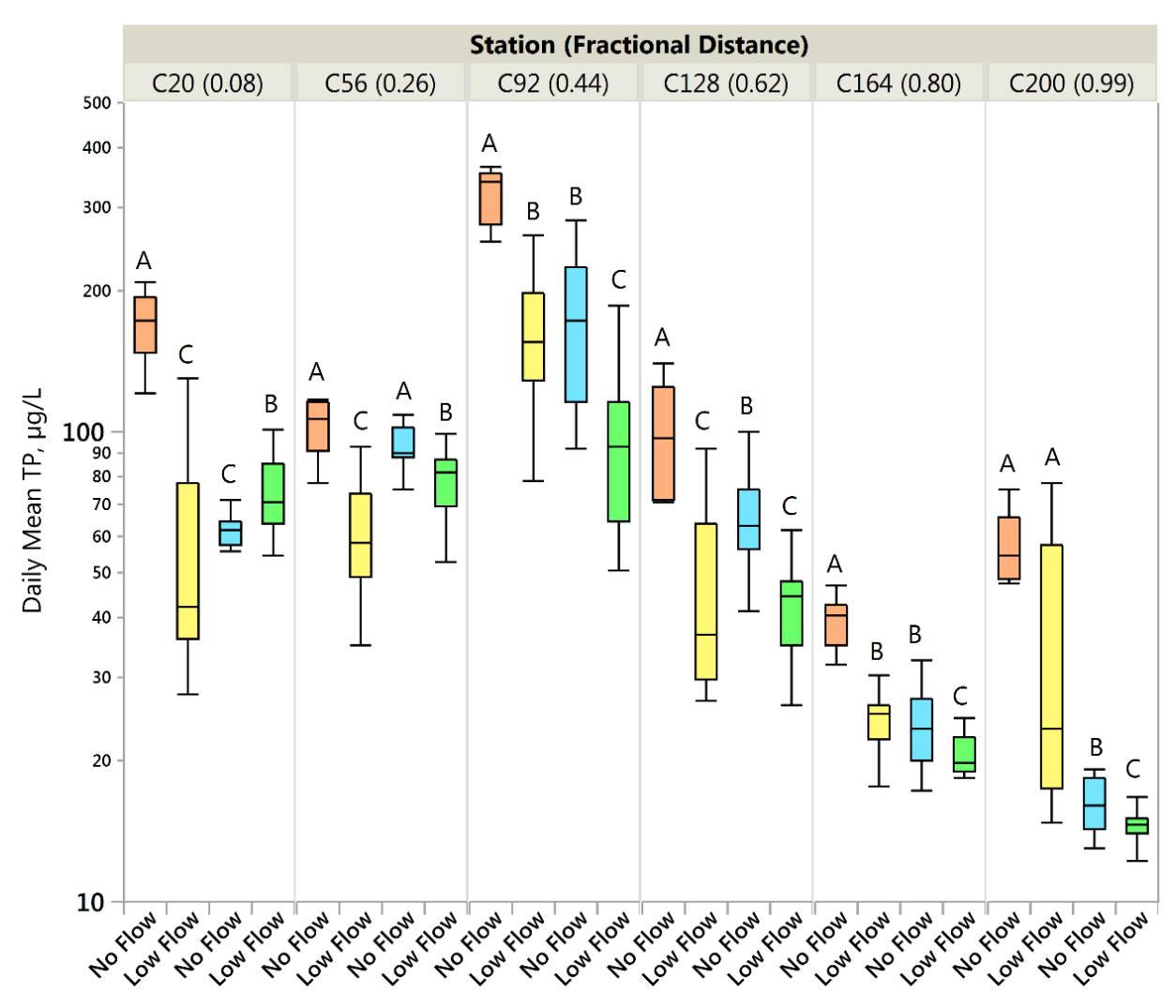


**Figure 8.** Daily mean TP concentrations in the auto samples collected every 4 hours at each monitoring station in STA-2 FW 3 during the second flow event (June 27–August 29, 2016). Fractional distance represents the distance between sampling station and inflow structure. For a given station, median TP concentrations with the same letter are not significantly different at a = 0.05 using Wilcoxon's multiple pairwise comparisons. Median TP values are indicated by the band inside the box. (Note: Y-axis is on a log-scale.)

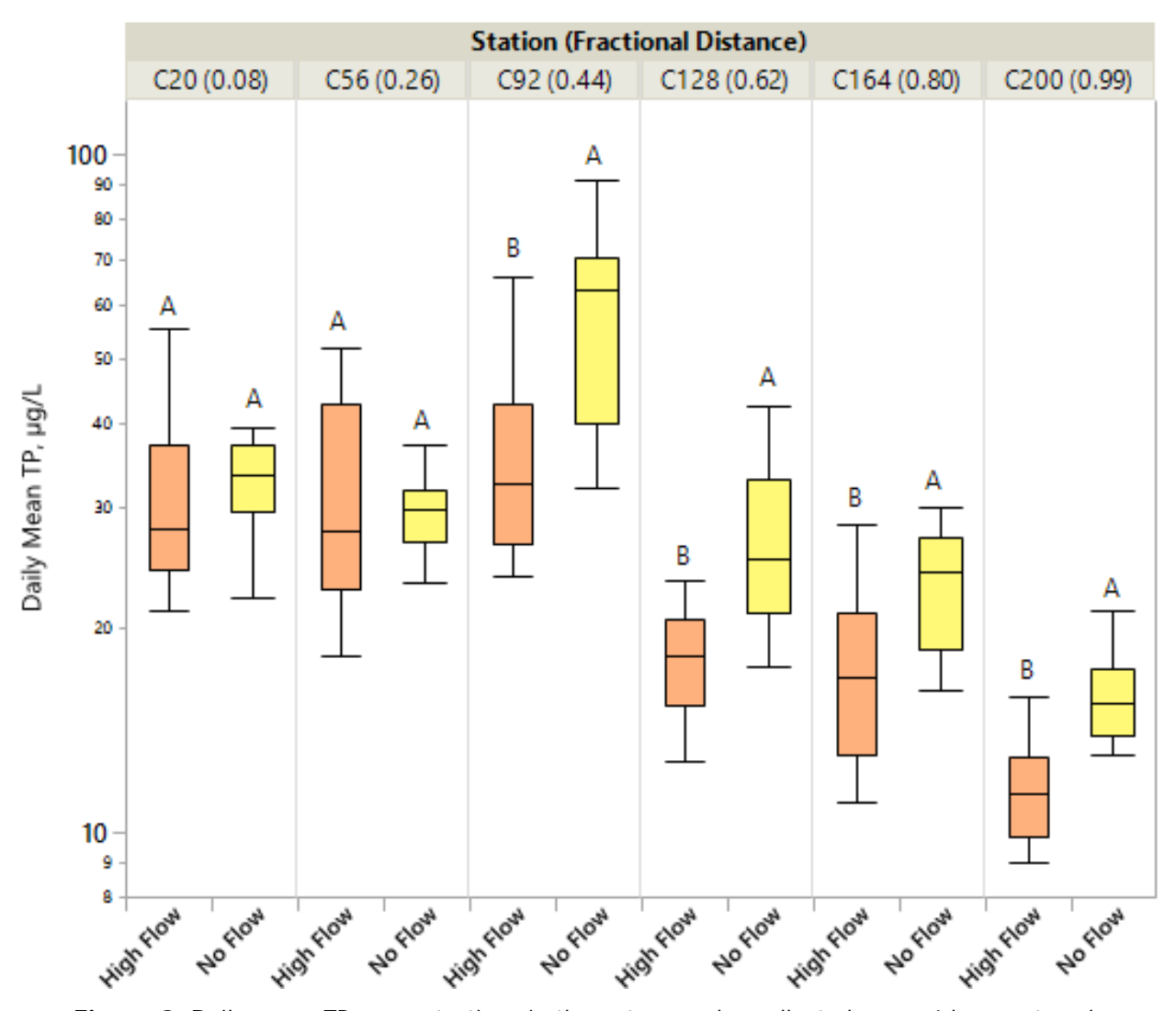
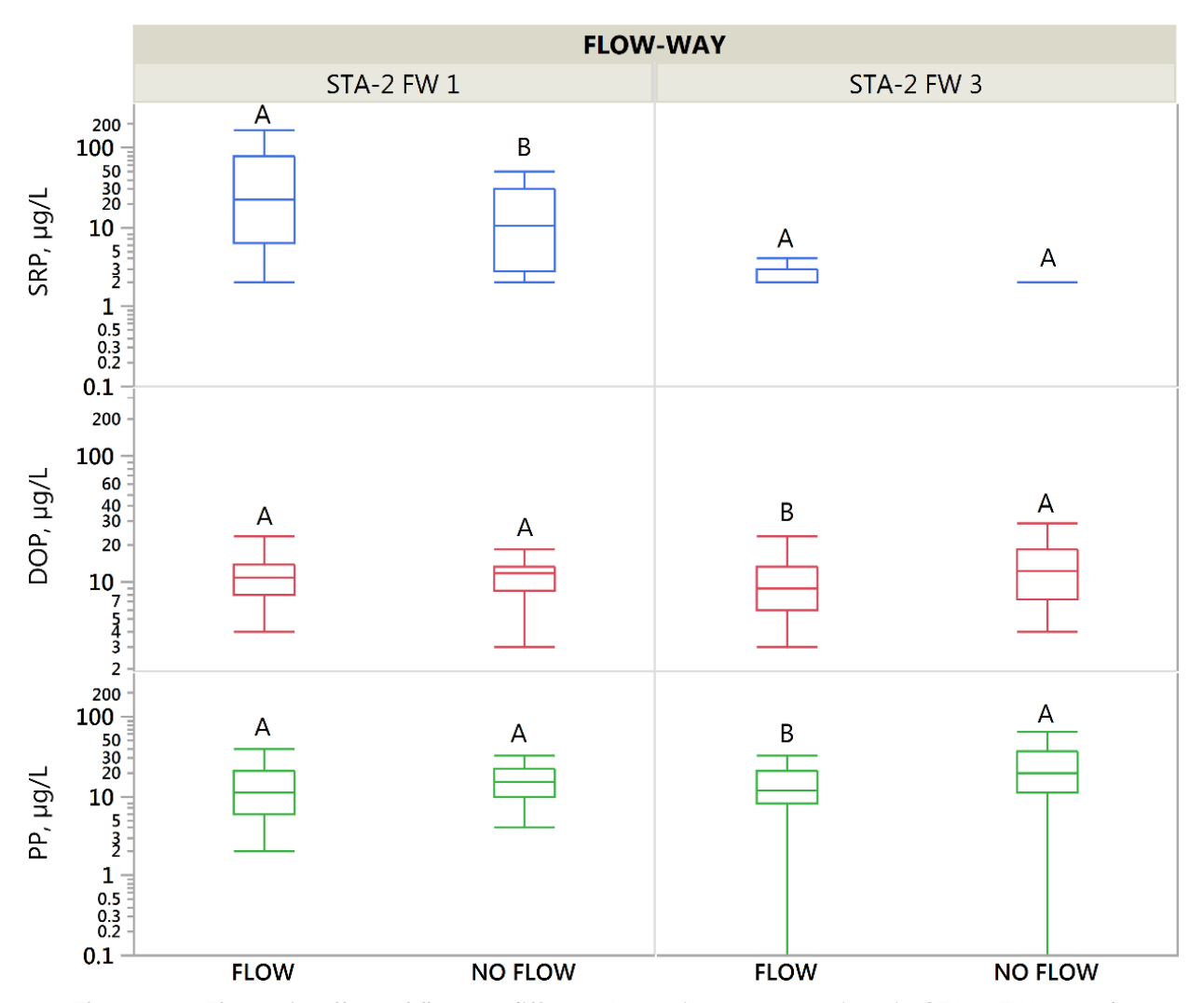


Figure 9. Daily mean TP concentrations in the auto samples collected every 4 hours at each monitoring station in STA-2 FW 3 during the third flow event (October 12–November 22, 2016). Fractional distance represents the distance between sampling station and inflow structure. For a given station, median TP concentrations with the same letter are not significantly different at a = 0.05 using Wilcoxon's multiple pairwise comparisons. Median TP values are indicated by the band inside the box. (Note: Y-axis is on a log-scale.)

### **Patterns in Different P Forms**

P cycling and movement within an STA is a function of various chemical, physical, and biological processes operating at different regions of the FW. The concentration and composition of P observed at the outflow structure is a net result of all these processes. P transformations along the transect during the flow events were evaluated using P speciation data from weekly grab samples. For each FW, data were pooled from all flow events and grouped into flow (combining data from low flow and high flow periods) and no flow to provide a data set large enough to determine if there are statistically significant differences. The overall effect of flow versus no flow condition on different P species concentrations varied between FWs (**Figure 10**). There was an increase in PP under no flow condition in both FWs, but the increase was significant for FW 3 only ( $\chi^2 = 8.43$ , p < 0.05). In FW 3, mean PP concentrations were 19  $\mu$ g/L for flow and 31  $\mu$ g/L for no flow conditions. In FW 1, PP concentrations averaged 15 and 18  $\mu$ g/L under flow and no flow conditions, respectively (**Table 2**).



**Figure 10.** The main effect of flow on different P species concentrations in STA-2 FWs 1 and 3 measured during six events. For a given FW, median P concentrations (indicated by the band inside the box) under flow and no flow conditions with the same letter are not significantly different at  $\alpha = 0.05$  using Wilcoxon's multiple pairwise comparisons. (Note: Y-axis is on a log-scale.)

No Flow

DOP

SRP

29

11

Concentration Statistic (µg/L) **Test** Number of Flow P Species **Observations** Flow-Way Condition **Minimum** Median Mean Maximum PΡ 60 2 11.0 15 58 DOP 60 4 Flow 11.0 11 23 SRP 2 60 22.0 48 279 **STA-2 FW 1** PP 4 30 15.0 18 87 No Flow DOP 3 11 30 11.5 21 SRP 30 2 10.5 18 76 PΡ 84 0 12.0 19 118 3 Flow DOP 84 9.0 10 56 SRP 84 2 2.0 5 33 **STA-2 FW 3** PP 0 31 60 19.5 263

**Table 2**. Summary statistics for the different P species concentrations in STA-2 FWs 1 and 3 under flow and no flow conditions.

DOP in both FWs showed similar trend as PP with a significant increase observed under no flow condition in FW 3 ( $\chi^2 = 6.21$ , P<0.05) but not in FW 1 (**Figure 10**). DOP concentrations were lower than PP concentrations in both FWs. Mean DOP concentrations were 11 and 13  $\mu$ g/L under flow and no flow conditions, respectively, in FW 3 and 11  $\mu$ g/L under both flow conditions in FW 1 (**Table 2**). In FW 1, SRP concentrations were significantly higher under flow than no flow condition ( $\chi^2 = 6.53$ , p < 0.05) but were similarly low under both flow conditions in FW 3. Mean SRP concentrations of 48  $\mu$ g/L under flow and 18  $\mu$ g/L under no flow conditions were observed in FW 1. SRP concentrations in FW 3 averaged 5  $\mu$ g/L under flow condition and 3  $\mu$ g/L under no flow condition (**Table 2**).

4

2

12.0

2.0

13

3

60

60

The distribution of the different P species along the flow path during periods of flow and no flow differed between FWs (Figures 11 and 12). In FW 1, SRP was the dominant P species under flow and no flow conditions (Figure 11). SRP was particularly high at stations close to the inflow region (Stations A3 and C3), accounting for over 70% of TP observed during the flow period (Table 3). The high SRP concentrations were attributed to high rainfall event in June 2017 that coincided with one of the flow events. During the two-week period of high flow, the PLR was 20 mg P/m<sup>2</sup>/d. As the water traveled downstream, SRP concentration decreased significantly at station F3 and was relatively unchanged until the water reached the OUT station (Figure 11) where mean SRP concentration declined significantly from 27 to the method detection limit (MDL) of 2 µg/L (**Table 3**). SRP concentration was also the dominant P species under no flow, but median concentrations were significantly lower than those observed under flowing condition (Figure 10). SRP concentration was significantly lower at the OUT station (Figure 11). DOP levels along the FW were low but steady with significantly lower concentrations at the outflow region under both flow and no flow conditions. Inflow to outflow mean DOP concentrations ranged from 13 to 6 µg/L under flowing condition and from 16 to 4 µg/L under no flow condition (Table 3). Similar to SRP, PP concentrations were highest at the inflow region and decreased along the flow path under flow and no flow conditions. Mean PP concentrations ranged from 26 to 4 µg/L and from 38 to 9 µg/L under flow and no flow conditions, respectively.

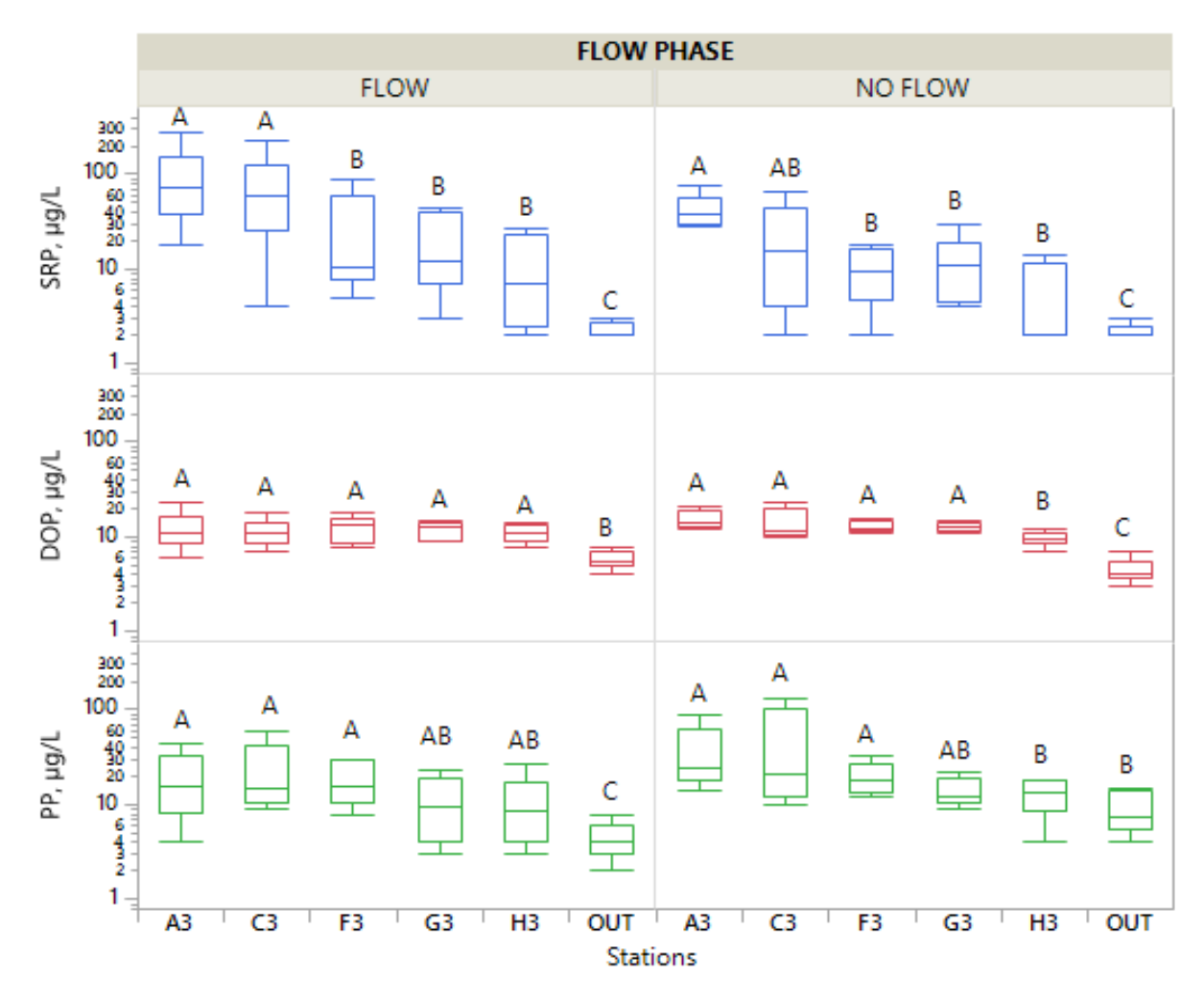


Figure 11. Water column P species concentrations along STA-2 FW 1 under flow and no flow conditions. For a given flow phase, median P concentrations (indicated by the band inside the box) along the transect with the same letter are not significantly different at  $\alpha = 0.05$  using Wilcoxon's multiple pairwise comparisons. (Note: Y-axis is on a log-scale.)

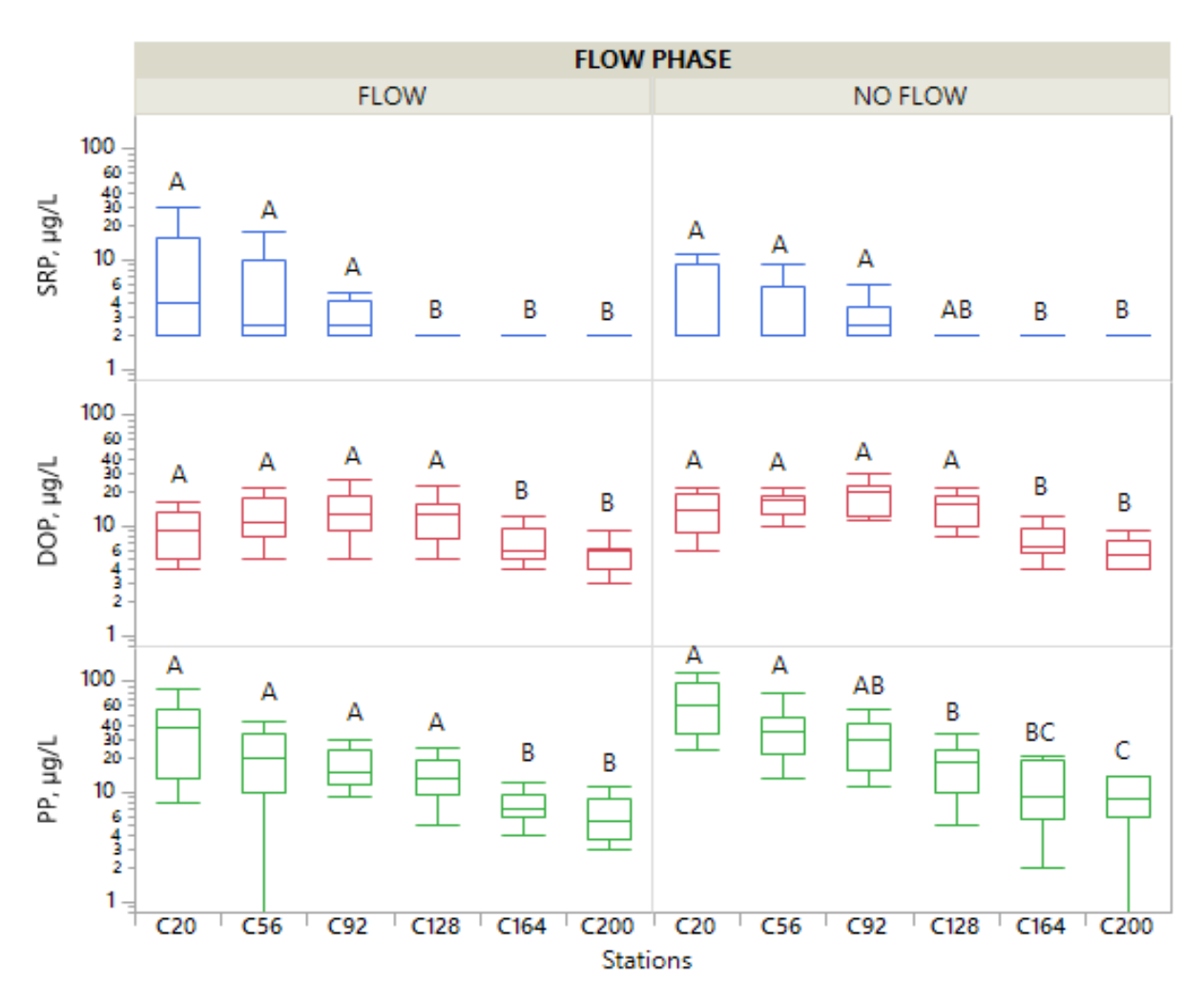


Figure 12. Water column P species concentrations along STA-2 FW 3 under flow and no flow conditions. For a given flow phase, median P concentrations (indicated by the band inside the box) along the transect with the same letter are not significantly different at  $\alpha = 0.05$  using Wilcoxon's multiple pairwise comparisons. (Note: Y-axis is on a log-scale.)

**Table 3**. Mean P species concentrations along the flow path under flow and no flow conditions in STA-2 FWs 1 and 3.

	Flow Condition		Concentrations from Inflow to Outflow Transect Locations (µg/L)					
Test FW		P Species	A3 (C20) <sup>a</sup>	C3 (C56)	F3 (C92)	G3 (C128)	H3 (C164)	OUT (C200)
		TP	137	128	63	57	49	12
	□lo	PP	20	26	18	11	11	4
	Flow	DOP	13	12	13	12	11	6
STA-2 FW 1		SRP	104	90	32	34	27	2
31A-2 FW 1	No Flow	TP	100	57	50	39	34	15
		PP	38	18	20	14	13	9
		DOP	16	11	13	13	10	4
		SRP	46	28	17	12	11	2
	Flow	TP	56	49	36	29	17	15
		PP	38	27	18	14	8	7
		DOP	9	15	13	13	7	6
STA-2 FW 3		SRP	9	7	5	2	2	2
51A-2 FW 5		TP	97	58	52	35	20	17
	No Flow	PP	79	38	30	18	11	9
		DOP	14	16	19	15	7	6
		SRP	4	4	3	2	2	2

a = Stations along STA-2 FW 3.

TP concentrations during the flow events were generally lower in FW 3 compared to TP concentrations observed in FW 1 (Table 3). While SRP dominated the water column P species in FW 1, PP was the dominant P form in FW 3, accounting for 68 and 81% of TP at the inflow region during flow and no flow conditions, respectively. There was a significant increase in PP concentrations along the FW following a period of flow (Figure 10). This indicates PP is generated in situ when the FW is stagnant. DB Environmental, Inc. reported phytoplankton to be the dominant component of surface water particles identified during the last flow event in FW 3 under similar stagnant condition (DBE 2017). Measures of phytoplankton density such as chlorophyll a concentration, cell density, and biovolume were positively correlated with PP concentration. PP concentrations declined as the water moved downstream with significant reductions observed at the OUT station under both flow and no flow conditions. SRP was reduced early in the FW with concentrations reaching the MDL (2 µg/L) at the midflow region down to the outflow of the FW under both flow conditions (Figures 11 and 12 and Table 3). This suggests that the bulk of inorganic P in the water column was consumed rapidly by biotic (i.e. biological uptake) and abiotic processes (i.e. P sorption/precipitation) near the inflow. DOP concentrations from inflow to outflow varied with some increase in the midflow of the FW but the concentration decreased significantly in the outflow region of the FW, with a mean outflow DOP concentration of 6 µg/L under flow condition and 4 µg/L under no flow condition. The residual P pool at the outflow region of both FWs was comprised mainly of PP and DOP with SRP at the MDL. The residual P pool under both flow conditions was slightly larger in FW 3 compared to FW 1 and was slightly bigger under no flow condition than flow condition in both FWs (Table 3).

# Relationship between TP and Selected Water Quality Parameters

One specific objective of the study was to identify key physical and biogeochemical factors influencing biogeochemical responses to different hydraulic and hydrologic conditions. The predictor screening platform in JMP Version. 13.1 was used to identify important predictors of TP from a suite of other water quality and field parameters measured along the FW during the flow events. The analysis was done on pooled data from all flow events and partitioned into flow and no flow. A total of 27 parameters were used in the prediction but only the top ten predictors based on their contribution to the variability explained by the model are presented (**Tables 4** and **5**). The "Portion" values in the predictor screening report represent the proportion of total contributions (reductions in error sums of squares due to splits) attributable to each predictor. These values come from dividing each contribution by the total of the contributions.

In STA-2 FW 1, the top ten predictors accounted for a combined 86% of the variability explained by the model with 37% attributed to total Fe, the most important predictor of TP under flow condition (**Table 4**). Near the top of the list are NH<sub>4</sub>-nitrogen (N), color, DO, and TN accounting for 31% of the explained variability in water column TP. Under no flow condition, the top ten predictors accounted for 86% of the variability in TP (**Table 4**). Similarly, both NH<sub>4</sub>-N and total Fe emerged as the two most important predictors contributing 37% to the variability explained by the model. TSS and Ca also appeared to be important predictors, ranking fourth and fifth, respectively, under no flow condition.

Table 4. Predictors of water column TP concentration ( $\mu$ g/L) in STA-2 FW 1 under flow and no flow conditions. The Contribution column shows the contribution of each predictor to the bootstrap forest model. The Portion column shows the percent contribution of each variable.

Flow Phase	Predictor	Contribution	Portion	Rank
	Iron, μg/L	36,394	0.369	1
	Ammonium-N, mg/L	10,199	0.104	2
	Color, PCU	7,766	0.079	3
	Dissolved Oxygen, mg/L	6,437	0.065	4
Flow	Total Nitrogen, mg/L	5,783	0.059	5
FIOW	Specific Conductivity, µS/cm	5,144	0.052	6
	Temperature, °C	3,746	0.038	7
	Alkalinity, mg/L CaCO <sub>3</sub>	3,572	0.036	8
	рН	3,487	0.035	9
	Sodium, mg/L	2,466	0.025	10
	Ammonium-N, mg/L	7,722	0.235	1
	Iron, μg/L	4,543	0.138	2
	Total Nitrogen, mg/L	4,428	0.135	3
	Total Suspended Solids, mg/L	2,194	0.067	4
No Flow	Calcium, mg/L	1,683	0.051	5
NO FIOW	Color, PCU	1,677	0.051	6
	Sulfate, mg/L	1,643	0.050	7
	Chlorophyll a, µg/L	1,551	0.047	8
	Magnesium, mg/L	1,481	0.045	9
	Alkalinity, mg/L CaCO₃	1,374	0.042	10

In STA-2 FW 3, the top ten variables were slightly better predictors of TP than those identified in STA-2 FW 1, accounting for 90 and 88% of the variability in water column TP under flow and no flow

conditions, respectively (**Table 5**). Chlorophyll *a* was the most important predictor of TP under both flow conditions, explaining over 23% of the variability. Total suspended solids, TN, pheophytin *a*, and total Fe appeared in the top six of the list under flow and no flow conditions but in a slightly different order of importance.

The emergence of metal cations as an important predictor of water column TP under flow and no flow conditions is consistent with the correlative relationships between TP and other water quality parameters previously reported for these STAs (Villapando and King 2018). Positive correlation of TP with iron and Ca suggests the importance of these metal cations in binding with P to form organic/inorganic precipitates. The ability of total suspended solids to predict TP concentration especially under no flow condition could be related to in-situ production and resuspension of particulates in the water column. The appearance of TN as a predictor of TP in both flow-ways under flow and no flow conditions supports previous findings that the transformations of P in the STAs are strongly coupled to that of nitrogen (Corstanje et al. 2016).

**Table 5**. Predictors of water column TP concentration ( $\mu$ g/L) in **STA-2 FW 3** under flow and no flow conditions. The Contribution column shows the contribution of each predictor to the bootstrap forest model. The Portion column shows the percent contribution of each variable.

Flow Phase	Predictor	Contributio n	Portion	Rank
	Chlorophyll a, mg/L CaCO₃	3,267	0.244	1
	Total Suspended Solids, mg/L	1,935	0.145	2
	Total Nitrogen, mg/L	1,730	0.129	3
	Pheophytin a, μg/L	1,562	0.117	4
Flow	Temperature, °C	1,343	0.100	5
FIOW	Iron, μg/L	1,109	0.083	6
	Dissolved Organic Carbon, mg/L	342	0.026	7
	рН	339	0.025	8
	Alkaline Phosphatase Activity, nmo/min-mL	236	0.018	9
	Potassium, mg/L	220	0.016	10
	Chlorophyll a, µg/L	8,044	0.232	1
	Iron, μg/L	5,029	0.145	2
	Total Suspended Solids, mg/L	5,001	0.144	3
	Pheophytin a, μg/L	4,152	0.120	4
No Flow	Total Nitrogen, mg/L	2,542	0.073	5
No Flow	Potassium, mg/L	1,779	0.051	6
	Alkalinity, mg/L CaCO₃	1,483	0.043	7
	Total Dissolved Solids, mg/L	902	0.026	8
	Color, PCU	892	0.025	9
	Specific Conductance, µS/cm	739	0.021	10

The predictor screening platform provides a method of identifying important predictors of an outcome (e.g. water column TP) from a large number of candidate variables. We hypothesize that the water column TP in the STAs is influenced not by one water parameter but a combination of different water quality parameters and other biogeochemical parameters such as floc chemistry, redox, and microbial activities among others, that were not included in the analysis. In an attempt to better understand the biogeochemical factors most important in influencing P retention and cycling along the treatment FW under different flow scenarios, different combinations of the predictors will be fitted into predictive statistical models. A predictive understanding of the factors and processes influencing P speciation along the FW also will be pursued using robust statistical analyses.

#### **SUMMARY**

Six controlled flow events, three each in STA-2 FWs 1 and 3, were conducted under different flow scenarios between August 2015 and December 2017. The flow events varied in duration and timing and consisted of either a low or a high flow period preceded and/or followed by a period of no flow. Despite a concerted effort to use agricultural runoff as the primary source of water for the study, it is likely that the flow-ways received invariably small flows from other sources such as the A-1 Flow Equalization Basin (FEB) and Lake Okeechobee during the flow events. A reduction gradient in TP concentrations from inflow to outflow was observed in both flow-ways. In STA-2 FW1, TP concentrations were reduced by 79 to 95%, with the greatest reduction occurring during high flow when basin runoff and inflow TP concentrations were highest, e.g. during and after an intensive rainfall event that occurred in June 2017. Averaged over flow periods and flow events, STA-2 FW 1 reduced TP concentration by 88%. SRP was the dominant P species in the inflow water and accounted for the majority of TP concentration reduction along the FW under flow and no flow conditions. This was expected as the bulk of the inorganic P in the water column is rapidly consumed through plant and microbial uptake, while a fraction of the inorganic P may also adsorb on particles containing metallic ions such as Ca, Mg, Fe, and Al or co-precipitate with any of these cations. PP and DOP concentrations in the water column were lower compared to SRP and steadily declined from the inflow to outflow region of the FWs. The reductions in the different P species concentrations were pronounced at the backend of the FW where SRP reached the MDL (2 µg/L) while PP and DOP combined for 10 and 13 µg/L under flow and no flow conditions, respectively.

Autosampler TP data from STA-2 FW 3 (SAV-dominated) also showed a reduction along the FW but the gradient was less defined compared to FW 1 due to an apparent hotspot at station C92 where TP concentrations were consistently elevated for all flow events. The inflow to outflow TP concentration reduction averaged over all flow periods and flow events in FW 3 was only 69%. TP concentrations in FW 3 during the flow events were generally lower compared to those seen in FW 1. This was attributed to a huge difference in the average PLR the FWs received during the flow events: 7.3 mg P/m<sup>2</sup>/d in FW 1 and 3.7 mg P/m<sup>2</sup>/d in FW 3. While SRP dominated water column P in FW 1, PP was the dominant P species in FW 3 and accounted for much of the reduction in TP concentration along the FW under both flow conditions. The huge reduction observed at stations close to the inflow region of the FW was due to rapid settling of particulate matter from the incoming water, a major P removal mechanism of constructed wetlands (Reddy and DeLaune 2008). Compared to DOP, SRP was reduced much earlier in the FW and was at the MDL at the midflow region all the way to the outflow region of the FW, indicating that SRP was consumed much more readily through biological and physico-chemical processes operating along the front half of the treatment FW. DOP concentrations along the FW were small relative to PP and consistent until the water reached the outflow region of the FW where concentration decreased significantly under both flow conditions. Similar to FW 1, the residual P pool at the outflow region of FW 3 was comprised primarily of PP and DOP, with concentrations slightly larger in FW 3 and slightly elevated under no flow than flow condition in both FWs. Since SAV and the associated periphyton community can sequester P rapidly and can store it within SAV biomass, SAV-based systems are generally regarded as more effective than EAVdominated systems at removing P from the water column (Dierberg et al. 2002, Knight et al. 2003). The results of the study however, are consistent with the long-term performance of these test FWs with STA-2 FW 1, a predominantly cattail community achieving an outflow TP flow-weighted mean concentration of  $14~\mu g/L$  compared to the SAV-based STA-2 FW 3, achieving  $18~\mu g/L$  for the entire period of record. Part of the reason could be the higher PP concentrations in FW3 that are generated in situ under no flow (stagnant) condition. Several processes controlling PP production have been suggested and they include phytoplankton growth, periphyton sloughing, litter fragmentation, resuspension via entrainment or bioturbation, and horizontal transport (DBE 2017, SFWMD 2013). The production of PP under no flow conditions has important implications in STA operations and performance, especially because FWs remain stagnant between flow events. One potential management option would be to avoid sending high flows to the STAs after a long period of no flow, when possible. The FEBs, which were constructed as part of the *Restoration Strategies Regional Water Quality Plan* (SFWMD 2012b), are anticipated to assist in this regard.

Key water quality parameters monitored during the flow events showed close association with TP in the water column under flow and no flow conditions. Fe and NH<sub>4</sub>-N emerged as the top two predictors of TP in STA-2 FW 1 under both flow conditions. In STA-2 FW 3, TSS and chlorophyll *a* were at the top of the list under both flow conditions. Predictive statistical modeling will be used to identify the factor(s) with significant influence on P retention and cycling along the treatment FW. It is likely that the influencing factors change depending on the location along the FW. Results from the study will be evaluated in relation to vegetation, soils, and microbial data to determine key biogeochemical factors and processes influencing P reduction in these STAs, especially at the lower reaches of the treatment FW.

# INTERNAL P LOADING MEASUREMENTS

Mike Jerauld<sup>1</sup>, John Juston<sup>2</sup>, and Tom DeBusk<sup>1</sup>

## INTRODUCTION

One factor that likely is important in achieving the WQBEL for the STAs is the contribution of internal loading on low P STA discharge concentrations. Internal loading is a return flux from labile P contained in biotic and/or edaphic solids (Kadlec and Wallace 2009). However, little is known of the total internal P loading rate (iPLR) or the relative magnitudes of different potential internal P sources and the environmental and operational factors that affect them in the low P domain.

#### **GENERAL APPROACH**

The internal loading rate in a wetland is difficult to measure directly because P removal processes continually act upon a combination of longitudinally-transported and internally-loaded P return fluxes at all points along a treatment gradient. When water flow shuts off to a flow-through wetland, the local water concentration is driven to equilibrium over a matter of a few days or weeks, in which uptake and release between the water column and internal sources and sinks become balanced (Juston et al. 2015, Kadlec 2001). Here, the dynamic response to equilibrium was measured in mesocosms (1.5-meter (m) diameter) installed directly in the STA-2 FW 3 marsh, encompassing both native soil and vegetation communities, during multiple two-week batch incubations. A modeling approach was then used to extract the net internal P loading rate that contributed to the measured dynamic responses, based on the assumption that this internal load was essentially constant during each incubation.

<sup>&</sup>lt;sup>1</sup> DB Environmental, Inc., Rockledge, Florida.<sup>2</sup>

<sup>&</sup>lt;sup>2</sup> Juston Konsult AB, Sweden.

The well-known k-C\* model (Kadlec and Wallace 2009) represents change in water P concentration during a batch incubation as the balance of 1<sup>st</sup> order P removal and zero-order P return fluxes:

$$\frac{\partial C}{\partial t} = -(k_0 * C_t) + (k_0 * C_E) \tag{1}$$

where:

t = time elapsed, days

 $C_t = P$  concentration at time, t, milligrams per liter (mg/L)

 $C_E$  = equilibrium P concentration, mg/L

 $k_0$  = batch volumetric rate constant, per day (d<sup>-1</sup>)

We note that this model application makes no attempt to represent specific P removal and return mechanisms, only their net consequences. However, in this way, k and  $C_E$  values were aggregated model parameters that were calibrated to the time series data (i.e.,  $C_t$ ). Then, the total effective internal loading rate was calculated for each response from these calibrated parameters:

$$iPLR = k_0 * h * C_E$$

where:

h =water depth, m.

The concept of "internal load" is similar to but slightly distinct from the "net flux" terminology used previously (Jerauld et al. 2018). P removal/uptake in wetlands typically occurs proportionally (first order) to the water column concentration, while internal loading is considered essentially constant (zero order). Therefore, when the initial water column concentration (and thus removal rate) is low, internal loading results in a net flux *to* the water column. At equilibrium, the removal rate of P ( $k_0 * C$ ) balances the iPLR. This is what is measured in typical chamber time series responses. If the water column concentration (and thus removal rate) is high, concentrations may decline, and net flux may be *out of* the water column, despite the internal loading.

#### **METHODS**

## **Field Methods**

Mesocosms were open top, open bottom, 1.5-m diameter plastic cylinders installed in triplicate in existing SAV beds at inflow (INF), midflow (MID), and outflow (OUT) regions of STA-2 FW 3 (**Figures 13** and **14**). The chambers have large open windows that allow free water exchange with the surrounding marsh, so that the enclosure experiences the same effects of P loading and other forcing factors as the rest of the FW (**Figure 14**). Following controlled, prescribed flow events, the mesocosm openings were sealed, preventing surface water exchanges. The water column in the chambers was sampled serially over a 14-day incubation period. Simultaneously, peepers were installed in duplicate outside each set of chambers, and were sampled after 14 days (Carignan 1984, Dierberg et al. 2012, Fisher and Reddy 2001, Hesslein 1976, Newman and Pietro 2001). These chambers were sealed and sampled during three no flow events lasting at least two weeks in duration between March and November 2016 (**Table 6**). These events occurred after various flow events in STA-2 FW 3. The SAV community inside the INF mesocosms disappeared between Events 1 and 2 (not as a result of Event 1 chamber closure) and could not be revived. Therefore, only data from Event 1 could be used for analysis. During Event 2, the mesocosms at MID had initial TP concentrations of ~120  $\mu$ g/L, which was ~90  $\mu$ g/L higher than measured in the ambient water column at the time of closure (t = 0) even though no noted field observations supported this phenomenon. We

excluded these apparently contaminated data from analysis. Lastly, it was not possible to maintain zero discharge conditions from the flow-way throughout Event 2, which required screening of day 14 samples (recall that the purpose of sampling during no flow events was to remove effect of P advection on local water P equilibria).

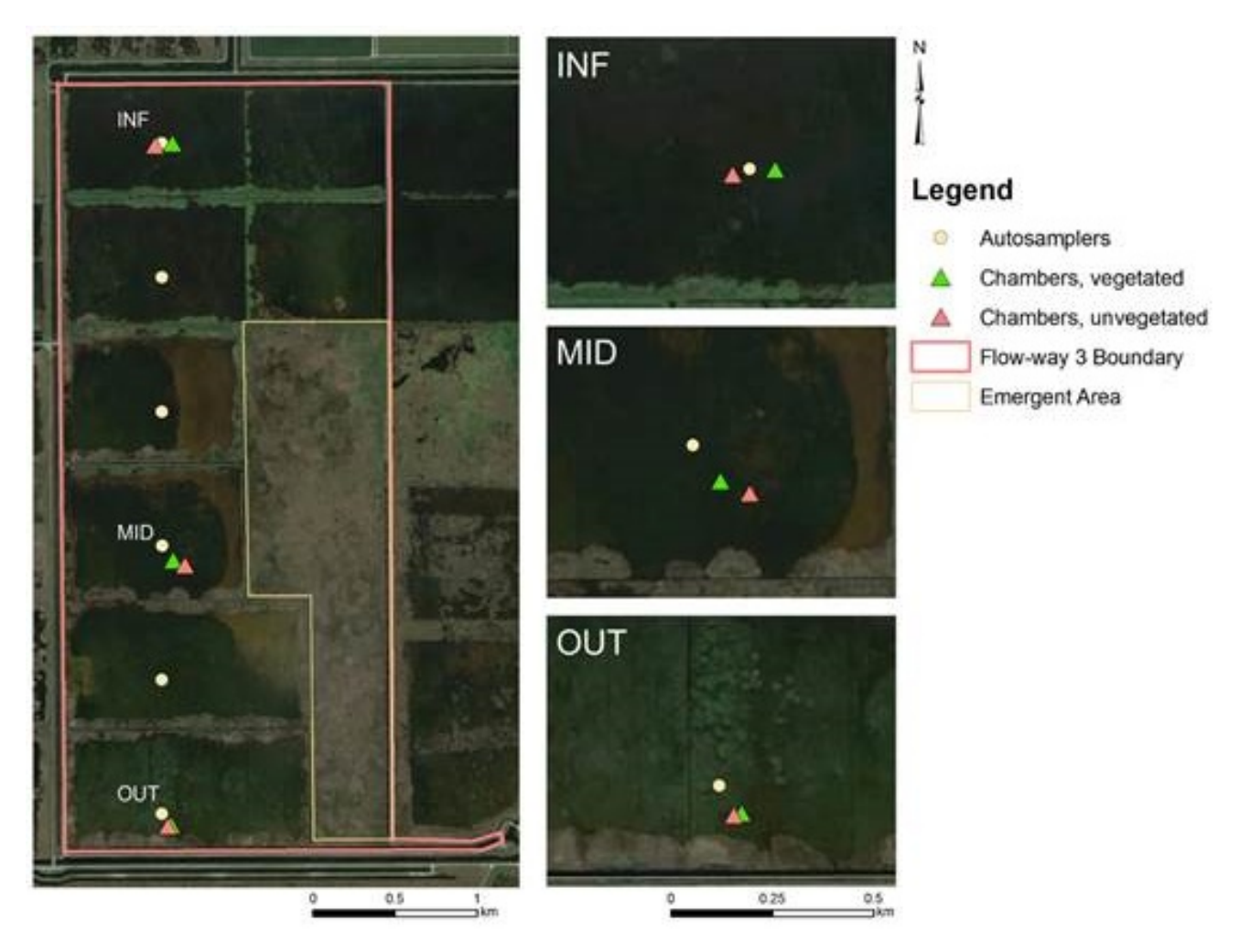


**Figure 13**. Location of the flux chambers installed in the vegetated and unvegetated patches of the inflow (INF), midflow (MID), and outflow (OUT) regions of STA-2 FW 3. The inset images correspond to the INF, MID, and OUT study sites identified in the left-hand panel.



**Figure 14.** Flux chambers installed in the outflow region of STA-2 FW 3, during a chamber closure/monitoring event (left) and an installed porewater equilibrator (right).

During Event 1 in March 2016, the top 0 to 4 centimeter (cm) of soil (corresponding to the top two porewater sample depths) adjacent to each peeper was sampled and analyzed for bulk density, carbon (C) and nutrient content, Ca, and 0.5-molar (M) sodium bicarbonate (NaHCO<sub>3</sub>)-extractable P ("plant-available" P). The P content was further characterized by a sequential extraction, in order: deionized water, 1.0-M ammonium chloride (NH<sub>4</sub>Cl), and 1.0-M hydrogen chloride (HCl).

# **Data Analysis**

#### Calculation of Vertical Diffusive Flux Rates

Net vertical diffusive fluxes of P (F, g/m<sup>2</sup>/yr) were estimated from Fick's First Law:

$$F = \frac{\varphi D_o}{\theta^2} \frac{\partial C}{\partial X} \tag{3}$$

The SRP concentration gradient,  $\partial C/\partial x$  (micrograms per liter per centimeter,  $\mu g/L/cm$ ), was calculated from vertical porewater profiles data using linear regression of measured SRP concentrations across the sediment-water interface (+4- to -4-cm depths). Average (sample size [n] = 18) soil porosity,  $\varphi$  (cubic centimeters per cubic centimeters, cm³/cm³), in the upper 0 to 4 cm in STA-2 FW 3 was ~0.9 (DBE unpublished data). The accompanying tortuosity factor,  $\theta^2$ , was estimated as 1.2 from available regression equations (Boudreau 1996). The diffusion coefficient,  $D_o$  (square centimeters per day, cm²/d), was set to 0.7 (Li and Gregory 1974). These methods and parameter values are consistent with those used in past studies in the STAs (Fisher and Reddy 2001, Newman and Pietro 2001, Dierberg et al. 2012).

### Model Application and Calibration to Incubation Time Series

**Equation 1** can be solved in closed-form for a formulation that can be directly calibrated to available time series data:

$$\frac{C - C_E}{C_i - C_E} = \exp(-k_0 t) \tag{4}$$

The initial concentration, Ci, for each 14-day time series prediction was the measured P concentration at t = 0 in the mesocosms. The batch volumetric rate constant,  $k_0$ , should be differentiated from long-term, mass balance-based rate constants identified in the STAs by Chen et al. (2015), which assume  $C^* = 0$ . The model was separately calibrated to each event response (n = 3) at each site (n = 3). Each of these calibrations had two calibration parameters:  $k_0$  and  $C_E$ . The model was also calibrated jointly by combining mesocosm data from all events at each site. This calibration had four calibration parameters: one joint  $k_0$  value and three site-specific  $C_E$  values (INF, MID, and OUT).

For each calibration, Bayesian Markov Chain Monte Carlo analysis was used with a formal probabilistic likelihood function to estimate model parameter and prediction uncertainty distributions. These methods are well established (Kuczera and Parent 1998) and application details followed those used in our past studies (Juston and DeBusk 2011, Juston et al. 2015). The error model was formulated to standardize error variance and its validity was confirmed with visual inspection (not shown). The approach of Bayesian inference coupled to the Markov Chain scheme resulted in a posterior set of model parameter distributions for each calibration. Probability density functions and 5 to 95% confidence intervals were calculated for calibrated model parameters directly from the Bayesian posterior. Similarly, internal load was calculated using **Equation 2** with all parameter sets in the posterior, again allowing for estimation of confidence intervals on internal load magnitudes.

**Table 6.** Summary of event conditions (average antecedent flow and load, range in parentheses). For comparison, the recent (2010–2016) average HLR and PLR in STA-2 FW 3 were 3.3 centimeter per day (cm/d) and 1.0 grams per square meter per year (g/m²/yr), respectively.

		14-Day Antece	dent Average	30-Day Antecedent	
Event	Chamber Closure & Water Sampling	HLR (cm/d)	PLR (g/m²/yr)	HLR (cm/d)	PLR (g/m²/yr)
1	March 7-21, 2016	10 (8–11)	1.7	8 (0–13)	2.1
2	July 25-August 8, 2016	3 (3–4)	0.6	2 (0-4)	0.2
3	November 7–21, 2016	8 (0–12)	2.0	9 (0–13)	3.2

#### RESULTS

#### **Diffusion from Soils**

Average diffusive P flux rates (F) across all three events were 0.1 grams per square meter per year (g/m²/yr) at the INF site, 0.01 g/m²/yr at MID, and 0.0 g/m²/yr at OUT, reflecting the strong monotonic longitudinal gradient in porewater SRP concentrations (**Figure 15**). Pairwise, the average diffusive flux at INF was significantly greater than at the other sites, but MID and OUT were not different from one another. The greatest diffusive flux rate calculated from the concentration gradient of an individual peeper was 0.19 g/m²/yr at INF. Soluble reactive P was not detected in any porewater samples at any depth from the OUT site (n = 12 individual peepers over three deployments), so consistently there was no motive force for diffusion from soil at that site (**Figure 15**).

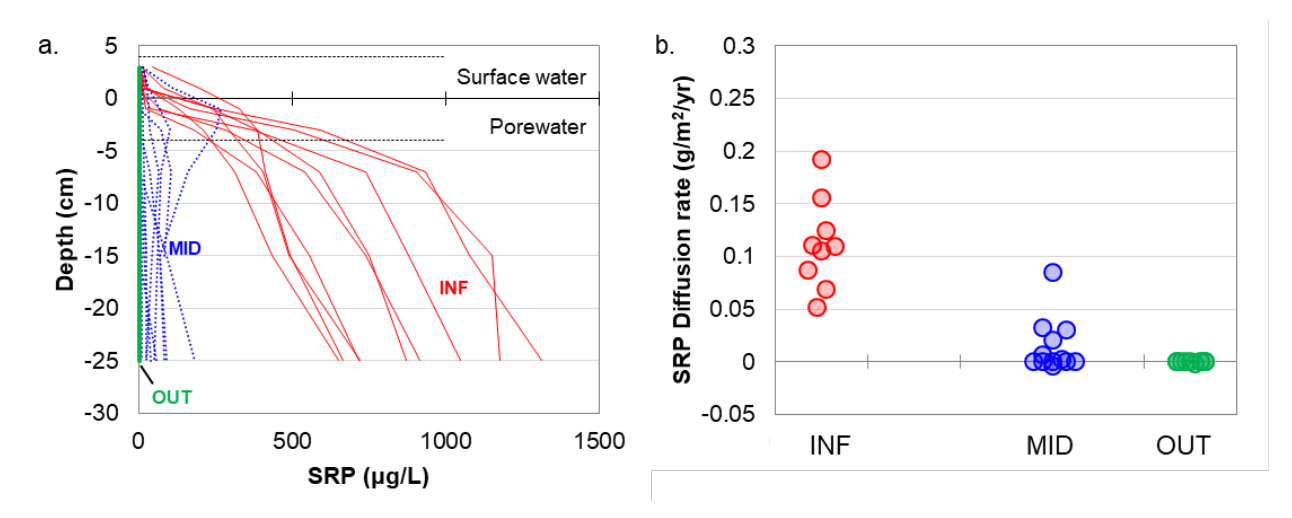


**Figure 15.** (a) Porewater SRP profiles for all individual peepers (n = 9 at INF; n = 12 at MID and OUT) and (b) Jitterplot of corresponding SRP diffusion rates calculated from the concentration gradient between +4 and -4 cm.

## MODEL CALIBRATION RESULTS

In general, the model (Eqn. 3) calibrated well to each event at each site (median  $r^2 = 0.5$ , range = 0.1 to 0.8, n = 6; **Table 7**). Calibrations were most successful where the response dynamics had the greatest ranges, such as INF and MID during Event 1 ( $r^2 \sim 0.8$ , simulated versus observed responses; **Table 7** and **Figure 16**). Calibration results of individual event responses at MID and OUT varied, largely due to the amplitude of the responses (**Table 7** and **Figure 16**). However, the model had very good ability to distinguish between-site response differences (INF-MID-OUT) during Events 1 and 3 when data were available from multiple sites ( $r^2 = 0.72-0.90$ ; 'Net' row in **Table 7**). This is a necessary condition for credibility of the calculated internal loading rates based on these calibrations (next section). An additional cross-event calibration was investigated based on all data pooled together at each site. As described in the *Methods* subsection, this exercise had four calibration parameters (one  $k_0$  and three  $C_E$  values for INF-MID-OUT). There was variability amongst the time series responses when plotted together, but also a distinct longitudinal pattern as well (**Figure 17**). The best-fit model calibration to the combined data tended to capture the average response at each site (**Figure 16**), and suitably represented between-site response differences ( $r^2 = 0.86$ ; Net Combined in **Table 7**).

**Table 7.** Model goodness-of-fit, expressed as the coefficient of determination ( $r^2$ ) of simulated versus observed time series responses (**Figure 16**). Blank cells indicate that there was no data available. The bottom 'net' row shows  $r^2$  values for combined results of INF-MID-OUT calibrations in the rows above.

r <sup>2</sup>		Event	Combined		
r-	#1	#2	#3	Combined	
INF	0.8	-	-	0.79	
MID	0.8	-	0.2	0.40	
OUT	0.5	0.1	0.6	0.28	
Net	0.90	-	0.72	0.86	

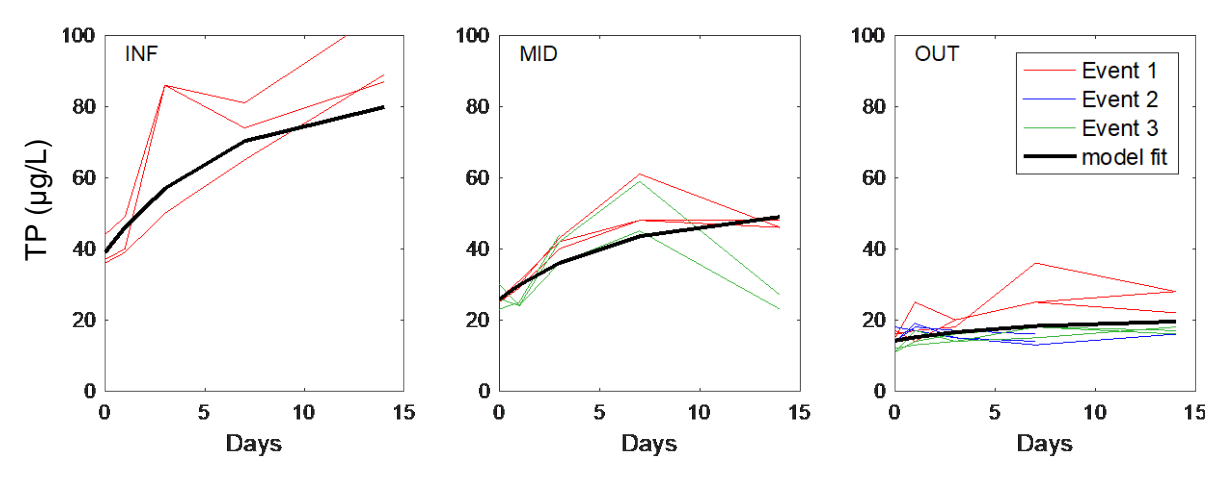


Figure 16. TP concentration responses from all events at each site.

## **ESTIMATION OF INTERNAL LOADING RATES**

Internal P loading rates (with confidence intervals) were calculated (**Equation 2**) from the Bayesian posterior distribution resulting from each model calibration (**Figure 17**). Due to the low data sample counts for model calibrations to individual events at each site, uncertainty intervals in iPLR estimates were in general high in these separate calibrations (e.g. average range of 5 to 95% confidence intervals > 2x best-fit values; (**Figure 17**). However, as more data were added to calibrations, such as in the combined and pooled data calibrations, resultant confidence intervals narrowed and there was more certainty in internal load estimates, as could be expected (**Figure 17**).

At INF, the average measured internal loading rate from the single event with available data was  $\sim 3 \text{ g/m}^2/\text{yr}$  (**Figure 17**). Calculated internal loading rates at MID ( $\sim 1$  to  $2 \text{ g/m}^2/\text{yr}$ ) tended to be less than at INF (**Figure 17**), but the upper confidence intervals at MID were within the lower ranges at INF. Internal loading rates calculated at OUT also tended to be less than at INF and MID (**Figure 17**). All confidence intervals for internal loading rates calculated at OUT overlapped one another (**Figure 17**). However, the upper confidence intervals for all iPLR calculations at OUT (n = 3) were less than the lower confidence intervals at INF. This indicates statistical significance between internal load responses at INF and OUT in STA-2 FW 3. The average measured internal loading rate at OUT was  $\sim 0.5 \text{ g/m}^2/\text{yr}$  (n = 3). In summary, there was no strong evidence of differences in internal load calculated for different measurement events, but a consistent gradient between sites (INF-OUT) was identified.

Internal loading rates (and the 5 to 95% confidence interval) calculated from the combined calibration (all events at all sites) were 2.7 g/m²/yr (1.7 to 4.4) at INF, 1.7 g/m²/yr at MID (1.0 to 2.7), and 0.7 g/m²/yr at OUT (0.4 to 1.1) (**Figure 18**). These values are very close to those identified above from the mean of individual events at each site. Confidence intervals from the pooled calibration were also narrow enough to assess that differences in internal load were significant between INF and OUT (**Figure 18**).

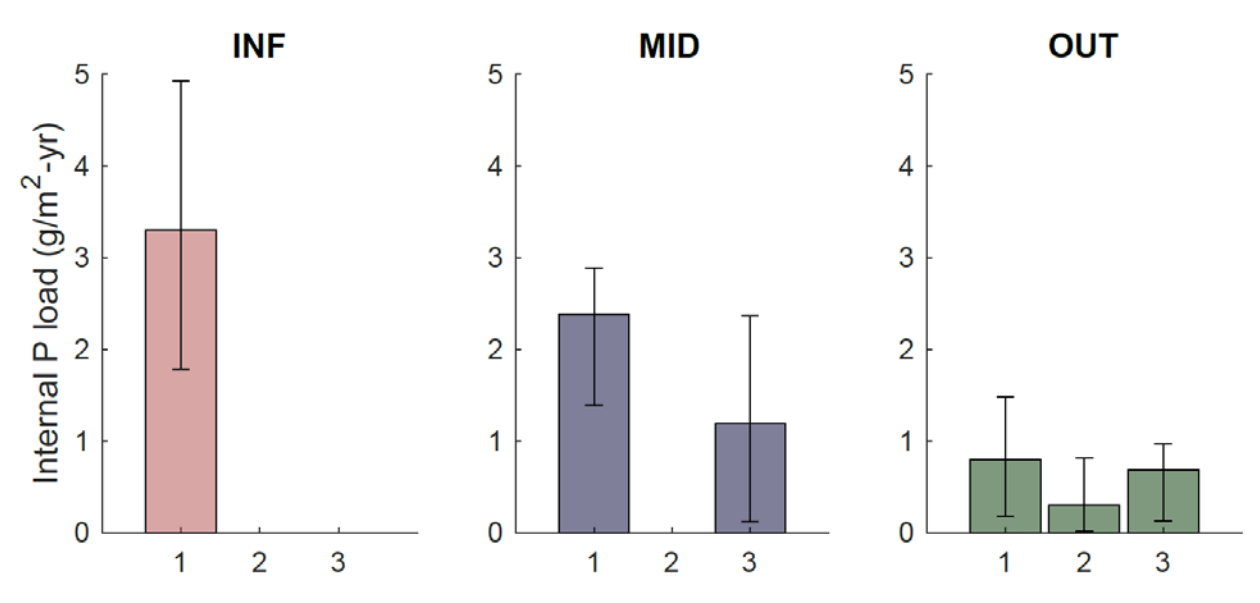


**Figure 17.** Net internal loading rates estimated from  $K_{V0}C_E$  model calibrations to mesocosm time series responses during each measurement event (**Table 6**). Error bars indicate the 5 to 95% confidence interval resulting from model calibration methods; significant differences occur between pairs of measurements if confidence intervals do not overlap.

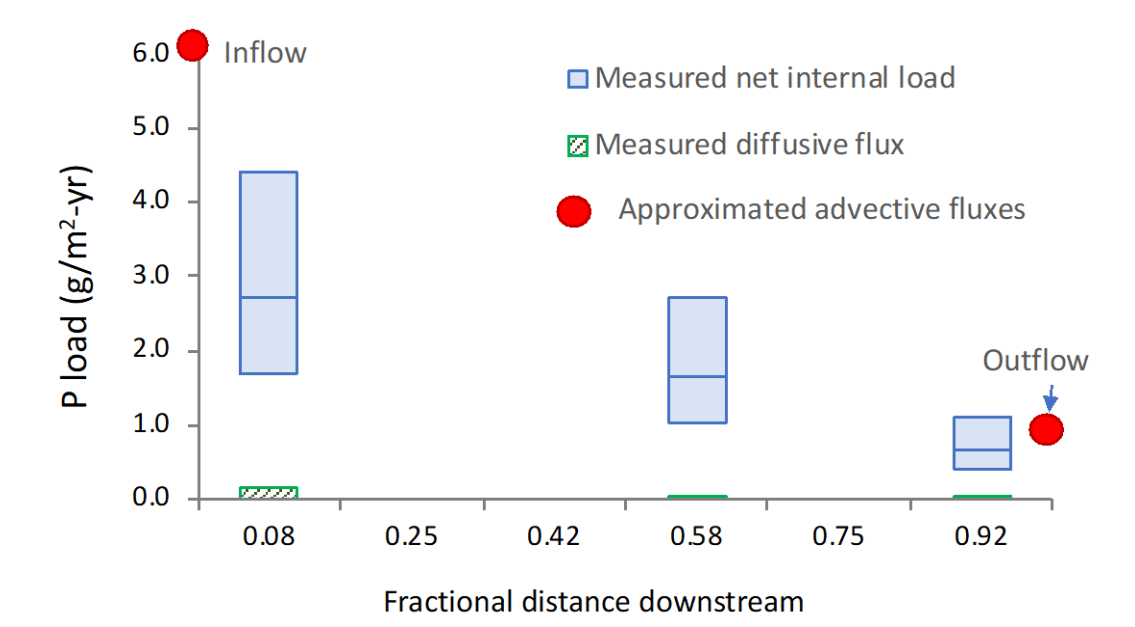


**Figure 18.** Measured internal loading rates as a function of longitudinal position. Approximated areal inflow-outflow advective fluxes are shown for context. Advective fluxes were approximated using measured long-term average mass transport rates at inflow and outflow structures (grams per year [g/yr]), divided by 1/6 of total cell area, roughly corresponding to physical compartmentalization (**Figure 13**).

#### DISCUSSION

#### **KC Model Framework**

The batch form of the conventional KC\* model was adapted to describe the P responses of the flux chambers, and termed KC<sub>E</sub> since the chamber equilibrium concentrations may differ along the FW longitudinal gradient. A process-based model like KC<sub>E</sub> provides a well-developed conceptual framework for understanding and evaluating chamber responses. This application provides a significant advancement from Jerauld et al. (2018) in the interpretation and understanding of internal loading in STA-2 FW 3.

## **Comparison of P Load Sources**

To provide context for the magnitude of the measured internal loads, above, the advected P loads at the inflow and outflow regions of STA-2 FW 3 were approximated. The long-term average P mass transport rates at inflow and outflow structures (g/yr) were each divided by 1/6 the area of the FW, corresponding to the size of the inlet and outlet compartments naturally defined by emergent vegetation strips (**Figure 13**). The magnitude of the measured internal load was comparable to that of the advected flux of P (**Figure 18**). The best-fit internal P load measured at INF ( $2.7 \text{ g/m}^2/\text{yr}$ ) was about half of the average advected P load delivered to the inflow region ( $6 \text{ g/m}^2/\text{yr}$ ; **Figure 18**). In the outflow region, the measured internal load was nearly equal to the advected P load in the discharge waters ( $0.9 \text{ g/m}^2/\text{yr}$ ). In other words, for a given parcel of marsh in the outflow region of STA-2 FW 3, the flux of P to the water column from internal sources was almost equivalent to the flux of P transported into that parcel by the flow of water.

The internal loads quantified in this study represent the "whole-ecosystem" flux and include loading from most of the ecosystem components that are potential P sources to the water such as diffusion from soil porewater, resuspension of soil particles, senescence of plant tissues and excretion by small biota. Strikingly, diffusive fluxes from the soil porewater were about two orders of magnitude less than concurrently measured iPLRs (**Figure 18**), contributing 4%, 0.7%, and 0.0% to the net flux at INF, MID, and OUT, respectively. Thus, diffusion from soil porewater was essentially negligible compared to other (unspecified) internal load vectors. The specific sources of internal P loading are currently under investigation, by this study and other associated projects (see, for example, the fauna study described in **Appendix 5C-4** of this volume).

# **Factors Affecting Internal Loading Rates**

Soils are hypothesized as the source of P to porewaters that is then available for diffusion into surface water (Bostic et al. 2010, Juston et al. 2015, Pant and Reddy 2003), and thus the diffusive flux may be expected to be related to P stored in the soil. Some interesting relative spatial patterns are evident in the soils data (**Table 8**). Among soil P fractions, only two relatively labile P pools, NaHCO<sub>3</sub>-extractable P and NH<sub>4</sub>Cl-extractable P, presented a monotonic (decreasing) longitudinal profile along the FW (**Table 8**), corresponding to the same pattern in diffusion (**Figure 15**) and total internal load rates (**Figure 18**). Conversely, soil TP was lower at MID (424 mg/kg) than at OUT (545 mg/kg) (**Table 8**). This suggests that diffusion and possibly total internal load are more closely related to the labile P than the TP in the soil. Further work beyond the scope of this study would be required to quantitatively link soil concentrations of these loosely-bound P pools to the diffusion rate, and to identify how these P fractions accumulate in the soil.

It is conceivable that the short-term antecedent external P load could affect internal loading rates, if recently sequestered P is available for release (e.g. Kröger et al. 2007). Internal loading was measured following events of different antecedent flow and P loading conditions (**Table 6**), although data availability was concentrated in Events 1 and 3, which had similar antecedent conditions. There were no significant between-event differences in the internal loading rates at any site (**Figure 17**), therefore there is no evidence

yet to support the hypothesis that the internal load varies dynamically in response to short-term loading events.

**Table 8.** Average (and range) of properties of the top 0 to 4cm of sediment at the STA-2 FW 3 internal load study sites from n = 4 soil cores from each site (n = 3 at INF) collected during Event 1 in March 2016. Small sample size precluded statistical analysis.

Parameter	Unit	INF	MID	OUT
NaHCO₃-extractable P	mg/kg	184 (163-195)	39 (26-58)	2 (1-4)
Water-extractable P	mg/kg	1.9 (1.2-3)	0.4 (0.3-0.4)	0.2 (0.2-0.3)
NH <sub>4</sub> Cl-extractable P	mg/kg	31.2 (28-34.3)	5.1 (2.8-7.1)	1.1 (0.6-1.8)
HCI-extractable P	mg/kg	556 (503-646)	103 (76-129)	114 (94-134)
TP	mg/kg	1131 (984-1340)	424 (326-502)	545 (415-701)
TOC	%	11 (10-13)	8 (6-9)	17 (12-24)
TN	%	0.9 (0.8-1.1)	0.8 (0.7-1)	1.6 (1.4-1.9)
Calcium	%	25 (24-27)	29 (28-30)	20 (15-24)
BD	g/cm <sup>3</sup>	0.16 (0.13-0.18)	0.1 (0.08-0.13)	0.11 (0.07-0.15)

#### Limitations

There are several important caveats to summarize. Our estimate of annual iPLR is based on three discrete measurements over one year and there may be additional intra-annual or long-term variability in iPLR that has not yet been captured. Two of the three measurement events had data either removed or not collected due to some difficulties in maintaining experimental conditions. Finally, the measurement technique necessitated no-flow conditions. Obviously, wetland discharges are produced during flow events. Therefore, additional study and likely time series modeling are necessary to establish how the measured iPLR in this study contributes to discharge TP magnitudes and limits.

#### **SUMMARY**

A novel technique was employed to measure the internal loading rate in STA-2 FW 3. In situ mesocosms allowed the observation of equilibration between water, soil, and biota, isolated from the effects of longitudinal transport (flow). The mesocosm responses were represented by a simple model that quantifiably partitioned the observed responses into removal and return (internal load) rates. The measured internal loads had a distinct longitudinal gradient, were comparable to the external loading rate, and were one to two orders of magnitude greater than the load from vertical soil porewater diffusion alone. Internal loading from processes other than diffusion is likely to be providing an important, possibly even dominant, influence on STA outflow concentrations.

The physical, ecological or biogeochemical mechanisms generating the observed internal loads should continue to be explored. Further evaluation is needed to determine the influence of factors such as soil chemistry or antecedent external loading events. Additional flux measurements in other FWs, as planned for this project, should help provide further insights. Companion efforts toward identifying additional sources and mechanisms of P release are underway, as documented in other sections of this report.

# MICROBIAL PATTERNS AND RESPONSE TO FLOW

Patrick Inglett<sup>3</sup>, Kathleen Pietro, Kanika Inglett<sup>3</sup>, and Jill King

## INTRODUCTION

In wetlands like the STAs, nutrients are mostly in organic forms, therefore, microbial organisms like algae, fungi, and bacteria can play a major role in nutrient cycling through the production of exoenzymes. Exoenzymes are proteins released into the environment to convert organic compounds to available C, P, and N. In well performing STAs, particularly at the midflow and outflow regions within the FWs, TP exists primarily in dissolved organic or particulate forms (**Figure 10**). In these areas, the microbial components and enzymes may be a driving mechanism in reducing water column TP concentrations via their degradation of DOP compounds into more available P forms for uptake.

Potential enzyme activity in benthic floc and litter, epiphytic periphyton, and surface water of STA FWs can provide understanding of nutrient cycling and substrate availability along the inflow to outflow nutrient gradient. The variable hydrology and nutrient loadings the STAs receive from basin stormwater runoff may alter microbial cycling of nutrients, thus affecting the outflow TP concentrations. A limited evaluation of enzyme activity in STAs is ongoing, and the objective of this research study is two-fold: (1) to quantify the enzyme activity along the nutrient gradient from the inflow to outflow regions of selected FWs and within the major vegetation communities and (2) to determine the effect of hydrologic flow on enzyme activity.

## **METHODS**

The enzyme activities in the floc and periphyton were measured under a range of inflow hydraulic conditions in STA-2. Sampling was conducted in FW 1 in 2017 and FW 3 in 2016. In both FWs, locations were established at inflow, midflow, and outflow stations along the FW transect gradient (**Figure 19**), where surface water chemistry, soil nutrient conditions, water depth, and light penetration were also being measured. The two FWs have distinctively different dominant vegetation; EAV dominates FW 1 while FW 3 consists mostly of SAV (**Figure 20**). Within each FW, there also were differences in the vegetation species among the sampling locations. In FW 1, at inflow station A3 cattail (*Typha domingensis* or *Typha latifolia*) and floating aquatic vegetation (*Pistia stratiotes* and *Eichhornia crassipes*) are found and the at midflow (F3) and outflow (Out) stations dense stands of *Typha*, spp. with some *Cladium* spp. are found. At all locations in FW 1, the water column contains abundant quantities of vegetation litter, mostly decomposing plant litter. STA-2 FW 3 contained a diversity of SAV that was different in each of the study sites. At the inflow (C20), there was open water with some *Chara* spp., the midflow location (C128) was dominated by extremely dense stands of *Chara*, and the outflow location was dominated by *Najas guadalupensis* and *Potamogeton* spp.

-

<sup>&</sup>lt;sup>3</sup> University of Florida, Gainsville, Florida.

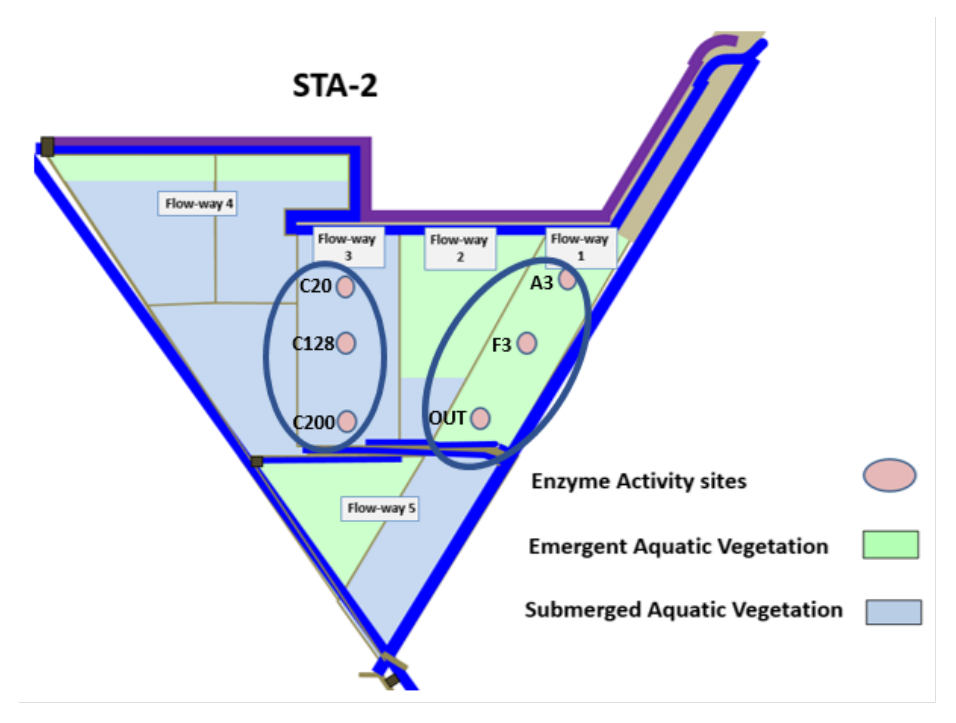


**Figure 19.** Sampling locations in STA-2 FW 1 and FW 3 for measurement of potential enzyme activity in the periphyton and floc.



Figure 20. Dominant vegetation communities in STA-2 FW 1 (left) and FW 3 (right).

As part of the P Flux Study design, a range of hydraulic conditions were imposed on the FWs and the enzyme assays were conducted biweekly on periphyton (7-day growth) samples after allowing for a 7- to 14-day accumulation period to account for hydraulic residence time. In STA-2 FW 1, there were 4 sampling events to measure periphyton enzyme activity during flow and 3 sampling events during no flow. In STA-2 FW 3, there were 7 sampling events during flow and 4 sampling events during no flow. The floc was collected from cores collected during each of the flow conditions (**Figure 21**). The periphyton used for enzyme assays was obtained from biomass accumulated on acrylic dowels deployed for 7-day periods. The floc samples were collected from triplicate cores and assayed as replicates, stored overnight and sectioned to collect the upper 2-cm of surficial floc material. A complete description of the methodology, event conditions, and full results for the floc, can be found in University of Florida's project reports (2016, 2017).

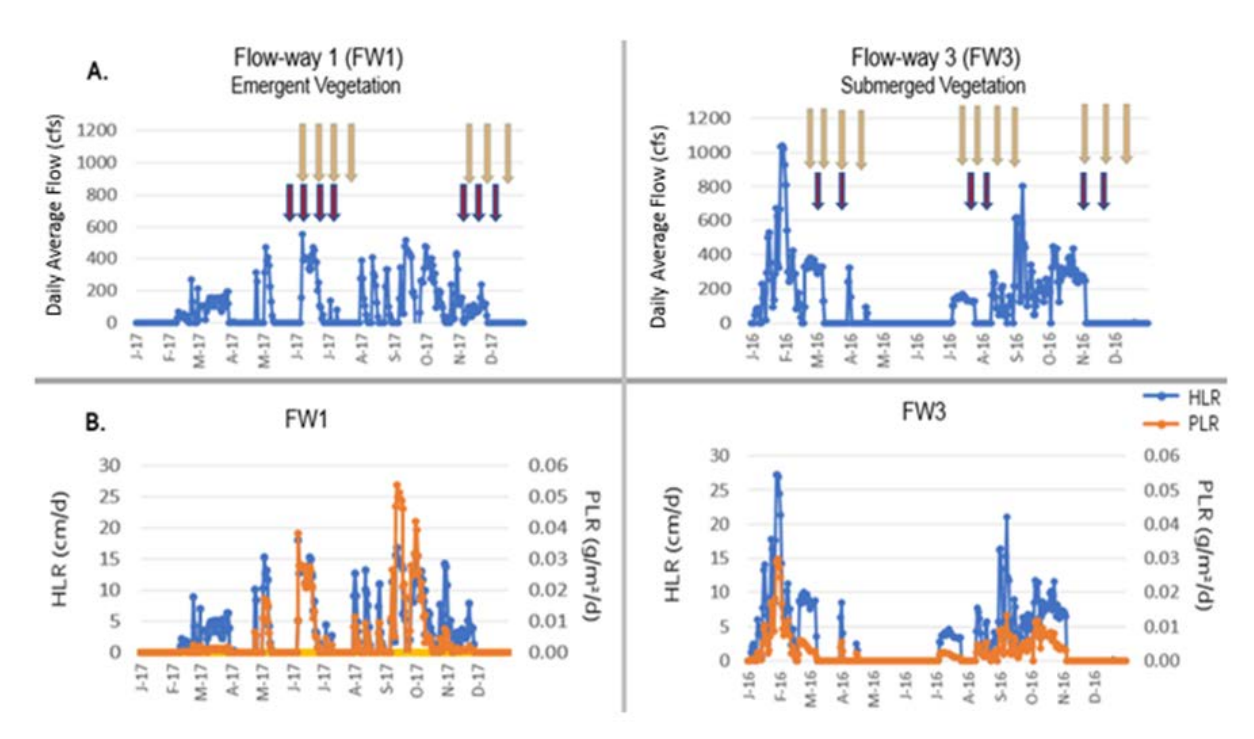


**Figure 21.** Hydrologic flow conditions (top figures) and HLR and PLR loading rates (bottom figures) into STA-2 FWs 1 and 3 during this study. The tan colored arrows designate the sampling dates for measuring enzyme activity in the periphyton and the dark red arrows designate the sampling dates for floc.

Because the microbial communities act upon a range of essential nutrients, the enzyme activity for a suite of enzymes involved in P, N, and C cycling were assayed. Enzyme activities related to P ( $E_P$ , alkaline phosphatase [AP]), and bis-phosphatase [BisP]), N ( $E_N$ , leucine aminopeptidase [LAP] and N-acetyl-glucosaminidase [NAG] also known as chitinase), and C ( $E_C$ ,  $\beta$ -glucosidase [BGA]) were analyzed in floc and periphyton samples collected during the flow events. Enzyme activity for NAG was only measured in the floc samples. The enzyme activity was measured using fluorometric substrates and the assays were conducted over a 45-minute period according to the approaches of Inglett and Inglett (2013) and Liao et al. (2014). Enzyme activity was calculated as potential enzyme activity per hour and expressed by dry weight of either periphyton biomass or floc material.

The enzyme activity is presented by flow or no flow conditions. The main effects of flow condition and transect location (inflow, midflow, and outflow) and their interaction on floc enzyme activities, microbial nutrients, and ratio values were tested using a multifactor analysis of variance (ANOVA). To account for seasonal type effects (e.g. temperature or inflow amount or composition), flow event (1 and 2 in FW 1 and 1 to 3 in FW 3) was also included as a blocking factor. Prior to statistical analyses, enzyme activities were log transformed where appropriate. All analyses were performed using JMP® Software 13.1 (SAS Institute Inc. 2016).

## **RESULTS**

#### Periphyton

Enzyme activity in the periphyton showed different responses along the nutrient gradient and in response to flow conditions (**Figure 22**). The combined activity of both P-acquiring enzymes (E<sub>P</sub>; AP + BIS-P) in both FWs was lowest at the inflows and highest at the outflows. Between the FWs, there was a

notable difference in  $E_P$  activity at the midflow locations. In FW 1, the average  $E_P$  activity at the midflow increased approximately 10 micromoles per gram dry weight per hour ( $\mu$ mol/g dw/h) compared to the inflow. Activity at the midflow site in FW 3 also increased but the increase was substantially greater compared to that observed in FW 1 (approximately 100  $\mu$ mol/g dw/h higher at the midflow compared to the inflow). In both FWs,  $E_P$  was greatest at the outflow sites. Among the different enzyme activity, generally AP activity was 30 to 50% greater than Bis-P activity at all locations except for the outflow in FW 3 where average Bis-P activity was higher compared to AP activity during flow.

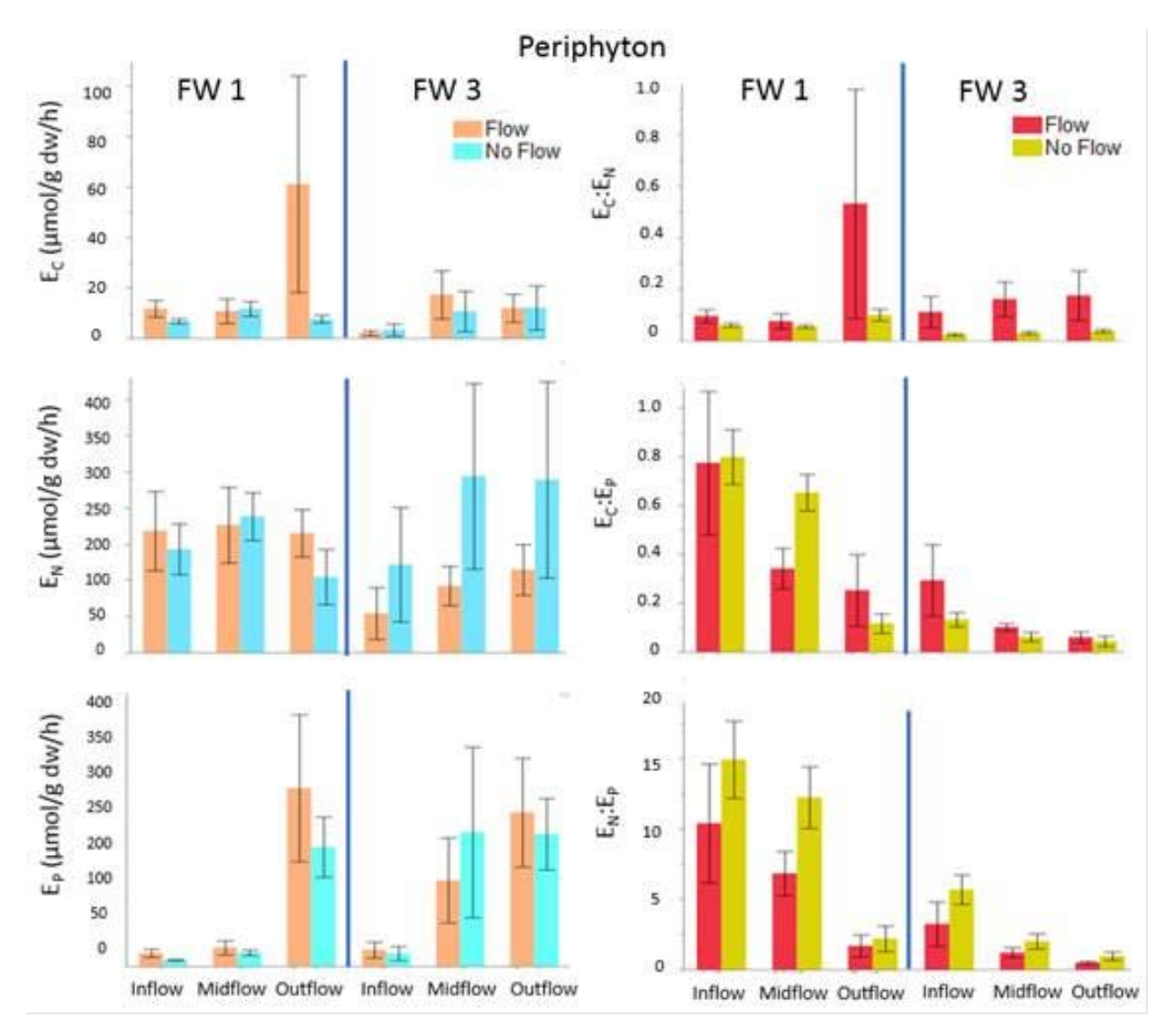


**Figure 22.** Left panel: Potential enzymatic activity measured in the periphyton for the C-acquiring enzyme ( $E_C$ ), N-acquiring enzyme ( $E_N$ ), and the combined sum of the P-acquiring enzymes (AP and phosphodiesterase [ $E_P$ )) in STA-2 FW 1 and FW 3. Right panel: ratios of the periphyton enzyme activity. Bars are means  $\pm$  standard error.

Between the FWs, there were differing responses in  $E_P$  activity with flow particularly at the midflow locations. In both FWs, the  $E_P$  activities at the inflow and outflow sites were higher during flow. In FW 1,  $E_P$  at the inflow averaged 9  $\mu$ mol/g dw/h during no flow and 19  $\mu$ mol/g dw/h during flow while in FW 3,  $E_P$  averaged 19  $\mu$ mol/g dw/h during no flow and increased to 24  $\mu$ mol/g dw/h during flow.  $E_P$  also increased

during flow at the outflow sites, averaging 177 and 197  $\mu$ mol/g dw/h during no flow and increasing to 265 and 229  $\mu$ mol/g dw/h during flow in FW 1 and FW 3, respectively. At the midflow sites, there was an opposite response between the FWs compared to flow conditions. In FW 1,  $E_P$  activity at the midflow was much lower compared to FW 3. As observed at the inflow and outflow sites,  $E_P$  activity in FW 1 increased, from 20  $\mu$ mol/g dw/h during no flow and increased to 27  $\mu$ mol/g dw/h during flow. But in FW 3, the  $E_P$  activity at the midflow decreased during flow, averaging 199  $\mu$ mol/g dw/h during no flow and 128  $\mu$ mol/g dw/h during flow.

The activity for the C-acquiring enzyme ( $E_C$ ; BGA) in the periphyton showed a mixed response of activity along the gradient to flow and no flow conditions (**Figure 22**). At some of the sites (FW 1 inflow and outflow, and FW 3 midflow),  $E_C$  increased during flow, while at the remaining locations (FW 1 midflow, and FW 3 inflow and outflow), average activity was essentially the same between the flow and no flow. Except for a single high value reported for FW 1 outflow location (230  $\mu$ mol/g dw/h), the  $E_C$  activity was similar between the FWs with maximum  $E_C$  activity ranging from 6 to 50  $\mu$ mol/g dw/h with averages among the two FWs ranging from 2 to 19  $\mu$ mol/g dw/h.

The response of the N-acquiring enzyme (LAP,  $E_N$ ) in the periphyton also was complicated and differed between the two FWs and in response to flow conditions (**Figure 22**). In FW 1, activity along the gradient was similar during flow conditions with averages ranging from 166  $\mu$ mol/g dw/h at the outflow to 177  $\mu$ mol/g dw/h at the midflow site. During no flow, activity was less at the inflow and outflow sites (143 and 105  $\mu$ mol/g dw/h, respectively, but increased at the midflow site (189  $\mu$ mol/g dw/h). In FW 3, a contrasting response was observed where  $E_N$  increased along the nutrient gradient and activity was greatest during no flow compared to flow conditions. The average  $E_N$  in FW 3 ranged from 122 to 239  $\mu$ mol/g dw/h during flow and increased to 436 to 772  $\mu$ mol/g dw/h during no flow conditions.

#### **Benthic Floc**

Differences between the floc microbial communities of FW 1 and FW 3 were observed in overall microbial biomass abundance (higher microbial biomass carbon [MBC], microbial biomass nitrogen [MBN], and microbial biomass phosphorus [P]) in FW 1 samples (**Figure 23**). Stoichiometric nutrients ratios (MBC:MBN, MBC:MBP, MBN:MBP) were similar between the two FWs, but there was a somewhat higher MBC:MBN and on average a lower MBN:MBP in the floc of FW 1 than in FW 3. In a similar fashion, overall enzyme activity was higher in the floc of FW 1 than FW 3 (**Figure 24**).

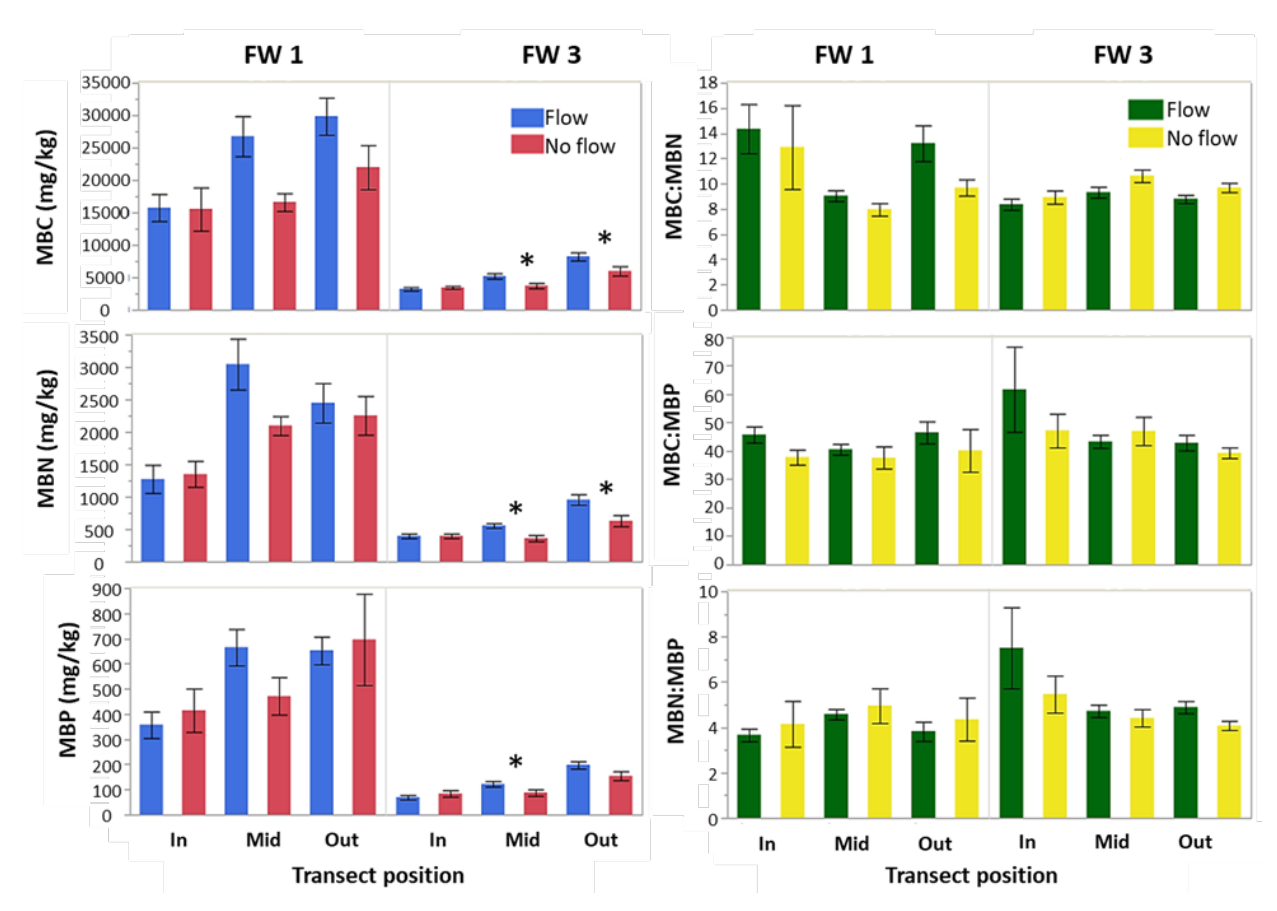


**Figure 23.** Patterns of MBC, MBN, MBP, and their ratios (MBC:MBN, MBC:MBP, and MBN:MBP) in floc samples collected from study sites during flow and no flow conditions in STA-2 FW 1 and FW 3. Bars are means ± standard error. Significant differences (p < 0.05) between flow and no flow effects at a single transect location are denoted by an asterisk (\*).

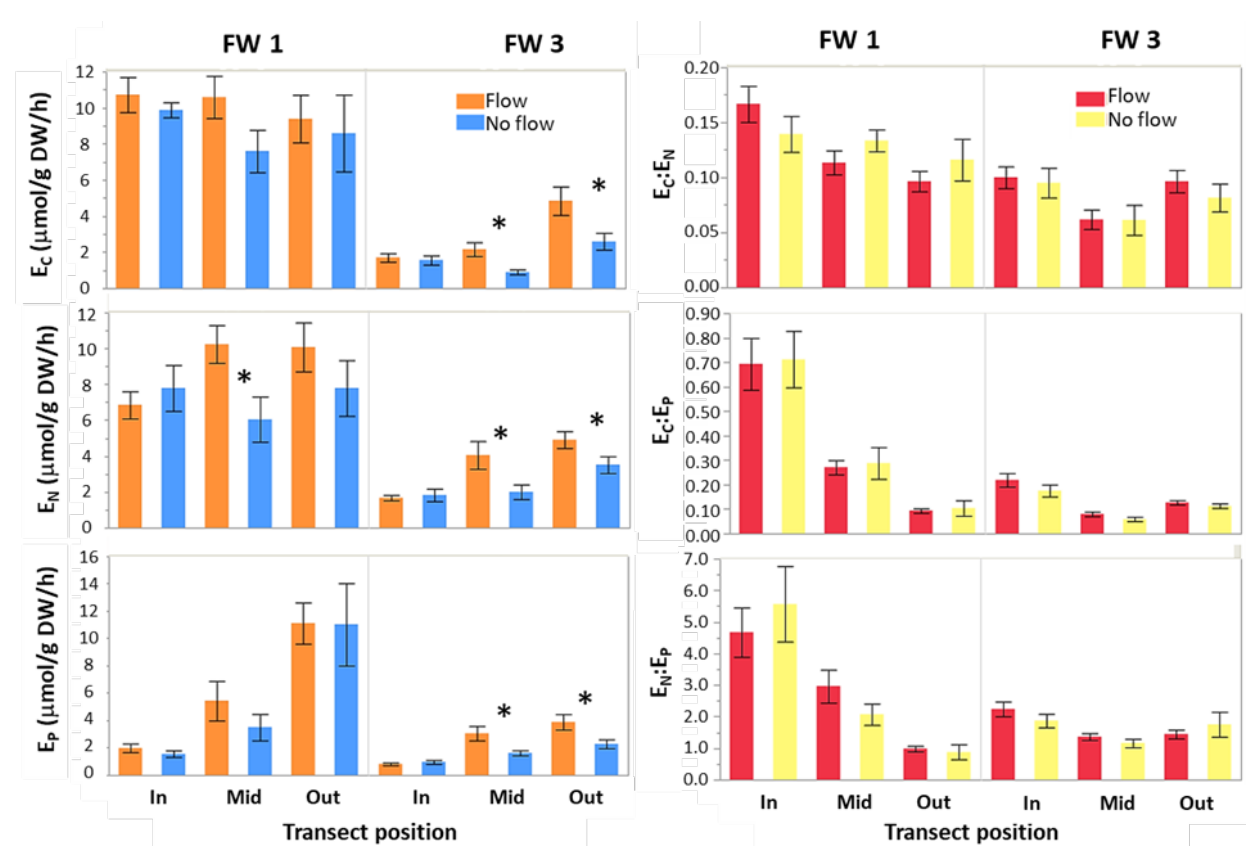


**Figure 24.** Patterns of microbial enzyme activities ( $E_C$ ,  $E_N$ , and  $E_P$ ) and ratios ( $E_C$ :  $E_N$ ,  $E_C$ :  $E_P$ , and  $E_N$ :  $E_P$ ) in benthic floc samples collected from study sites during flow and no flow conditions in STA-2 FWs 1 and 3 at the inflow (IN), midflow (MID), and outflow (OUT) locations. Bars are means  $\pm$  standard error. Significant differences (p < 0.05) between flow and no flow effects at a single transect location are denoted by an asterisk (\*).

In general, the presence of flow increased floc microbial biomass especially at the midflow and outflow sites (**Figure 23**), but the effect was only significant in FW 3 (though MBC exhibited a p value < 0.1 in FW 1) (**Table 9**). Both MBC and MBN significantly increased under flowing conditions in FW 3. MBC:MBN was likewise significantly affected with flow in both FWs (**Figure 23**), but with contrasting changes, where MBC:MBN increased and decreased with flowing conditions in FW 1 and FW 3, respectively.

Floc enzyme activities also increased significantly due to flow (**Table 10**) where NAG enzyme was most affected in FW 1, while in FW 3, all enzyme systems were significantly affected by flow. Similar to microbial biomass, the greatest changes in enzymes with flow occurred at the midflow and outflow sites. In FW 1, hydrologic flow significantly increased  $E_N$  (LAP + NAG) by 68% at the midflow and by 30% at the outflow sites (**Figure 24**).

In FW 3, phosphorus enzymes ( $E_P$ , phosphatase + phosphodiesterase activity) increased 86 and 70% with flow at the midflow and outflow sites, respectively. At the same sites,  $E_C$  (BGA) was elevated 141 and 86%, respectively while  $E_N$  was observed to increase 100 and 39%, respectively, with flowing conditions. Ratios of enzymes normalize effects of changes in total microbial biomass. Using this approach, the only observed effect of flow on floc enzyme stoichiometry was a slight (but significant) overall increase in  $E_C$ : $E_P$  in FW 3 (**Table 10** and **Figure 24**).

**Table 9**. Fit least squares model results for floc MBC, MBN, and MBP and their ratios during flow/no flow conditions in STA-2 FW 1 and FW 3. Values are bolded if p < 0.05.

Test FW	Source of Variation	Response Variable (Probability > F)						
		МВС	MBN	MBP	MBC:MBN	MBC:MBP	MBN:MBP	
	Flow Event	0.369	0.794	0.039	0.120	0.031	0.004	
CTA O FIN 4	Location	0.007	<.001	0.006	0.017	0.753	0.102	
STA-2 FW 1	Flow	0.068	0.735	0.400	0.048	0.087	0.532	
	Location * Flow	0.497	0.455	0.391	0.854	0.832	0.972	
STA-2 FW 3	Flow Event	0.287	0.420	0.150	0.075	0.049	0.373	
	Location	<.0001	<.0001	<.0001	0.014	0.392	0.096	
	Flow	0.006	0.001	0.125	0.015	0.568	0.113	
	Location * Flow	0.037	0.043	0.051	0.794	0.665	0.844	

**Table 10**. Fit least squares model results for floc microbial enzyme parameters during flow/no flow conditions in STA-2 FW 1 and FW 3. Values are bolded if p < 0.05.

Test	Source of	Response Varial						able (Prob > F)				
FW	Variation	AP	Bis-P	AP+Bis-P (E <sub>P</sub> )	BGA (E <sub>c</sub> )	LAP	NAG	LAP+NAG (E <sub>N</sub> )	E <sub>C</sub> :E <sub>N</sub>	E <sub>C</sub> :E <sub>P</sub>	E <sub>N</sub> :E <sub>P</sub>	
	Flow Event	< 0.0001	0.005	< 0.0001	0.001	0.026	0.553	0.074	0.097	0.030	0.002	
STA-2	Location	< 0.0001	< 0.0001	< 0.0001	0.248	0.226	0.006	0.726	0.012	< 0.0001	< 0.0001	
FW 1	Flow	0.241	0.282	0.130	0.134	0.053	0.003	0.073	0.530	0.701	0.970	
	Location x Flow	0.659	0.598	0.598	0.518	0.169	0.744	0.095	0.221	0.839	0.317	
	Flow Event	0.062	0.003	0.029	0.001	0.001	0.153	0.002	< 0.0001	< 0.0001	0.174	
STA-2	Location	< 0.0001	< 0.0001	< 0.0001	< 0.0001	< 0.0001	0.002	< 0.0001	< 0.0001	< 0.0001	< 0.001	
FW 3	Flow	0.076	0.004	0.016	< 0.001	0.002	< 0.0001	0.001	0.470	0.045	0.292	
	Location x Flow	0.023	0.159	0.063	0.064	0.070	0.133	0.070	0.799	0.540	0.313	

## DISCUSSION

## Trends along the FW Gradient

Within the STAs, patterns of microbial nutrient content and enzymes reveal dynamics of microbial abundance, activity, and potential nutrient limitation. The magnitude in enzyme response was greatest in the periphyton, which is 100 times higher for the C- and P-acquiring enzymes and 33 times higher for the N-acquiring enzymes compared to floc. The elevated activity measured in the periphyton is related to the biomass that accumulated over the 7-day deployment period. This newly accumulated biomass is extremely active and may be reflective of active production of substrates for metabolizing organisms with smaller proportions of dead or inorganic material than the floc components.

For periphyton, FW 3 consistently showed an increasing trend in enzymatic activities from inflow to outflow. The trend was also observed for P enzymes in FW 1, but there was little consistency in either  $E_C$  or  $E_N$  along the transect (**Figure 22**). Similar to the results for periphyton, there were also strong gradients

in all floc enzyme activities along the inflow to outflow gradient in FW 3 but strong gradients in FW 1 were observed only for  $E_p$  (**Figure 24**).

Enzyme ratios, which normalize for microbial biomass, are often used as a good indication of relative limitation of microbial biomass (**Figures 22** and **24**). For  $E_C:E_P$  and  $E_N:E_P$ , the results for floc and periphyton are similar with general declining trends from inflow and outflow. The declining trends in both  $E_C:E_P$  and  $E_N:E_P$  demonstrate a shift from more C and N cycling and demand near the inflows to a preponderance of P limitation (i.e., high phosphatase activity) at the outflows.

Despite the similarity in trends for individual enzyme activities along the FW, there were differences between the periphyton and benthic floc in the enzyme ratios. For example, in the periphyton, there is a general increase from inflow to outflow for  $E_C$ : $E_N$ , while in floc there is a general decrease from inflow to outflow in this ratio. This difference between the two components may be related to the differences in C quality where periphytic communities have abundant simple C compounds, sugars, and polysaccharides while floc materials include more recalcitrant C forms from structural plant components (e.g. cellulose).

The differences between the two vegetation types in the STAs are evident in floc enzyme activities. For example, there is a generally higher abundance of microbes and enzyme expression in the floc of FW 1 than in FW 3 (**Figures 23** and **24**). Much of this difference is likely due to the vegetation types of the two FWs, where FW 1 has a higher abundance of available carbon in structural compounds of decomposing emergent macrophyte litter, and FW 3 is likely to have higher abundance of more mineral C compounds being based more on SAV and algae, which are low in structural C components.

Differences in C quantity and quality between the two FWs may also be seen in the ratios of floc  $E_C:E_N$  and  $E_C:E_P$  (**Figure 24**) where FW 1 floc microbes express higher overall amounts of C-based enzymes than those for nutrients ( $E_N$  and  $E_P$ ). Also, the higher  $E_N:E_P$  ratio observed at the inflow and midflow of FW 1 indicates that N is potentially more limiting in these areas compared to FW 3. In contrast, the very high  $E_P$  and low  $E_N:E_P$  at the FW 1 outflow, suggests a high degree of P limitation, even when compared to FW 3.

## **Effects of Hydrologic Flow**

The periphyton and floc enzyme activities in the STA respond differently to flow conditions. Periphyton patterns and results were more variable than those for floc. For example, the only major effect of flow observed for periphyton in this study was an increase in  $E_P$  at the outflow locations in both FWs and a general suppression of  $E_N$  and increased  $E_C$ :  $E_N$  under flowing conditions in FW 3 (**Figure 22**).

In contrast, benthic floc microbial communities responded more consistently to flow. Overall, the effect was an increase in microbial abundance and stimulated enzyme activity. In FW 1, the effect was inconsistent and only statistically significant for N-related variables such as MBC:MBN and activity of NAG, though it is important to note that statistical probability (p) values for other variables (MBC, MBC:MBP, and LAP) were also low and very close to established significance level (**Table 9**). In FW 3, the effect of flow was significant (p < 0.05) and consistent with observable increases in MBC and MBN and expression of all enzymes (**Figures 23** and **24**, and **Tables 9** and **10**) during flowing conditions. This effect of flow in FW 3 was also related to transect location (significant Location x Flow interaction, **Table 10**) with downstream midflow and outflow sites showing the most response (**Figures 23** and **24**).

The stimulatory effect of flow on both microbial biomass and enzyme activities in floc may be the result of both system-level and specific organism responses. For example, during a hydrologic flow event, nutrients (N and P), as well as C, can be transported from upstream to downstream in both dissolved and particulate forms. As a result, additional substrates may be supplied to downstream (midflow and outflow) sites resulting in greater microbial growth and activity throughout the FW. The additional substrates may also create limiting conditions of some of the nutrients leading to increased enzymatic activity. Microorganisms, especially algae, can vary their physiology (growth rates, respiration, and nutrient uptake) in response to changing hydrodynamics (Moisander et al. 2002, Wang et al. 2012). These effects, based on

changes in nutrient distributions and diffusion rates at the cellular level, are highly organism-specific resulting in both stimulation and inhibition.

In the case of FW 3, the effect of flow may indeed reflect redistribution of C and nutrients as indicated by significant flow effects on floc microbial biomass and enzyme activity stoichiometry (**Tables 9** and **10**). These effects were particularly evident downstream, near outflow sites where MBC:MBN ratios declined (indicating higher nitrogen abundance) and  $E_C$ : $E_P$  ratios increased (suggesting abundance of carbon degradation). During flow, it is possible that inputs of the dissolved and particulate forms of the nutrients result in more C and N relative to P and enhanced  $E_P$  in downstream areas.

Differences in enzyme activities between the two FWs may be explained by the difference in the availability and quality of organic materials. In FW 1, litter materials provide abundant microbial substrates while in FW 3, benthic materials are highly decomposed and mostly mineral requiring regular inputs to sustain microbial growth. N-based decomposition processes (LAP and NAG) were largely stimulated by flow in FW 1 indicating a potential for more N limitation relative to P (supported by higher MBC:MBN and lower MBN:MBP, **Figure 23**). In contrast, the effect of flow in FW 3 was more based around enhanced P limitation as evidenced by increases in E<sub>p</sub> and relative increases in MBC:MBP and MBN:MBP.

The different responses to flow observed between floc and periphyton enzyme activities may also reflect the biological differences between the microbial communities, i.e. water column organisms in the periphyton are more photosynthetic (i.e., fix their own C source) while benthic floc communities, particularly in SAV dominated systems, require external C inputs for their heterotrophic metabolism. In this way, results of benthic communities would be more dependent on flow provision of resources while water column microbes in the periphyton would be affected by more nutrients (in particular P) and environmental parameters (e.g. light availability).

#### **SUMMARY**

Results of this study demonstrate that biomass nutrient ratios and activity of the microbial components, in particular enzymes, can sensitively detect process-level characteristics of the STAs. Water column components like periphyton are highly variable but showed high enzyme activity with some useful trends and similarities to those in the benthic floc. In benthic components like floc and litter, enzymes and microbial nutrient ratios showed that EAV systems are more C rich than those with SAV. For this reason, differences in the systems as well as the internal communities (i.e. water column versus benthic) help explain the different responses to external variables like flow.

Flow appears to have a significant effect on microbial abundance and activities, and with different responses between the periphyton and benthic communities. The response is also related to vegetation type in that FW 3, which is dominated by SAV, shows a greater overall response in floc microbial and enzyme parameters than in FW1, which is dominated by EAV. Also, floc microbial activities indicate that the stronger response of SAV systems to flow may be related to flow providing nutrients and C substrates causing higher activity (i.e. more biomass and enzyme expression) in downstream microbes. In the periphyton, the effect of flow on enzyme activity was more variable and likely involved both chemical (nutrients) and physical (water depth and light penetration) components.

In both vegetation systems, flow appears to enhance nutrient limitation in the floc, with EAV systems tending toward more N limitation and SAV systems toward more P limitation. With flow and higher microbial activity, especially in the outflow areas, SAV-dominated systems exhibited higher levels of phosphatase enzymes in the benthic floc. In the periphyton, there was mixed responses to flow in enzyme activity between EAV and SAV systems. In both systems, flow appeared to enhance P limitation of periphyton (lower  $E_N:E_P$ ), but in EAV systems, this P limitation appeared to result from increased  $E_P$  while in SAV systems, the lower periphyton  $E_N:E_P$  seemed more related to a repression of  $E_N$  with flow.

These patterns of microbial nutrients and enzymes have implications for using separate management strategies based on the vegetation type in the STAs. This could include, for example, more consideration of nitrogen limitation near the inflows or levels of available C in the outflow regions of SAV systems. In this study, phosphatase enzyme expression also showed lower P levels and higher P limitation under flowing conditions. This finding combined with results for the other microbial biomass nutrients, enzymatic activities, and ratios suggests that optimizing flow may lead to further P reduction through balanced macrophyte growth and distribution of C and N within the FW. Results also indicate that there is a high degree of variability in microbial communities, both between system components (i.e. litter, floc, periphyton, and water column) and even within a given component. Therefore, a higher degree of sampling frequency, protocols, and replication will likely be necessary to effectively separate treatment effects from environmental variation. It is also clear from the differential response of benthic and water column microbial communities (periphyton) that these communities are being controlled by and respond to different factors. As a result, higher frequency water quality data are needed to link floc and periphyton responses to changes in nutrient conditions at both the water column and benthic levels.

Along with higher frequency chemistry data, additional controlled flow rate experiments (i.e. with more flow levels and greater consistency) are needed to more precisely quantify the effect of flow rate on microbial processes. Also, the enzymatic activities presented here are only potential measures based on forms and optimal concentrations of added nutrient. These approaches do not necessarily reflect actual enzyme function (i.e. hydrolysis, decomposition, and organic P conversion) in the system. Therefore, experiments to determine the in-situ function of elevated enzyme activities under flowing conditions could provide insight into the mechanisms and rates of organic P hydrolysis in the system, as well as identify potential limitations and inhibitors of the process. Ultimately, these rates and relationships will allow microbial scale processes to be incorporated into system-level models to enhance our prediction of flow rate effects on P removal, storage, and stability in the STAs.

# SETTLING AND ENTRAINMENT PROPERTIES OF STA PARTICULATES

Leonard J. Scinto<sup>4</sup>, Serge Thomas<sup>5</sup>, David C. Fugate<sup>5</sup>, Shimelis Dessu<sup>4</sup>, Colin Saunders, Jill King, Rene M. Price<sup>5</sup>, Jarrell Smith<sup>6</sup>, and David Perkey<sup>6</sup>

#### INTRODUCTION

Previous research on P reduction in the STAs has shown that approximately 50% of outflow TP is particulate (PP). The objective of this substudy is to evaluate hydrodynamic conditions potentially leading to particulate entrainment and export. In particular, this study evaluates spatial flow characteristics under several different hydraulic loads and the potential for particulate movement through the STAs that may affect PP export. This report presents preliminary data, as data collection was still ongoing as of the initiation of this report. The study was conducted in two STA FWs: STA-2 FW 3 and STA-3/4. The results from STA-2 are presented here.

## Site Selection, Sampling, and Measurements

Study sites at the inflow (S21F), midflow (S2MD), and outflow (S2OB) of STA-2 FW 3 (**Figure 25**) were established based on the observed scouring, presence of and/or proximity to remnant canals, distance from inflow/outflow structures, vegetation, and soil/sediment and bathymetric characteristics. The water at the inflow region of the FW had an abundance of easily observable particulates with dark, organic benthic sediments and filamentous green algae. The western side of the midflow and outflow regions of the FW had dense SAV, primarily *Chara* spp., which were heavily covered with periphyton. Vegetation was less dense on the eastern side of the FW and consisted primarily of *Potamogeton* with patches of *Nymphae*. The soils near the outflow region of the FW consisted of 10 to 15 cm of light, golden, sediment over dark-colored muck soil.

Sediment cores were collected in June 2016 from the three sites and two additional locations in STA-2 FW 3: the midflow in emergent vegetation and the outflow in a remnant agricultural ditch identified as potential high flow scouring area. One set of cores was collected for physicochemical analysis and a set of replicate cores was collected for erosion experiments.

SONTEKTM acoustic Doppler velocimeters were deployed at approximately 0.6 times the water depth at each site to measure instantaneous flow velocity (**Figure 25**). These measured flow velocity every 15 minutes during each flow event. Three pairs of sediment traps were deployed at each site to evaluate sediment settling. A "pair" of traps consisted of a high-aspect ratio tube trap and a low-aspect ratio plate trap to measure total downward particle flux and instantaneous or net downward sedimentation, respectively.

<sup>&</sup>lt;sup>4</sup> Florida International University, Miami, Florida.

<sup>&</sup>lt;sup>5</sup> Florida Gulf Coast University, Ft. Myers, Florida.

<sup>&</sup>lt;sup>6</sup> United States Army Corps of Engineers Research and Development Center, Vicksburg, Mississippi.

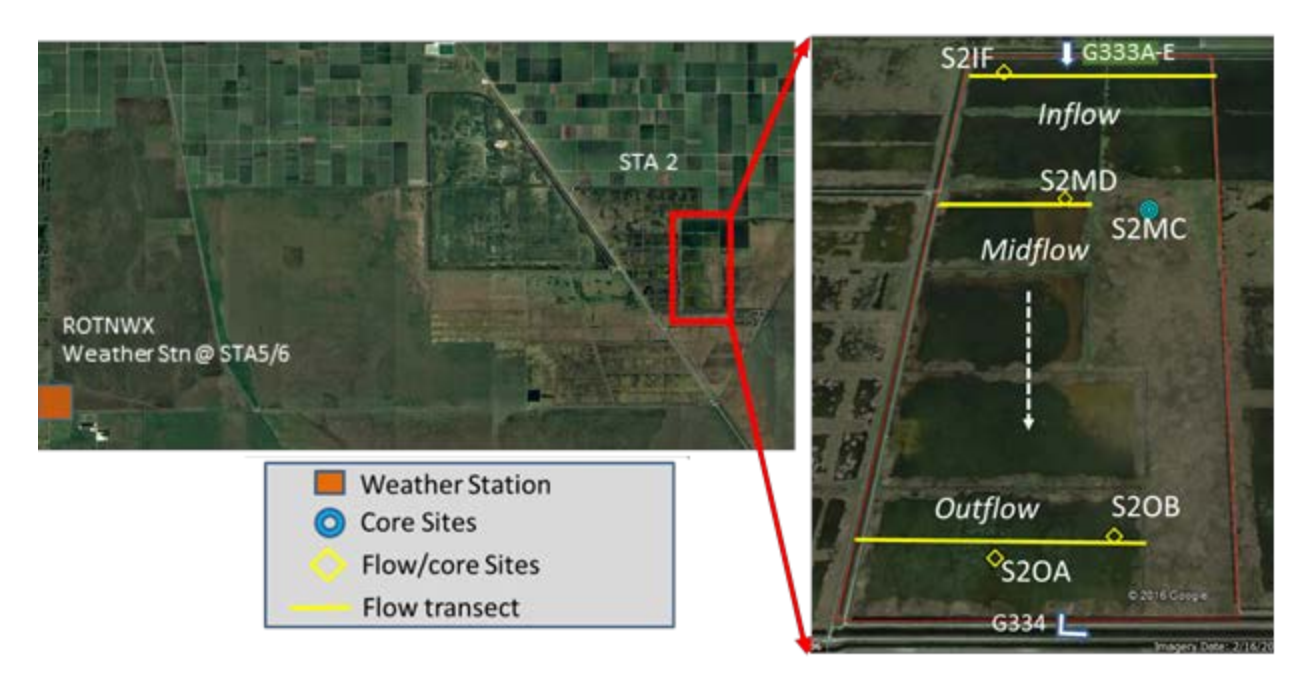


Figure 25. STA-2 FW 3 showing locations of transects, core collection sites, and flow monitoring sites.

#### Soil/Sediment Cores

The potential mass of sediment available for resuspension and possible subsequent release and transport of TP depends on soil/sediment characteristics as well as the physical flow of water. Surficial sediments are most susceptible to entrainment in water flows and therefore, data on the distribution of sediment and sediment nutrients in a vertical profile are needed. Previous work on STA soil/sediments has shown gradients develop in vertical profiles of the RAS that has formed since STA operations began (e.g. Scinto et al. 2011).

Soil cores collected for physicochemical characterization were extruded in 1-cm increments until the "pre-STA" soil was reached. Pre-STA soil was collected as a single increment of varying thickness (to bedrock). Samples were dried at 80° Celsius, ground, and analyzed for TP, dry bulk density, and organic matter content.

In general, TP concentration in the RAS decreased with depth, which is most evident at the inflow (**Figure 26**). TP in pre-STA soil (lowest increment) varied between 347 and 755 milligram per kilogram (mg/kg), typically less than the TP in RAS. At the inflow, soil TP was > 1,500 mg/kg. RAS TP decreased from inflow to outflow locations, indicating sequestration of P along the treatment FW. The RAS bulk density generally increased with depth. In all cores, the upper 1 to 2 cm of RAS had the lowest bulk density, corresponding to a lighter floc layer. The RAS bulk density was higher than that of pre-STA soil in most cases. Organic matter was higher at the inflow than at midflow and outflow locations, indicating greater production of floc/RAS at the inflow than other locations. The midflow and outflow locations had OM contents generally less than 20%, which is indicative of an accretion process dominated by carbonaceous sediments formed by calcareous periphyton and macroalgae (*Chara* spp.).

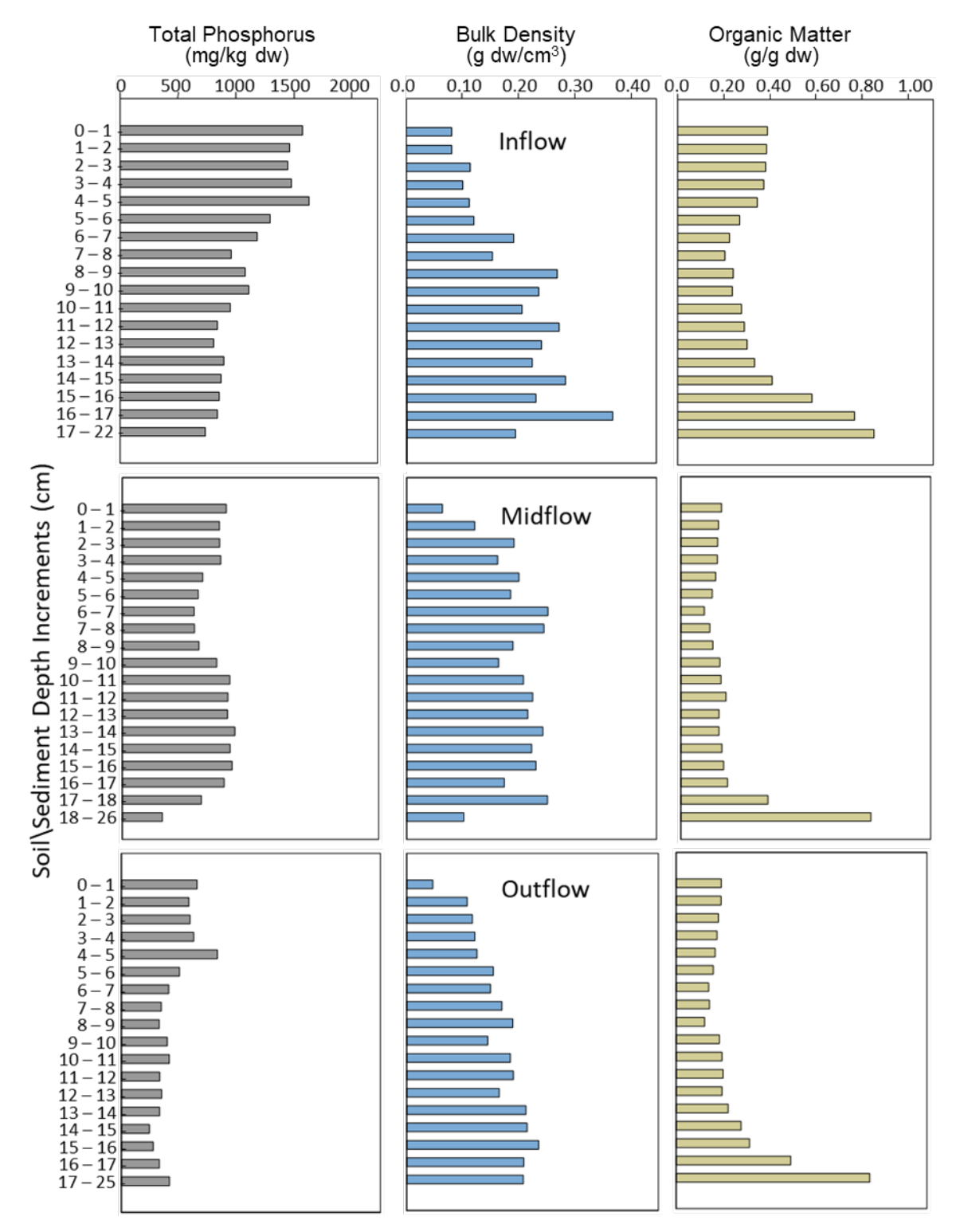


**Figure 26.** TP in milligrams dry weight (mg dw), bulk density grams dry weight per cubic centimeter (g dw/cm³), and organic matter content (in grams per grams dry weight (g/g dw) of soil cores collected at the inflow (S2IF), midflow (S2MD), and outflow (S2OA) of STA-2 FW 3. Cores were sectioned into 1-cm increments of RAS. The lowest increment represents the pre-STA soil analyzed as a single sample of varying thickness.

## **Erosion Assessment: Determining Critical Shear Stress**

## **GUST Chamber Analysis**

A Gust chamber (Dickhudt et al. 2009) was used to determine the erodibility and critical shear stress for flocculent or unconsolidated sediments. Duplicate cores were subjected to nearly constant shear stresses immediately following collection. Overlying water was pumped from the chamber into a turbidimeter and then collected and weighed. Mass of particles collected was then used to calibrate the turbidimeter. Gravimetric analyses were used to measure mass material eroded at a given shear stress, which was incrementally increased from 0.01 to 0.60 Pascals (Pa). The data were used to estimate erodibility and critical shear stress (e.g. Gust and Mueller 1997, Sanford and Maa 2001, Dickhudt et al. 2011, Ferre et al. 2010).

A plot from a core collected at S2IF demonstrates how shear stress affects erosion rate (**Figure 27**). Erosion started at 0.2 Pa when a large spike in resuspension occurred. This is the critical shear stress of the uppermost surface sediment of the core. Subsequently increased shear stress causes erosion rates to spike followed by decreasing rates as the sediments become more consolidated. A constant erosion rate occurred at the last shear stress of 0.60 Pa. The analysis revealed measurements of changes in critical shear stress at a very high vertical spatial resolution. As more sediment mass is eroded away, deeper parts of the core are exposed for analysis. The cumulative eroded mass provides a proxy to visualize changing critical shear stress with sediment depth. In this representative core, the critical shear stress at the surface is about 0.2 Pa and deeper in the core the critical shear stress averaged around 0.40 Pa and did not change with depth. Examination of the critical shear stress by eroded mass profiles for all cores collected in duplicate showed small difference among the sites (although one STA-2 FW 3 midflow core showed higher erodibility than the others) (**Figure 28**). The median critical shear stresses of surface sediments showed small difference between the sites and ranged between 0.1 and 0.2 Pa.

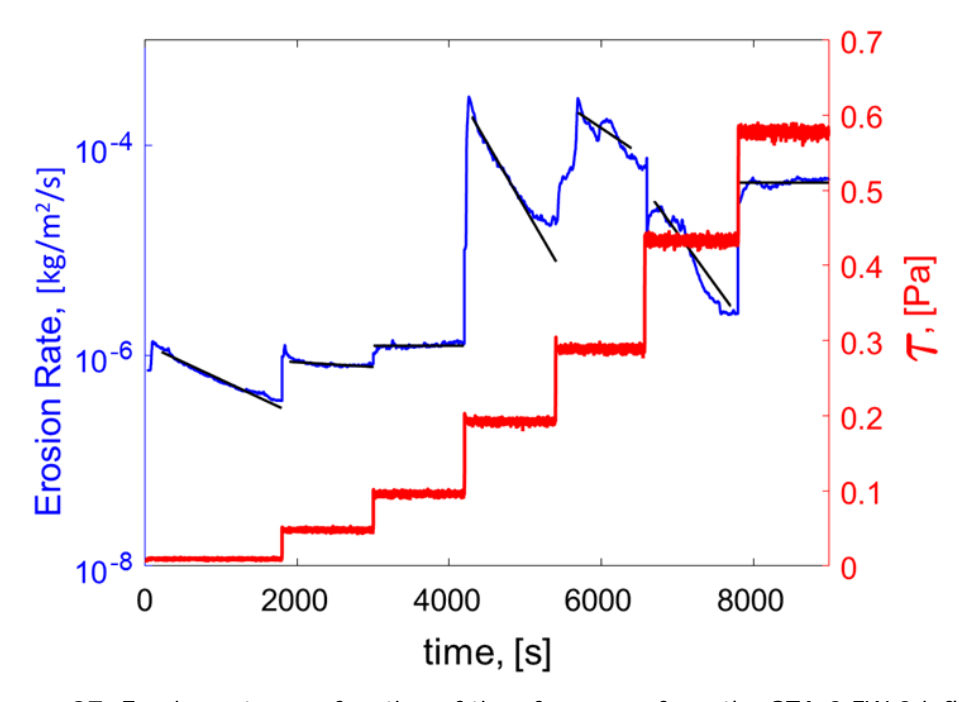
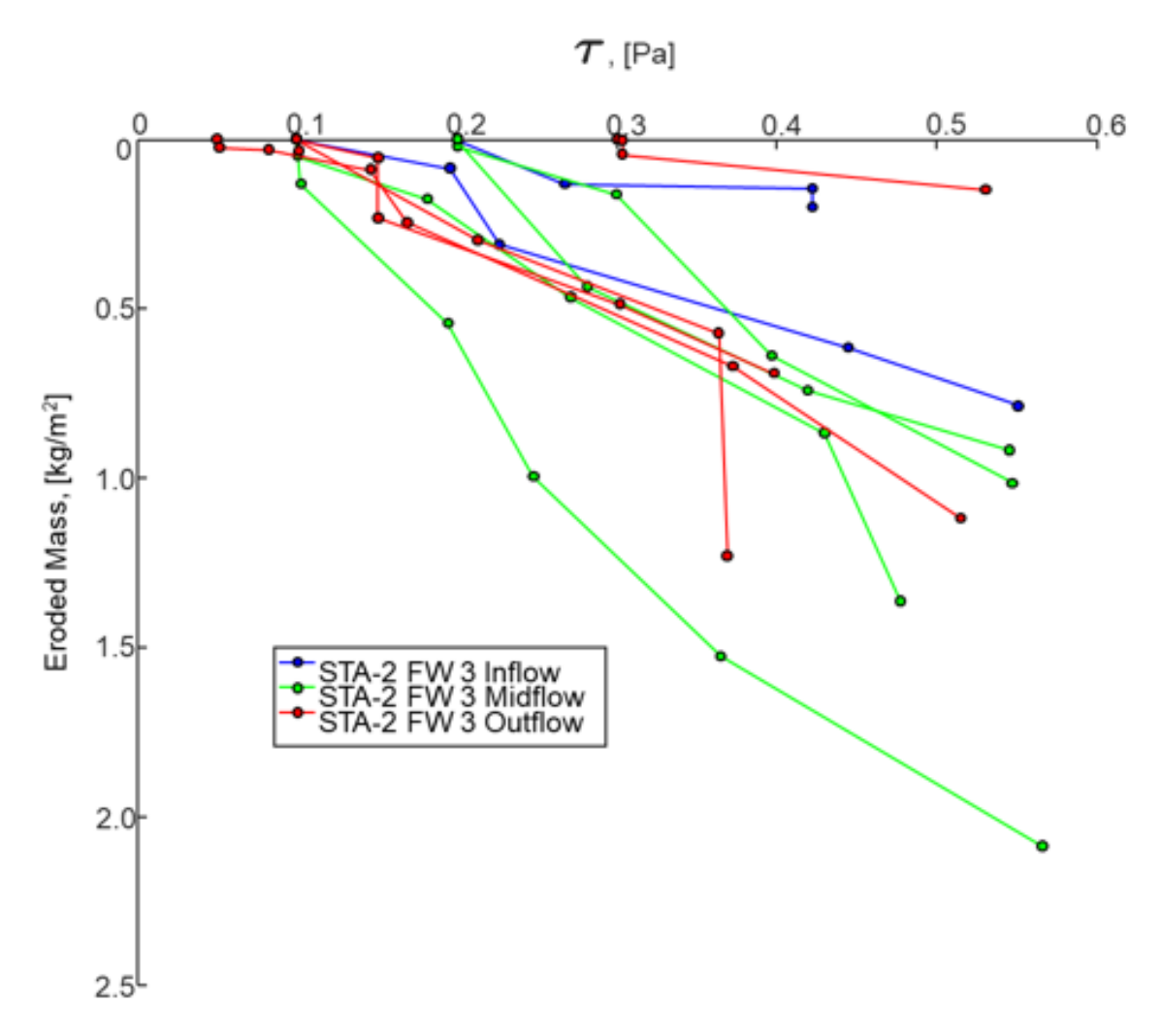


Figure 27. Erosion rate as a function of time for a core from the STA-2 FW 3 inflow.



**Figure 28.** Eroded mass as a function of shear stress for 12 total cores collected and analyzed as duplicates from five locations in STA-2 FW 3.

#### Sedflume Chamber Analysis

A Sedflume chamber is a "high velocity" flow system that applies a consistent turbulent flow across a sediment core surface creating critical shear stress in the range of 0.1 to 10.0 Pa (McNeil et al. 1996). It is best suited to measure erosion of consolidated material. The chamber was used to assess potential erosion at shear stresses greater than Gust chamber capabilities (> 0.60 Pa). As in the Gust, erosion of surface sediment occurs when the applied shear stress exceeds the critical stress for erosion,  $\tau_c$  under incrementally increasing shear stresses. Sedflume data were fit to the equation  $E = A\tau^N$  where E is erosion velocity in centimeters per second (cm/s),  $\tau$  is the applied shear stress in Pa, and A and N are parameters determined from the log-linear regression to the data. Critical shear stress is determined from the regression parameters, such that  $\tau_c$  corresponds to an erosion velocity, Ec of  $10^{-4}$  cm/s (or 3.6 millimeters per hour [mm/hr]).

Particle size distribution, water content, and other physical properties were measured at 3- to 5-cm intervals during erosion experiments. Size distributions were determined with samples dispersed in a 0.4% sodium metaphosphate solution and sonified prior to measurement in a Malvern Mastersizer 2000 laser diffraction particle sizer.

Cores collected at all stations behaved similarly. Erosion resistance from an example core, STA-2 FW 3 outflow station, increased with depth, especially below 5 to 7 cm ( $\tau_c$  = 0.56 Pa; **Figure 29**). Eroded sediment

for three depth increments had maximum particle size distribution of approximately 50 micrometers (μm) (**Figure 30**). The surface critical shear stresses for all sample locations ranged from 0.02 to 0.15 Pa, which was less than those typically estimated from the Gust method (~0.20 Pa). Consistent with Gust results, erosion thresholds increased with depth. Over all sites, the grain size distribution and the sediment composition did not vary; increased erosion resistance therefore appears to be associated with increases in packing density, which increased with depth.

The differences in shear stress measurements between the Gust and Sedflume reflect the differences in methodology. The Gust chamber measures the critical shear stress necessary to suspend sediment from the benthos into the water column (operationally to 10 cm above the bed). The Sedflume measures the critical shear stress necessary to achieve bedload transport, which does not reach high into the water column. The differences in the Gust and Sedflume estimates of critical shear stress indicate that bedload transport can occur at lower shear stresses than needed to resuspend sediment into the water column.

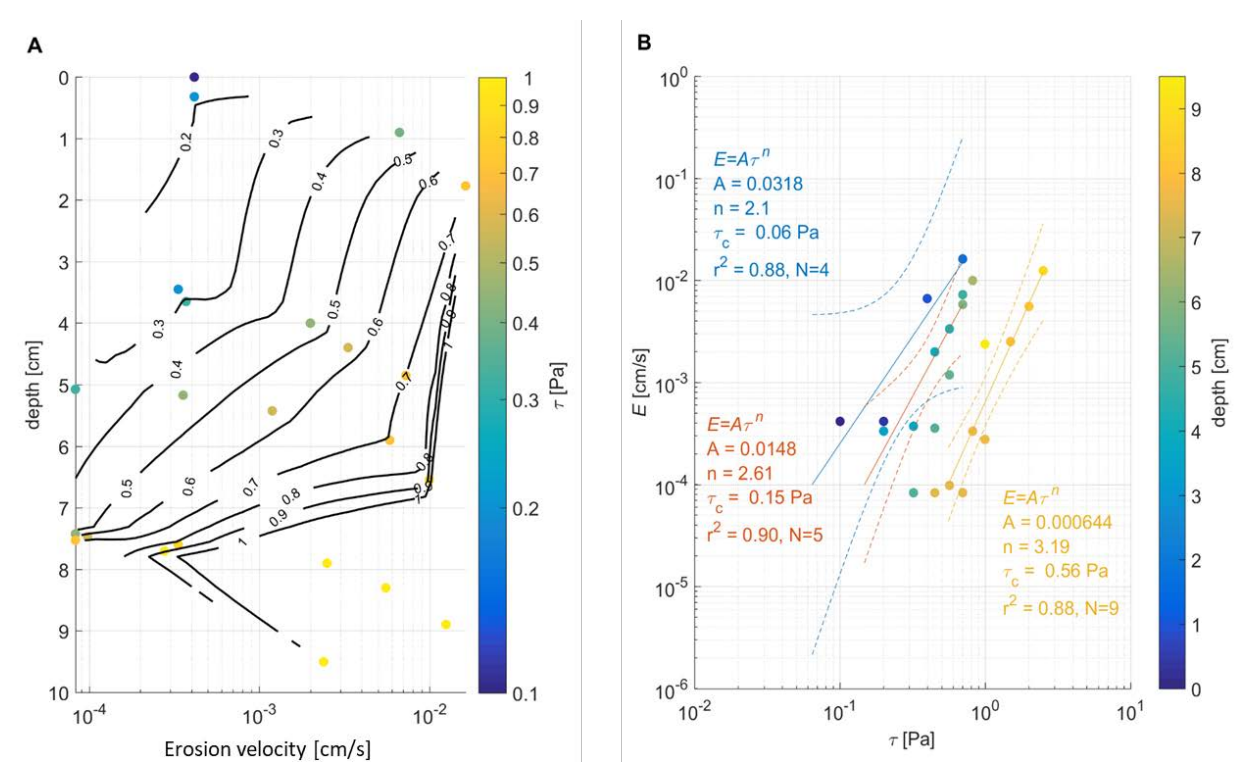


**Figure 29**. Results of sedflume analysis for a core collected at STA-2 FW 3 outflow station. Erosion velocity versus depth where the isolines represent the applied shear stress (A) and erosion velocity versus shear stress (B). The color of the data point corresponds to the depth below the sedimentwater interface. Regression lines and fit parameters are provided for the layers evident in the data. The dashed lines represent the 95% confidence intervals in fit parameters.

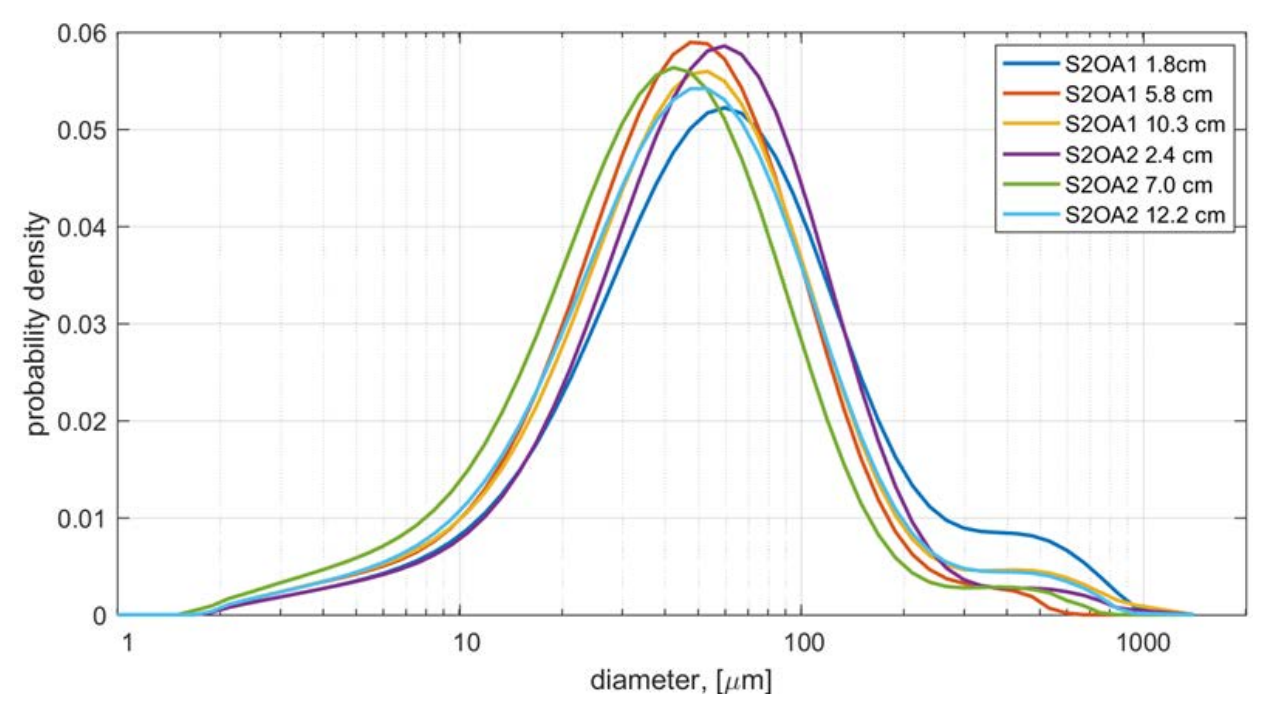


**Figure 30**. Particle size distribution for subsamples collected for given depths from duplicate cores at STA-2 FW 3 outflow station A.

## Water Velocities during Flow Events

Water velocity was measured for approximately six weeks over each of two flow events in STA-2 FW 3 (Event 1 – June 27 to August 29, 2016 and Event 2 – October 12 to November 22, 2016; see *Flow-Way Water Quality Assessments* section above) during active flow tests and post-flow periods. Events generally included two-week phases of given flows (determined by South Florida Water Management District [SFWMD or District] operations), followed by a no flow phase, and then a return to another phase of a given flow condition. However, numerous factors occasionally caused deviations from the plan.

The first flow test occurred in STA-2 FW 3 under conditions described as "low flow" where the inflow velocity during the experimental period averaged ~3.5 m³/s (**Figure 31a**). The effect of the outflow gate closure was observed on the individual velocity measurements at the three sampling sites. The outflow site velocity responded to the operation of outflow gate G-334. During the event, an additional three-dimensional acoustic flow velocity profiler (ArgonautXR) was installed inside a remnant canal (S2OA) near the outflow. Flow velocities here changed in response to the outflow gate operation. The flow velocity at the midflow responded to the operation of both inflow and outflow structures. The velocity response of the inflow site did not show explicit correlation with the inflow rate through the G333A-E structure. A high flow event in STA-2 FW 3 occurred on October 28 through December 12, 2016. The inflow and outflow gates were open until November 3, 2016 and were closed for the remainder of the experimental period (**Figure 31b**). Hence, the flow condition did not return to normal operation after two weeks of no flow. The outflow rate was at least 50% greater than the inflow rate during the experimental period. Similar to the low flow event (**Figure 31a**), the southward velocity at the outflow site responded to outflow gate operations.

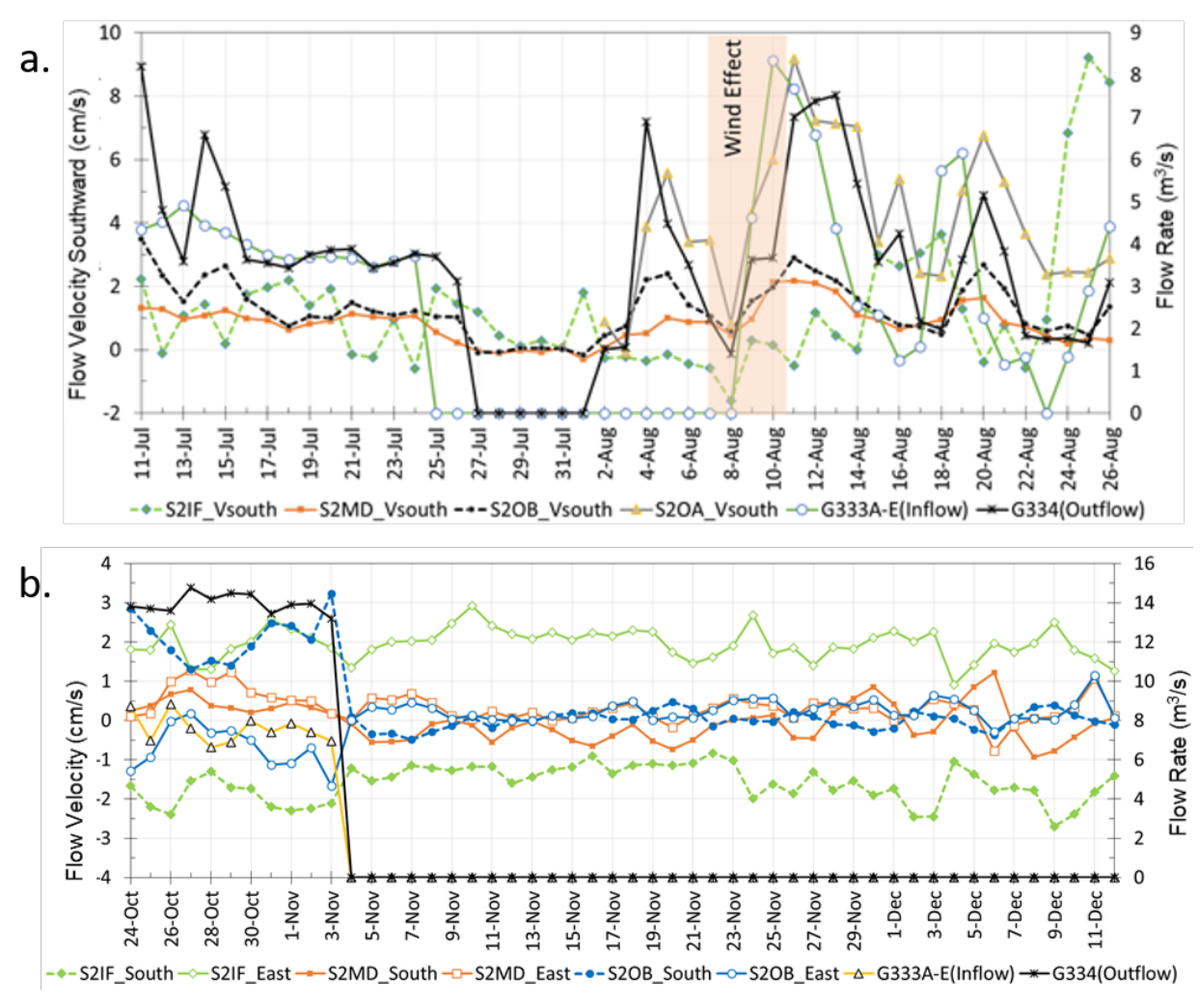


**Figure 31**. Daily average inflow/outflow rate and acoustic Doppler velocimeter velocity profiles in STA-2 FW 3 for (a) low flow and (b) high flow events.

## **Settling of Suspended Solids: Sediment Traps**

To measure particle settling due to downward flux of either water column derived particulates or suspended sediments, three replicate high aspect ratio traps (tubes) were paired with a set of three low aspect ratio traps (plates) at the inflow, midflow, and outflow sites for 1-week deployments during each flow event. Trap pairs were arranged along an axis perpendicular to the assumed north to south direction of flow. The tube traps openings were 31.7 square centimeters (cm²) and have a depth much greater than the aperture (also known as the high aspect ratio) to assess the total downward flux of particles. This includes material settling from or produced in the water column (e.g. sloughing periphyton) or resuspended from bottom sediments and becoming trapped without the possibility of recurrent resuspension. Tube traps were installed with the aperture 4 cm above the sediment to avoid trapping saltated particulates. The plate traps were a modified version of the well-tested Teller traps (Kozerski 1999, 2000, 2003). Plate traps provide a large sampling area but with minimal trap depth (smooth plate = low aspect ratio). Therefore, the mass particulates on the plate traps are subject to removal and resuspension and represent instantaneous or net downward sedimentation. After a 1-week deployment, sedimented material was collected from all traps. Material on the plate traps was collected by carefully enclosing the plate surface with a flanged dome and

securely clamping to the plate. The traps were removed from the water, inverted, gently agitated and all material now in the dome funneled into sample bottles. Any material remaining on the plates was scraped into the collection bottles with a spatula. Periphytometers (acrylic surfaces parallel to the water column) were used to correct for possible growth on the plate trap surfaces. Tube traps were capped under water and transported to the lab were material was decanted. Trapped sediment materials were separated per size class by sequential filtration and by particle size analysis using a digital floc camera. Filtered material was processed for TP, ash free dry weight, and total carbon (TC) and/or TN where applicable. Laboratory analysis is under way.

The net sedimentation flux was calculated from the material deposited on the sediment plate and expressed as mass per unit surface area per unit time (grams dry weight per square meter per day, g/m²/d). The downward sedimentation flux was calculated using the material collected in the tubes. Finally, the upward particulate flux (i.e. resuspended particulates) was determined for each trap pair by subtracting the downward sedimentation flux (plates) from the total downward flux in tubes.

For all locations and events, the high aspect ratio (tube) traps collected more sediment than the low aspect ratio traps (plates). Further, sedimentation rates decreased from inflow to outflow. Trap measurements are represented by the STA-2 FW 3 high flow event and show upward fluxes were driven by downward fluxes since the net fluxes (i.e. plate traps) were much less than the tubes (**Figure 32**). There was a decrease in the downward fluxes from upstream to downstream as demonstrated by the decreasing mass in trapped sediments moving from inflow to outflow. The differences between the tube vs plate traps was greatest at the inflow site. This suggests that resuspension may have been greater at the inflow where the lack of a densely vegetated water column, and a large fetch increase the likelihood of wind increased water velocity (see below). However, particulate fluxes at the inflow were mainly driven by large particles represented by fragments of the filamentous green algae *Spirogyra* sp. (> 2,000 µm) and particles between 120 and 10 µm. At the midflow and outflow, the majority of particles measured between 210 and 600 µm (not shown). There was also greater net deposition (plates) of particulates at the midflow and outflow than at inflow and likely represent increase sloughing of periphytonic material from the dense SAV.

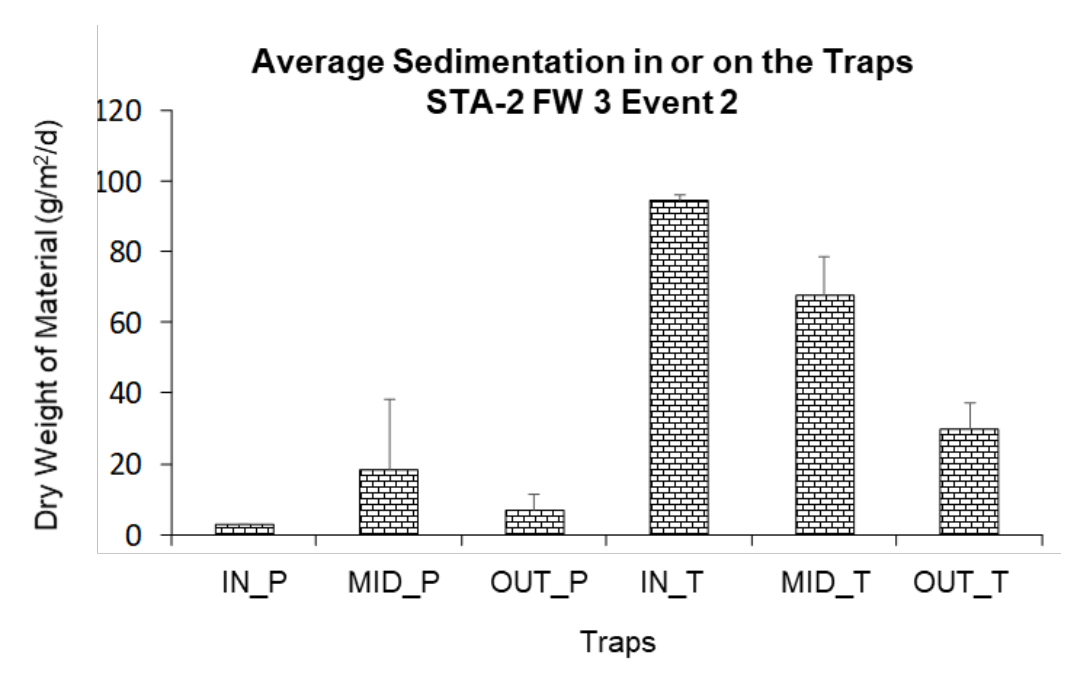


**Figure 32.** Average net sedimentation flux (plates) at inflow (IN\_P), midflow (MID\_P), and outflow (OUT\_P) and the downward net sedimentation flux (tubes) at inflow (IN\_T), midflow (MID\_T), and outflow (OUT\_T). (Note: P = plate type and T = tube traps.)

## Meteorological Conditions Affecting Flow and Potential Particle Suspension

The effects of meteorological conditions, namely wind speed, on water flow and subsequent particle movement were assessed in STA-2. Average hourly water velocities over approximately 20 days during the August 2016 flow tests were plotted against wind speed to determine the effects on velocity (**Figure 33**). Wind speed and direction were obtained from the SFWMD wind monitor at STA-5/6 (ROTNWX, **Figure 25**). The wind effect depended on the location of the station relative to the direction of the wind. The effects of wind on water velocity was greatest at the inflow where the long fetch and lack of vegetated water column allowed wind-driven flows. These effects were greatly reduced at the midflow and outflow.

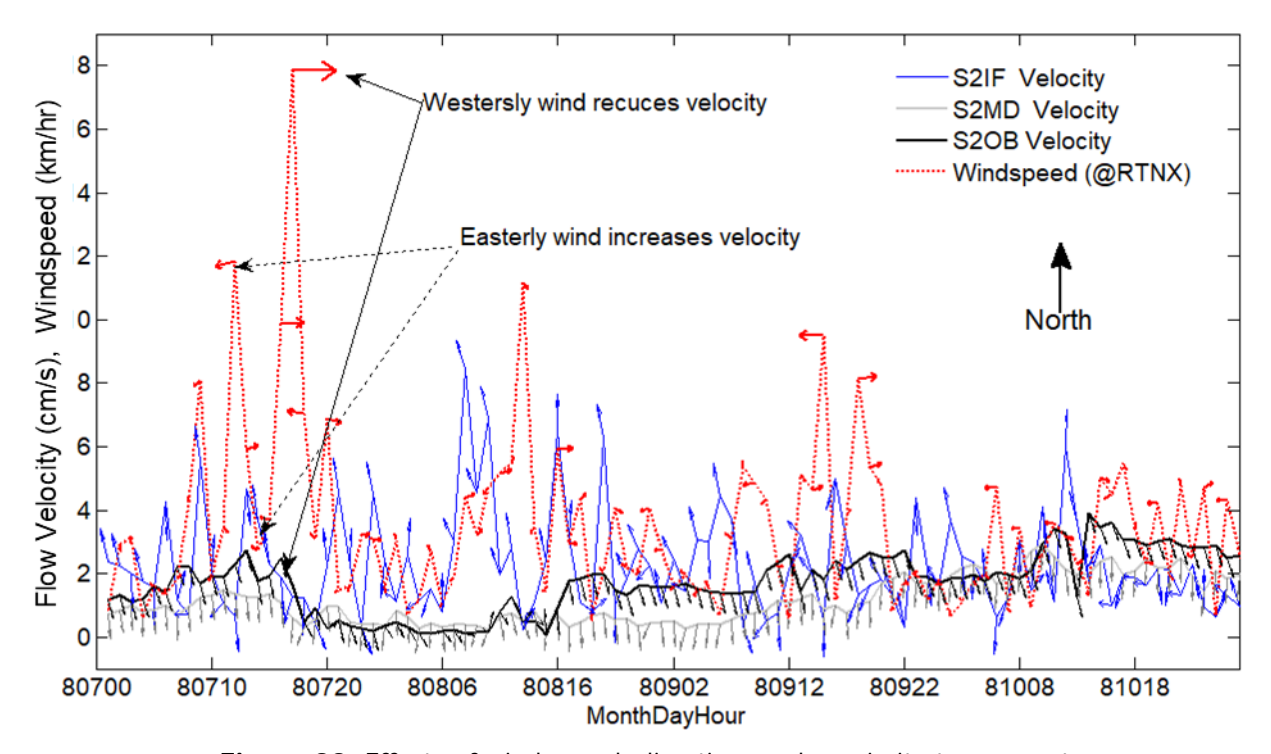


**Figure 33.** Effects of wind speed, direction, and proximity to remnant canals during a 20-day period in August 2016 in STA-2 FW 3.

Analysis of potential viscous versus turbulent flows affecting resuspension determined that water column friction in the STA was due to turbulent shear. Shear stress and turbulent kinetic energy (TKE) were obtained by deploying an acoustic Doppler velocimeter operating in burst mode on 15-minute intervals at the STA-2 midflow station during the June–August 2016 flow event. The high sampling frequency was used to estimate vertical flux momentum in the water column by the Reynolds stress (i.e. covariance method). The resultant turbulent shear stress was related to the amount of TKE in the water column, which are known to have a near linear relationship (Kim et al. 2000).

Horizontal mean velocities were generally less than 0.03 meters per second (m/s), and Reynolds stresses were approximately 10<sup>-3</sup> Pa (**Figure 34**). The acoustic backscatter, or echo amplitude (a proxy for suspended sediment in the water column) and the TKE (a measure for current), exhibited a diurnal pattern that was driven by peak afternoon winds. Therefore, ROTNWX winds were converted to median values by hour of day for the July 19–August 27, 2016, period and compared to hourly median TKE, shear stress, and acoustic backscatter.

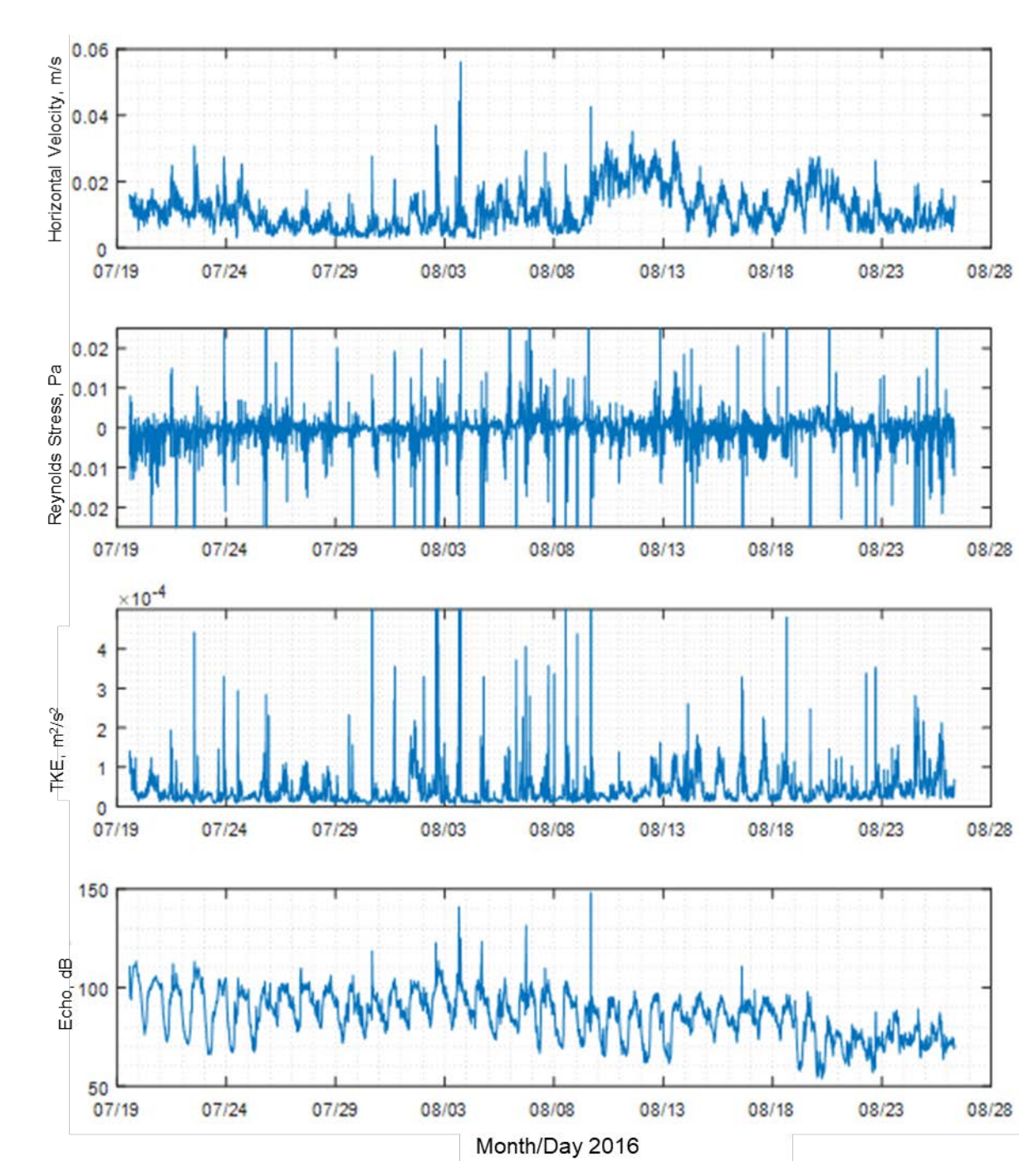


**Figure 34**. From top to bottom: Horizontal velocity, Reynolds stress, turbulent kinetic energy, and echo at STA-2 FW 3 (S2MD) during Event 2 (low flow) in July-August 2016.

This resulted in clear patterns emerging where wind data show a diurnal pattern of peak wind speeds around 1500 hours and rapidly decreasing wind between 1600 and 1800 hours (**Figure 35a**). Both TKE and shear stress show peaks around 1700 hours and rapidly decreasing afterwards (**Figures 35b** and **35c**). Diurnal median peak shear stresses were around 0.001 Pa. The effect of the wind wave generated turbulence was evident in the acoustic backscatter (**Figure 35d**) where the suspended sediment concentrations (SSC) follow the increasing portion of the wind time series. However, SSC did not drop off as rapidly as TKE and shear stress after the cessation of the wind. Instead, the suspended sediment settled slowly during the quiescent period. The pattern reveals that a much higher critical shear stress is needed for resuspension than for deposition. That is, there is turbulent friction in the water column below which particles will settle. At water column turbulent friction greater than this, suspended particles will remain suspended. The water column turbulent friction is much lower than the critical shear stress. Correlations between wind-driven and operational flow showed that the wind explained 41% of the variance in the mean flow current.

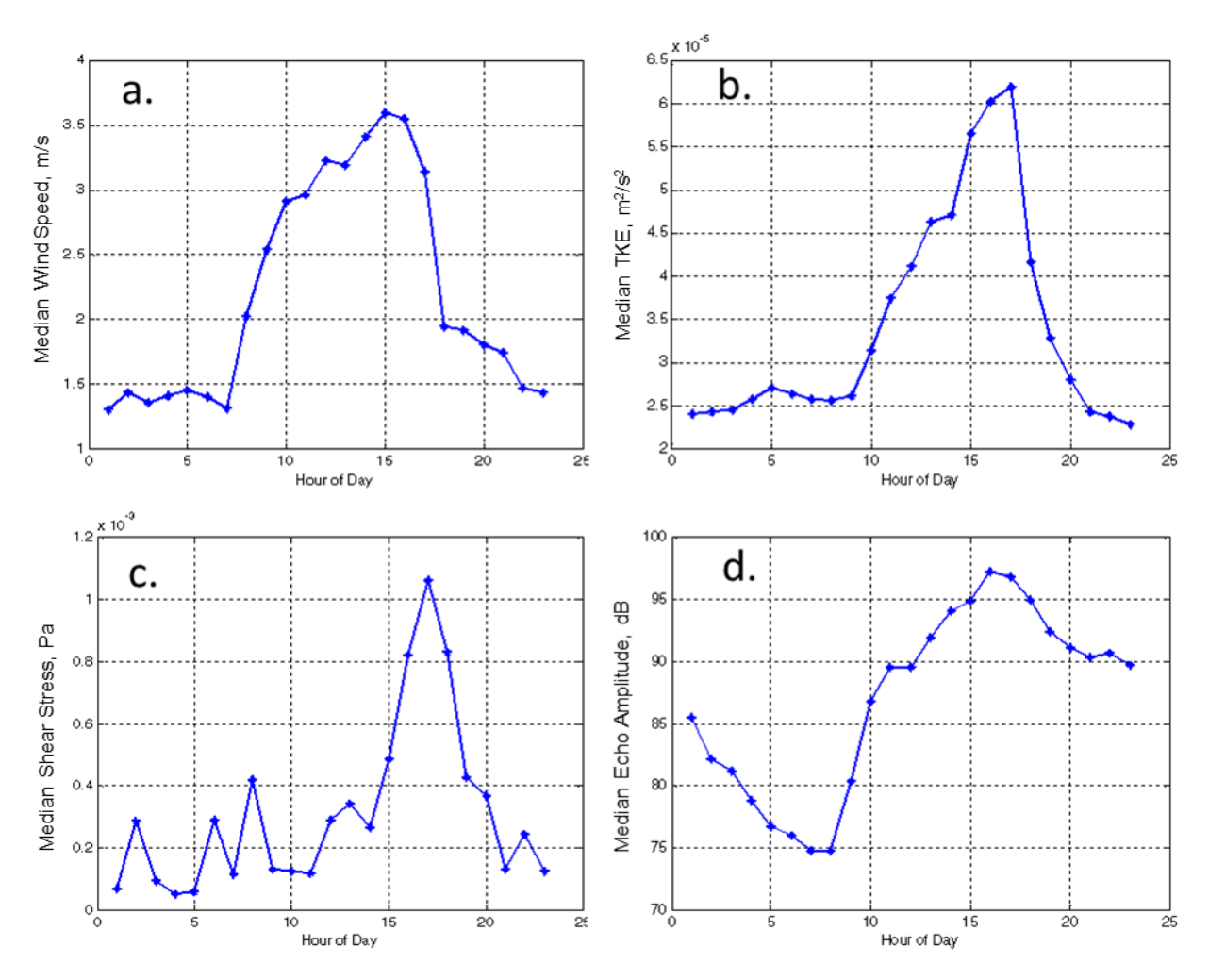


**Figure 35.** (a) Median wind speed, (b) median TKE, (c) median shear stress, and (d) mean echo amplitude (proxy for suspended sediment concentration) as a function of the hour of the day at STA-2 FW 3 from July 19 to August 27, 2016.

## Spatial Identification of Flow Fields and Preferential Flow Paths: Velocity Transects

A transect flow analysis was conducted to determine the extent sufficient velocities to entrain particles can be affected by bed morphology and preferential flow paths in the STAs, especially near outflow area. Transects in STA-2 FW 3 were established at the inflow, midflow, and outflow sites perpendicular (west to east) to expected flow (north to south) with geographically positioned endpoints (Figure 25). Measured points along transects were distributed to capture representative characteristics of the landscape heterogeneity (e.g. vegetated and non-vegetated sections, scoured and depositional areas). Flow velocity was measured with SONTEK<sup>TM</sup> Flow Trackers that were moved through the system on foot. Flow velocities and directions were recorded at intervals of 0.010 to 0.025 times the length of the transect. If conditions changed over shorter distances, additional measurements were made. Coordinates were recorded using a global positioning system at each velocity measurement point. The positive X direction was oriented toward the outflow, perpendicular to the transect line. The positive Y direction was set to the direction of the transect line. For a north-south flow and a transect running from west to east, the X direction was pointing south and Y direction pointing east. At each point, the surface water depth and floc depth were measured using a "Paluga pole" to draw bed topography and floc profile. Velocity along these transects in STA-2 FW 3 were measured during the high flow event on October 28 and 30, 2016. The velocities recorded in the X and Y directions were input to a MatLab program developed specifically to calculate and map the velocity vector for each measurement. Maps were made using water velocities and depth measurements along the three transects.

The velocity vector directions varied along each transect for the three STA-2 FW 3 transects (Figure 36). In general, the Y component of the velocities pointed to the nearest depression or old agriculture canal. For the inflow transect, higher floc depth was measured where the X velocity direction was northward. Comparatively, southward flow was associated with scoured locations. The inflow has two sections on the west and east side by a deep canal and the velocity profiles as well as the floc depth of the two sections differ despite their hydraulic connectivity. The east and west end of the inflow transect had a northward flow during our flow measurement period. The high wind during the inflow transect measurements may have induced the large east-west velocity. A strong preferential flow at the southwestern corner in the inflow transect corresponded to a break in the internal levee for airboat access (filled in 2017). A more consistent southward flow was observed in the outflow transect compared to the inflow and midflow transects (Figure 36). The outflow transect also showed apparent preferential flow paths along old canals. The inflow transect located in proximity to the STA inflow structures, had considerably less floc on the sediment bed than was found at either the midflow or outflow transects (Figure 36). At the midflow transect, the water flow was relatively uniform moving in a southward direction. The outflow transects showed high velocities with localized preferential flow paths along remnant canals especially when in proximity to cell outflow openings. There was a thicker floc bed generally at the outflow than the inflow and the midflow suggesting that floc thickness develops along the inflow to outflow portions of the cells.

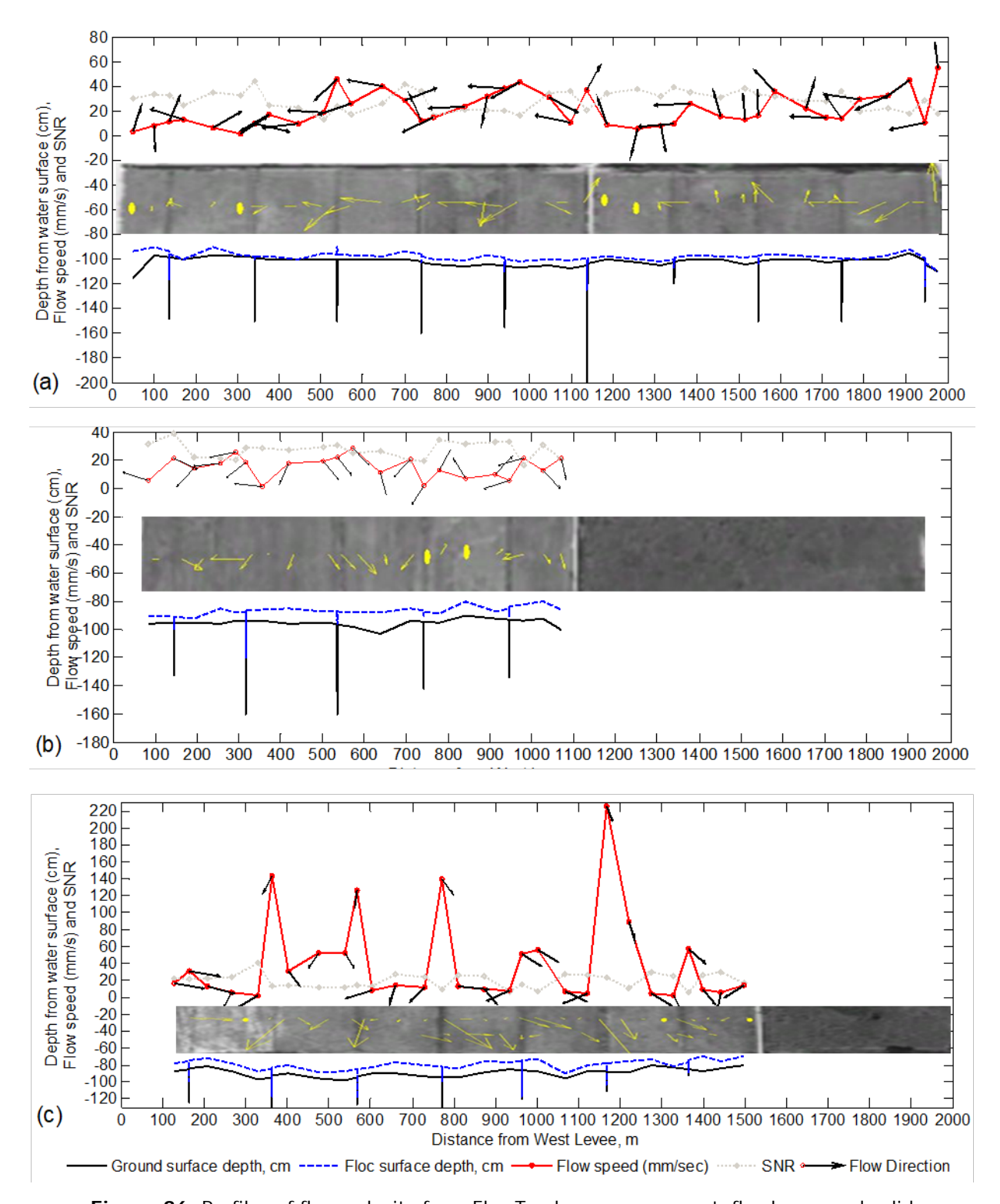


**Figure 36.** Profiles of flow velocity from FlowTracker measurement, floc layer, and solid ground depth from water surface using a "Paluga" pole along (a) inflow, (b) mid-flow, and (c) outflow transects in STA-2 FW 3 as measured on October 28 and 30, 2016.

#### **SUMMARY**

Several characteristics of flow effects in STAs are apparent from the study results. The sediments accumulating in the FWs of the STAs show P sequestration with the concentrations of TP in sediments decreasing with distance through the FWs. The highest TP concentrations are generally in the surface sediments in all areas, i.e. inflow, midflow, and outflow. However, the sediment characteristics in STA-2 FW 3 are spatially variable with the inflow sediments being more highly organic and having higher TP than in the outflow region. The abundant calcifying periphyton and *Chara* in the midflow and outflow regions of the FW produced RAS with a greater mineral content (low organic matter content) than at the inflow. The critical shear stress determined by both the Gust and the Sedflume methods suggest that surficial layers have a critical shear of about 0.02 to 0.2 Pa and that deeper in the sediment column, where the sediment is more consolidated, the critical shear stress increases to about 0.60 Pa. Flows and water velocities varied in response to flow-way operation (e.g. flow manipulations, gate openings, etc.) but also responded to bed morphology, especially the presence of remnant agricultural canals, proximity to control structures, and weather patterns, which also affected the potential for sediment resuspension. Given the low flows during experimental tests and the relatively high critical shear stress of the sediments, particle entrainment and movement from the sediments is likely an episodic phenomenon, or highly localized phenomena, as the highest velocities were observed in remnant ditches in the outflow sections of the FW. Wind-driven flows were greatest in the afternoons and were correlated to flows but at velocities that create peak shear stresses of approximately 0.001 Pa, which is an order of magnitude less than needed to exceed sediment critical shear stresses. The RAS and presumably the water column particulates vary from highly organic at the inflow of this FW to more mineral at the midflow and outflow suggesting that particulates are not moving between these areas of the flow-way. Further analysis of data, including physicochemical properties of water and particulate material, is underway. Incorporation of the chemical data as related to flow should provide a clearer understanding of these processes.

## SOIL PHOSPHORUS FORMS

K. R. Reddy<sup>3</sup>, Lilit Vardanyan<sup>3</sup>, Rupesh Bhomia<sup>3</sup>, Jing Hu<sup>3</sup>, Taylor Smith<sup>3</sup>, W.G. Harris<sup>3</sup>, Odi Villapando, and Sue Newman

#### INTRODUCTION

Wetlands serve both as a sink and a source of P. Wetlands can store large amounts of particulate matter in soils through settling and deposition and are also known to generate dissolved constituents that can be potentially transported downstream. Mobility and reactivity of P in wetlands are controlled by the chemical composition of P in soil and water, relative sizes of various P pools in the soil, interactions of soluble fractions with solid phases, and decomposition of organic substrates including soil organic matter (Reddy and DeLaune 2008).

The primary question posed in the study was how and to what extent the type of vegetation and nutrient loading alter the storage, forms, and reactivity of P in accreted soils. It was hypothesized that EAV and SAV will support different biogeochemical processes that will alter the relative proportion of organic and inorganic P forms in the accreted material. It was also hypothesized that nutrient loading will increase labile pools of P in soils in the upstream areas of the STA. The overall objective of the study was to determine the forms and distribution of P in floc, RAS, and pre-STA soil layers at the sampling locations established along the flow path of the study FWs. The results presented here are for STA-2 FW 1 and FW 3.

## **METHODS**

Intact soil cores were collected from 11 transect locations in STA-2 FW 1 and FW 3 in September 2016 (**Figure 37**). The description of the study sites is given in the *Flow-Way Water Quality Assessments* section of the appendix. The inflow, midflow, and outflow locations along each transect were marked as benchmark sites. The soil cores were sectioned into floc, RAS, and pre-STA soil (sectioned into depth categories of 0–5 cm for pre-STA 1 and 5–15 cm for pre-STA 2) and analyzed for select physico-chemical properties. Samples were fractionated sequentially for various pools of P.

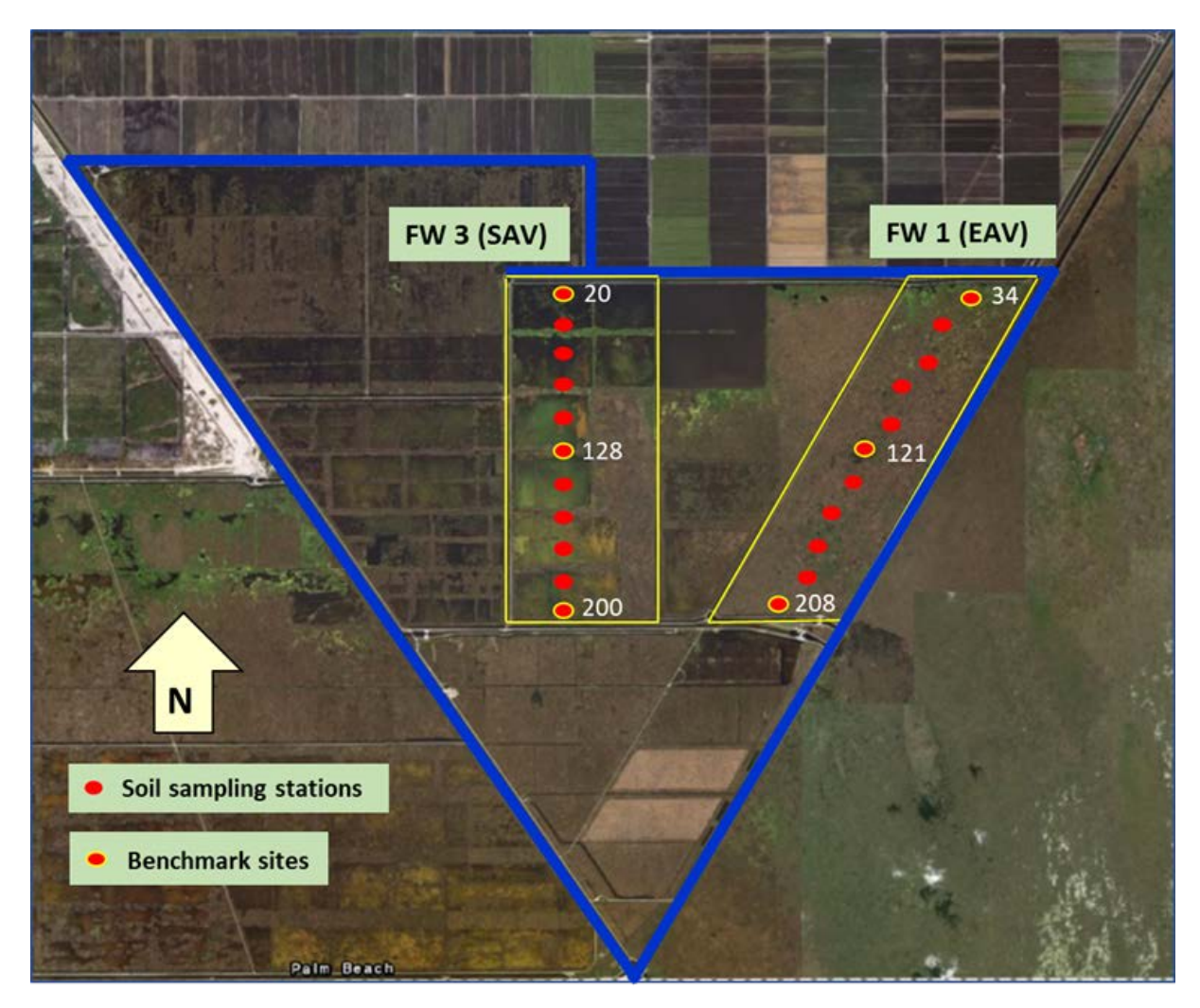


**Figure 37.** Map showing the transect points in STA-2 FWs 1 and 3. Sampling locations along the flow path are shown in red circles and benchmark stations are indicated with yellow circle.

## **Soil Phosphorus Fractionation**

The procedure used in the study is based on the solubility of inorganic and organic P pools in either acid or alkali solutions (Ivanoff et al. 1998, Reddy et al. 2013). This method has been used in several studies on wetland soils to determine operationally defined pools of P (**Figure 38**).

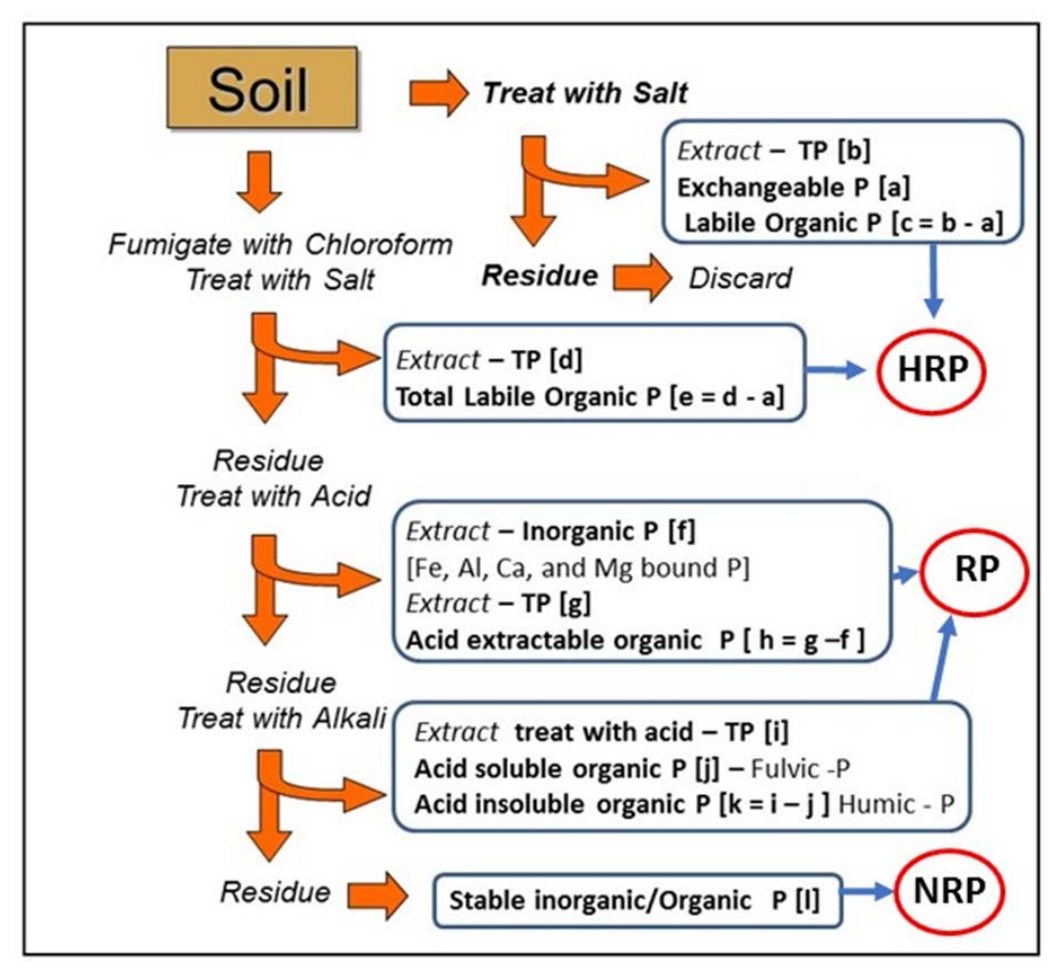


**Figure 38.** Soil P fractionation scheme used to quantify reactive and non-reactive pools of P in wetland soils (modified from Ivanoff et al. 1998 and Reddy et al. 2013). (Notes: HRP = highly reactive; RP = reactive P; and NRP = non-reactive P. Total labile organic P includes both labile P and microbial biomass P.)

## <sup>31</sup>P Nuclear Magnetic Resonance Spectroscopy

The floc and soil samples from benchmark locations in each FW were analyzed for organic P forms using the nuclear magnetic resonance (NMR) method described by Cade-Menun and Liu (2013) and Cheesman et al. (2012). The method identifies organic P groups including phosphomonoesters, phosphodiesters, polyphosphates, pyrophosphates, and others. Results of NMR and conventional P fractionation methods were compared.

## X-Ray Diffraction Analysis

The mineral composition of RAS samples from benchmark locations was determined by X-ray powder diffraction (XRD) analysis using a computer-controlled x-ray diffractometer (Harris and White 2008). Minerals were identified by referencing x-ray diffraction data for minerals (Joint Committee on Powder Diffraction Standards 1980).

#### **RESULTS**

TP concentration was generally higher in the floc and decreased with depth in both EAV (FW 1) and SAV (FW 3) systems (**Figure 39**). Concentrations typically followed FW nutrient gradients of surface water and vegetation. Floc and RAS in the EAV are generally more P-enriched than in the SAV cell. TP concentrations in the floc ranged from 860 to 2,320 milligrams P per kilogram (mg P/kg) in EAV and 360 to 1,080 mg P/kg in SAV, with high values observed at stations near inflows of both systems. In the EAV system, two distinct zones of floc P were observed with higher values (1,970 to 2,320 mg P/kg) from the inflow to midflow region and lower values (860 to 1,650 mg P/kg) from the midflow to outflow region (center to outflow) of the FW. In the SAV system, P enrichment in the floc was also higher in the first four stations near inflow (up to 1.5 kilometers [km] from inflow) than in the remaining stations along the transect.

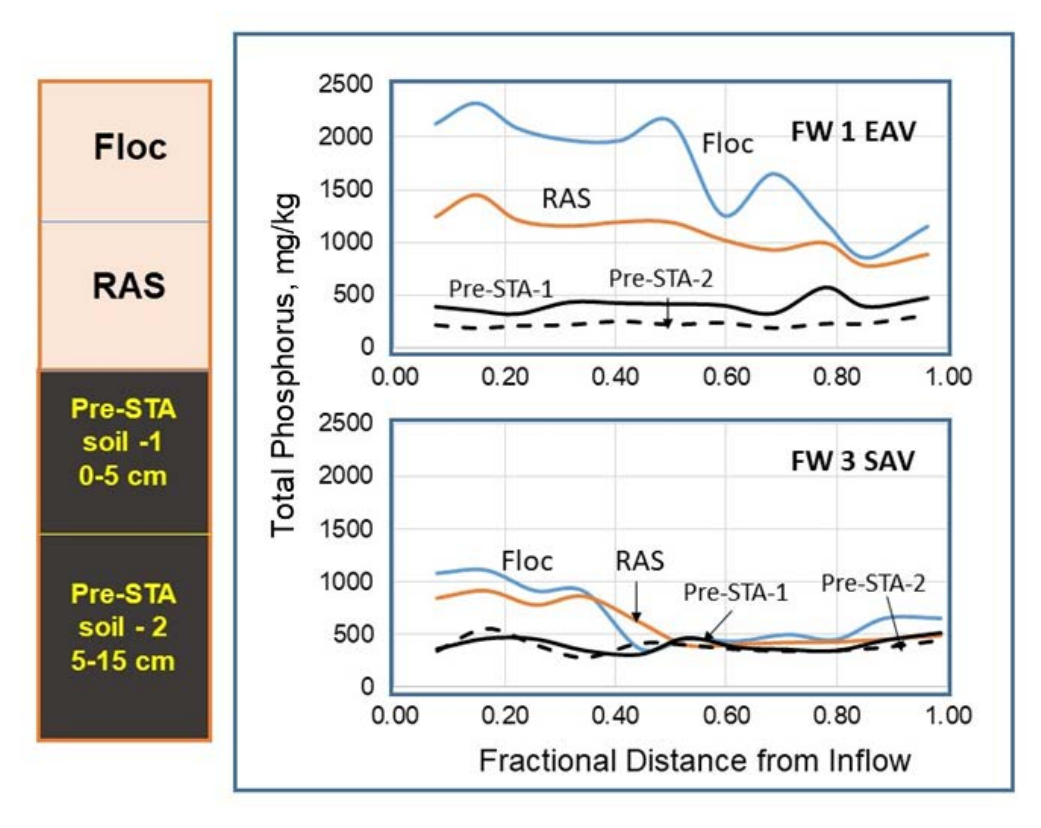


**Figure 39**. TP concentration in floc, RAS, and pre-STA soils along the distance from inflows of STA-2 FW 1 and FW 3.

## **Phosphorus Forms**

P forms in the floc, RAS, and pre-STA soils are grouped into three broad categories based on their solubility in acid or alkali. The **Highly Reactive P** (**HRP**) group includes (1) bicarbonate extractable inorganic P that is loosely adsorbed, bioavailable, and can be readily released into the water column; (2) bicarbonate extractable organic P that includes all non-living sources of microbial organic P, and (3) MBP. The **Reactive P** (**RP**) group includes (1) acid (HCl) extractable inorganic P that includes P associated with Fe, Al, Ca, and Mg; and (2) acid extractable organic P and alkali (sodium hydroxide [NaOH])-extractable organic P (fulvic- and humic-bound P). The **Non-reactive P(NRP**) group includes residual P not extracted either with acid or alkali and considered permanently accreted with organic matter

in soils. The relative size of various P pools varied between FWs but showed similar spatial pattern for floc and RAS in both EAV and SAV systems, while pre-STA soils showed no consistent pattern in both systems.

## Highly Reactive Phosphorus

Labile inorganic P (labile Pi) concentrations in the floc and RAS of EAV cell were generally higher at stations near inflow (up to 2.2 km) decreasing steadily along the flow path (**Table 11** and **Figure 40**). Similarly, labile Pi in SAV was highest near inflow station decreasing with distance from inflow. Labile Pi in EAV accounted for 1 to 15% of the TP in floc and 1 to 5% of the TP in RAS (**Figure 40**). Labile Pi in SAV accounted for 5 and 25% of the TP in floc and RAS, respectively (**Figure 40**).

Approximately 1 to 6% of the TP in floc and RAS was labile bicarbonate extractable organic P (labile Po) in EAV and 0.1 to 6% of the TP in floc and RAS in SAV and showed no consistent pattern along the flow path. MBP accounted for 6 to 37% of the TP in the floc and 5 to 19% of the TP in the RAS and increased with distance from inflow. Similarly, in the SAV system, MBP accounted for approximately 6 to 28% of TP in the floc and with high values in the second half of the transect (> 2.4 km) and increased with distance towards the outflow. Total labile organic P (that includes both labile Po and MBP) as a percent of TP was also lower at the inflow and increased with distance from the inflow (**Figure 40**).

**Table 11.** HRP pools including labile Pi, labile Po, and MBP in floc, RAS, and pre-STA soils from benchmark locations in STA-2. Values are mean ± standard deviation.

Flow- Way	Sampling Station	Distance from Inflow (m)	Floc	RAS	Pre-STA 1	Pre-STA 2		
Labile Inorganic P (Labile Pi) (mg/kg)								
	34	400	$138 \pm 63$	$47 \pm 3$	11 ± 2	$9.4 \pm 4$		
FW 1	121	2,700	88 ± 21	27 ± 8	13 ± 3	17 ± 1		
	208	5,200	$7.7 \pm 4$	18 ± 19	13 ± 2	16 ± 2		
	20	350	276 ± 41	194 ± 40	14 ± 2	11 ± 4		
FW 3	128	2,800	36 ± 14	$34 \pm 9$	15 ± 3	24 ± 2		
	200	4,450	$36 \pm 7$	21 ± 3	10 ± 3	8 ± 1		
Labile Organic P (Labile Po) (mg/kg)								
	34	400	84 ± 12	25 ± 15	3.0 ± 1	$3.2 \pm 2$		
FW 1	121	2,700	59 ± 18	26 ± 18	1.7 ± 1	$0.4 \pm 1$		
	208	5,200	$40 \pm 6b$	24 ± 11	$6.0 \pm 3$	$4.5 \pm 5$		
	20	350	55.6 ± 10	33.9 ± 2	4.6 ± 4	5.7 ± 2		
FW 3	128	2,800	$10.0 \pm 3$	$10.8 \pm 2$	$6.6 \pm 3$	$11.5 \pm 0.4$		
	200	4,450	10.5 ± 9	1.3 ± 1	$3.4 \pm 1$	$2.2 \pm 0.3$		
		Microbia	I Biomass P (ME	3P) (mg/kg)				
	34	400	238 ± 40	56 ± 28	16 ± 11	16 ± 8		
FW 1	121	2,700	454 ± 38	137 ± 108	14 ± 5	$8.8 \pm 3$		
	208	5,200	285 ± 8	155 ± 15	31 ± 15	20 ± 6		
	20	350	66 ± 58	45 ± 10	10 ± 2	11 ± 2		
FW 3	128	2,800	52 ± 9	$33 \pm 27$	11 ± 4	13 ± 2		
	200	4,450	72 ± 10	9 ± 5	1 ± 1	7 ± 3		

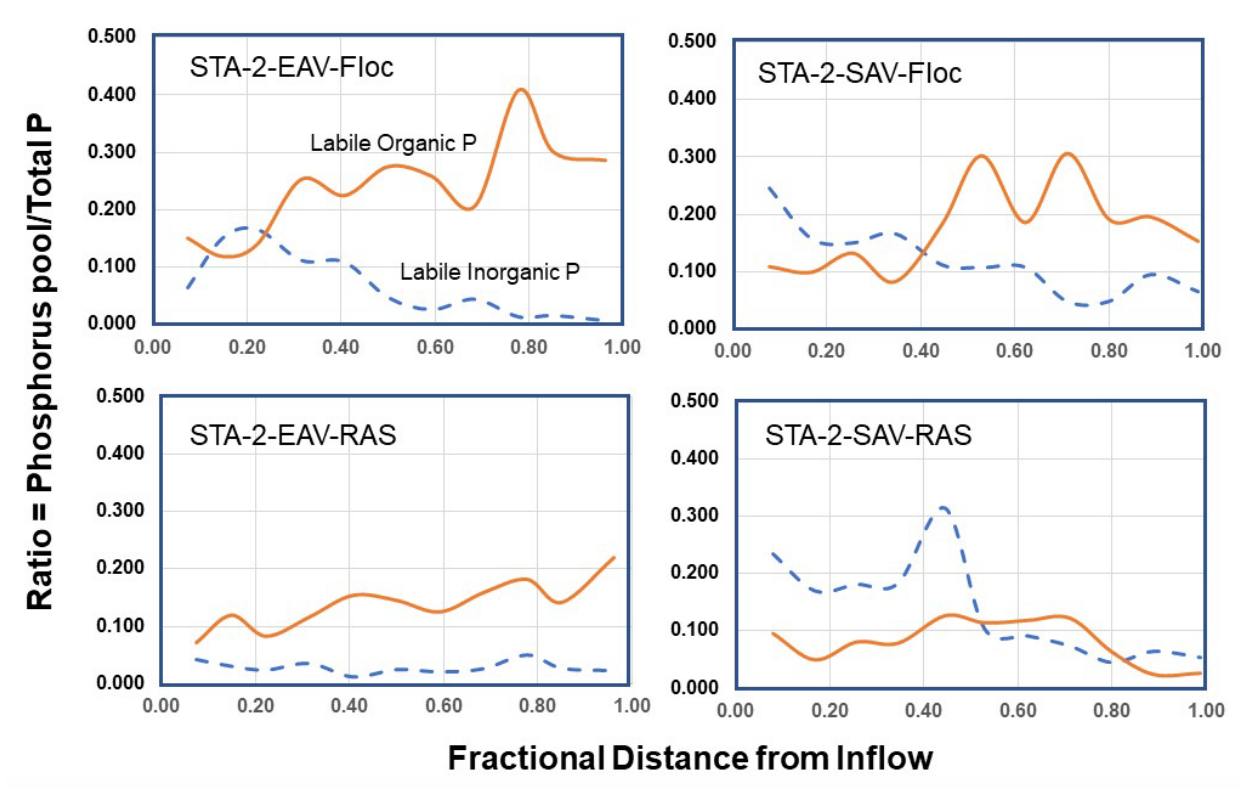


Figure 40. Ratio of HRP (Po and Pi) to total P in floc and RAS soil sections from FW 1 (EAV) and FW 3 (SAV) of STA-2.

#### Reactive Phosphorus

Reactive inorganic P (referred herein as HCl-Pi) concentrations in floc and RAS of EAV were generally higher at stations near the inflow (up to 3.2 km) and decreased steadily along the hydrologic flow path. Similarly, HCl-Pi in SAV was also high near the inflow station and decreased with distance from the inflow. HCl-Pi accounted for 17 to 29% of the TP in floc and RAS of FW 1 (Figure 41) and from 23 to 55% of the TP in floc and RAS of FW 1 (Table 12 and Figure 41). Acid extractable organic P (referred to as HCl-Po) ranged from 1 to 7% of TP in floc of both FWs. In both pre-STA soil sections of EAV system, HCl-Po ranged from 4 to 10% of TP. In the SAV system, HCl-Po accounted for 2 to 7% of TP in the pre-STA (0-to 5-cm layer) soil section in the first half of the transect (< 2.4 km) and from 12 to 21% in the second half of the transect. Alkali extractable RP includes both fulvic acid (FA-Po) and humic acid (HA-Po) associated P. In terms of stability, HA-P is more stable than FA-P. In EAV system, fulvic acid-P represents approximately 7 to 23% of TP in floc, 1 to 24% in RAS, and 17 to 30% in pre-STA soils. Similarly, HA-Po accounts for approximately 6 to 18% of TP in floc, 10 to 28% in RAS, and 22 to 45% in pre-STA soils.

**Table 12.** RP and NRP pools of Pi and Po in floc, RAS, and pre-STA soils from benchmark locations in STA-2. Values are mean ± standard deviation.

Flow- Way	Sampling Station	Distance from Inflow (m)	Floc	RAS	Pre-STA 1	Pre-STA 2			
Acid Extractable Inorganic P (HCI-Pi) (mg/kg)									
FW 1	34	400	376 ± 69	266 ± 13	44 ± 2	15 ± 2			
	121	2,700	428 ± 27	$248 \pm 94$	$45 \pm 8$	18 ± 4			
	208	5,200	331 ± 155	139 ± 83	$53 \pm 34$	17 ± 1			
	20	350	410 ± 25	351 ± 62	105 ± 18	111 ± 18			
FW 3	128	2,800	104 ± 14	118 ± 14	47 ± 2	57 ± 5			
	200	4,450	204 ± 26	168 ± 20	143 ± 5	156 ± 60			
		Acid Extrac	table Organic P	(HCI-Po) (mg/kg	1)				
	34	400	148 ± 54	91 ± 17	24 ± 4	13 ± 6			
FW 1	121	2,700	50 ± 15	$73 \pm 6$	27 ± 5	14 ± 7			
	208	5,200	35 ± 25	39 ± 15	26 ± 6	17 ± 4			
	20	350	67 ± 2	34 ± 6	25 ± 2	19 ± 2			
FW 3	128	2,800	11 ± 9	20 ± 12	52 ± 10	26 ± 10			
	200	4,450	4 ± 4	24 ± 4	53 ± 2	42 ± 12			
		Alkali Extra	ctable Organic	P (FA-P) (mg/kg	)				
FW 1	34	400	364 ± 113	207 ± 91	77 ± 19	49 ± 3			
	121	2,700	298 ± 26	170 ± 65	61 ± 21	$33 \pm 4$			
	208	5,200	164 ± 11	94 ± 10	89 ± 9	$66 \pm 20$			
	20	350	75 ± 15	44 ± 14	45 ± 3	$38 \pm 7$			
FW 3	128	2,800	49 ± 13	68 ± 22	139 ± 16	$93 \pm 7$			
	200	4,450	84 ± 12	81 ± 25	104 ± 38	101 ± 12			
		Alkali Extra	ctable Organic	P (HA-P) (mg/kg	)				
	34	400	274 ± 84	162 ± 103	85 ± 18	62 ± 17			
FW 1	121	2,700	242 ± 52	193 ± 106	83 ± 31	45 ± 6			
	208	5,200	189 ± 42	227 ± 22	172 ± 31	106 ± 19			
	20	350	28 ± 20	20 ± 12	56 ± 4	56 ± 1			
FW 3	128	2,800	$32 \pm 29$	14 ± 10	88 ± 27	74 ± 25			
	200	4,450	$44 \pm 30$	23 ± 17	61 ± 53	72 ± 45			
		Residual Inor	ganic and Orgai	nic P (NRP) (mg/	kg)				
	34	400	515 ± 126	260 ± 43	56 ± 4	22 ± 2			
FW 1	121	2,700	241 ± 11	240 ± 49	69 ± 3	$30 \pm 5$			
	208	5,200	82 ± 17	118 ± 9	62 ± 10	$30 \pm 2$			
	20	350	141 ± 23	104 ± 21	25 ± 4	24 ± 4			
FW 3	128	2,800	38 ± 8	71 ± 6	22 ± 4	18 ± 2			
	200	4,450	82 ± 13	49 ± 13	37 ± 10	27 ± 5			

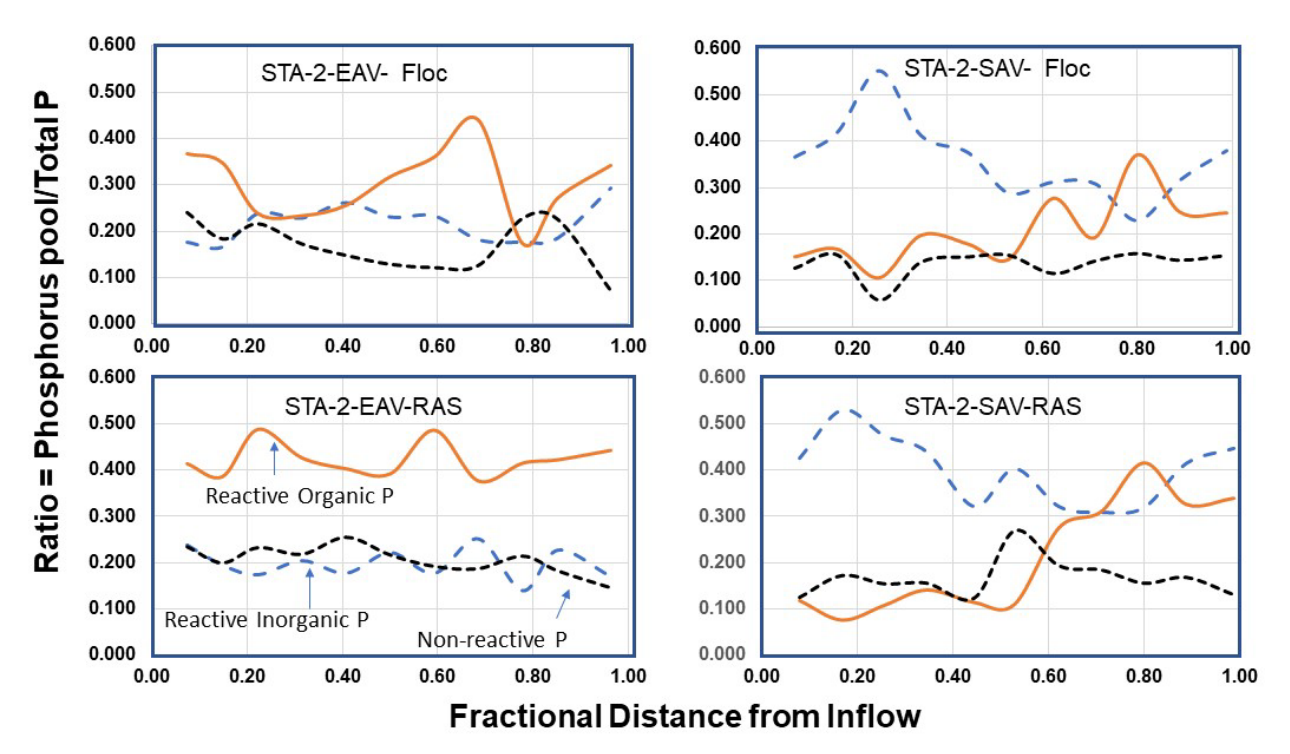


Figure 41. Ratio of reactive organic and inorganic P to total P in the floc and RAS soil sections of FW 1 (EAV) and FW 3 (SAV) of STA-2.

#### Non-Reactive Phosphorus

The residual form is considered highly refractory but may be slowly bioavailable (**Table 12**). In the EAV system, residual stable P accounted for 7 to 24% of TP in floc and 15 to 25% in the RAS. In the SAV system, residual P accounted for 6 to 15% of TP in floc and 13 to 27% in the RAS, respectively. Although residual P concentrations in floc and RAS in both systems decreased along the flow path gradient, no consistent patterns in NRP pool as percent of TP was observed.

## Total Inorganic and Organic Phosphorus

Total inorganic P includes the sum of bicarbonate extractable Pi and HCl extractable Pi. The relative proportion of inorganic and organic P pools was influenced by vegetation type, with the EAV system dominated by organic P and SAV system dominated by inorganic P in all soil layers. In the EAV system, approximately 39% of the TP was in inorganic P pool compared to 43% of the TP in organic P pool in floc and RAS of the soil layers (**Figure 42**). In the SAV system, approximately 75% of the TP was in inorganic P pool compared to 16% of the TP in organic P pool in floc and RAS layers (**Figure 42**). In pre-STA soils of EAV, 65% of the TP was present in the organic P pool and 15% in the inorganic P pool while in SAV system, approximately 15% of the TP was organic and 76% inorganic.

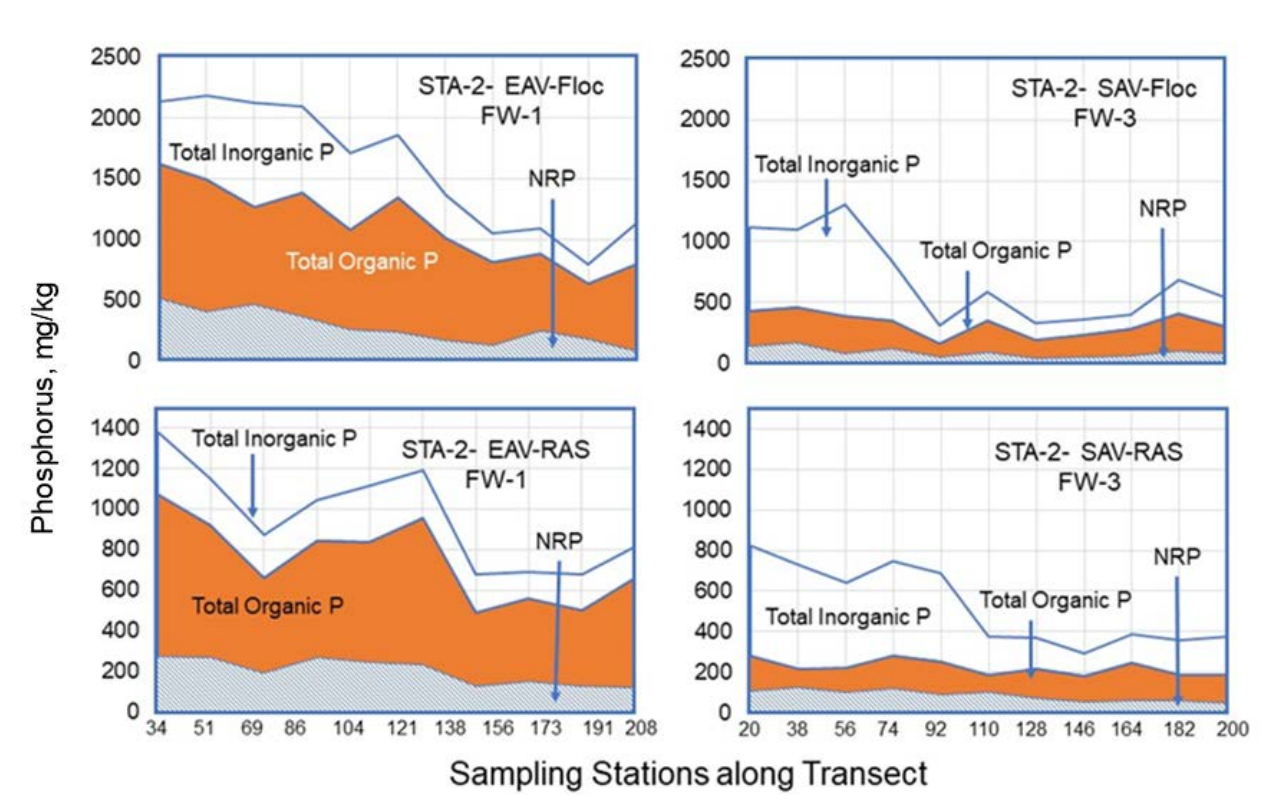


Figure 42. Total inorganic HRP+RP, organic HRP+RP, and NRP (expressed on a soil dry weight basis) in floc and RAS along the flow paths of STA-2 FW 1 (EAV) and FW 3 (SAV).

## **Phosphorus Storage**

The storage of various P pools and related macro-elements in the floc, RAS, and pre-STA soils from STA-2 FWs 1 and 3 was calculated as follows:

Storage 
$$(g/m^2) = C_m \times BD \times D \times [0.01]$$
 (5)

where,  $C_m$  is the concentration of an element or P pools expressed on dry weight basis (mg/kg or micrograms per gram [ $\mu$ g/g]); BD is the bulk density (grams per cubic centimeter [g/cm³]); D is the thickness of soil layer (cm); and [0.01] is the coefficient to convert units to grams per square meter (g/m²).

P storage was high in the floc and RAS near the inflow and decreased along the flow path. Average TP storage in the floc and RAS (combined) along the flow path was 5 g P/m² in FW 1 (EAV) and 16 g P/m² in FW 3 (SAV) (**Table 13**). Both treatment FWs have been in operation for the past 14 years (WY2002–WY2016) and for calculation purposes it was assumed that accretion of both floc and RAS occurred during this period. Some of the elemental storage was probably incorporated into the top layer (0- to 5- cm depth) of the pre-STA soil. In EAV belowground biomass, a large component of nutrient storage is not reflected in the floc and RAS. Thus, it is likely that storage values in EAV floc + RAS are underestimated.

Simple empirical equations relating TP storage to HRP, RP, and NRP storages were developed (**Table 14**) and relative proportion of each P pool is estimated using these equations. HRP represented 24 and 29% of the TP storage in the EAV and SAV FWs, respectively. The RP pool accounted for a larger proportion with 57 and 59% of the TP stored in EAV and SAV systems, while 22 and 12% of the TP was present in NRP pool of EAV and SAV systems, respectively. In the EAV system, approximately 33% of the TP was inorganic (HRP-Pi + RP-Pi) and 45% was organic (HRP-Po + RP-Po). In the SAV system, 68% of the TP stored was inorganic and only 9% was organic. In the EAV pre-STA soils, approximately 85%

of the TP stored was organic and 9% was inorganic. Similarly, in the SAV pre-STA soils, 51% of the TP stored was inorganic and 42% was organic.

**Table 13**. TP storage in floc, RAS, and pre-STA soils from FW 1 (EAV) and FW 3 (SAV). Values are mean  $\pm$  standard deviation (n = 11).

Soil Layer	Depth (cm)	Bulk Density (g/cm³)	Mean (g P/m²)	Minimum (g P/m²)	Maximum (g P/m²)
		STA-2 FW	1		
Floc	$4.7 \pm 2.0$	$0.043 \pm 0.018$	$2.8 \pm 1.1$	0.7	4.3
RAS	$2.9 \pm 1.3$	$0.075 \pm 0.016$	2.1 ± 1.4	0.8	5.5
Pre-STA 1	5.0	$0.163 \pm 0.030$	$2.8 \pm 0.6$	2.1	3.7
Pre-STA 2	13.8 ± 1.2	$0.169 \pm 0.019$	$4.7 \pm 1.3$	3.1	7.2
		STA-2 FW	3		
Floc	7.6 ± 1.8	0.151 ± 0.037	$9.0 \pm 7.1$	2.0	21.4
RAS	$3.8 \pm 1.3$	$0.261 \pm 0.092$	$6.7 \pm 5.8$	1.4	13.2
Pre-STA 1	5.0	$0.307 \pm 0.033$	5.1 ± 1.0	3.3	7.0
Pre-STA 2	13.5 ± 2.9	$0.281 \pm 0.070$	$13.2 \pm 6.2$	5.1	26.2

**Table 14.** Relationship between P storage in various pools and TP storage in the floc, RAS, and pre-STA soils from STA-2 FW 1 (EAV) and FW 3 (SAV).

Parameter	Regression Equation	R²	Sample Size	p-value						
STA-2 FW 1 (EAV)										
Floc and RAS										
Highly-reactive phosphorus (HRP) pools	Y = 0.24 [TP] - 0.07	0.92	22	<0.0001						
Reactive phosphorus (RP) pools	Y = 0.57 [TP] + 0.01	0.91	22	<0.0001						
Non-reactive phosphorus (NRP) pool	Y = 0.22 [TP] - 0.06	0.85	22	<0.0001						
Total	Total phosphorus – all P pools									
Total inorganic P (TPi)	Y = 0.33 [TP] - 0.16	0.85	22	<0.0001						
Total organic P (TPo)	Y = 0.45 [TP] + 0.22	0.91	22	<0.0001						
Pre-STA soils										
Total inorganic P (TPi)	Y = 0.09 [TP] + 0.23	0.62	22	<0.0001						
Total organic P (TPo)	Y = 0.85 [TP] - 0.55	0.98	22	<0.0001						
	STA-2 FW 3 (SAV)									
	Floc and RAS									
Highly-reactive phosphorus (HRP) pools	Y = 0.29 [TP] - 0.05	0.89	22	<0.0001						
Reactive phosphorus (RP) pools	Y = 0.59 [TP] - 0.09	0.97	22	<0.0001						
Non-reactive phosphorus (NRP) pool	Y = 0.12 [TP] - 0.14	0.79	22	<0.0001						
Total phosphorus – all P pools										
Total inorganic P (TPi)	Y = 0.68 [TP] - 0.71	0.97	22	<0.0001						
Total organic P (TPo)	Y = 0.20 [TP] + 0.57	0.77	22	<0.0001						
Pre-STA soils										
Total inorganic P (TPi)	Y = 0.51 [TP]- 0.89	0.81	22	<0.0001						
Total organic P (TPo)	Y = 0.42 [TP] + 0.75	0.75	22	<0.0001						

#### DISCUSSION

STA-2 FW 1 (EAV) and FW 3 (SAV) are configured parallel to each other with similar long-term hydraulic and nutrient loading rates (**Figure 37**). Total lengths of FW 1 and FW 3 are 5.2 and 4.5 km, respectively. Floc and RAS represent materials accreted since the operation of STAs along with overall nutrient budgets are good indicators to evaluate STA performance to store P. As STAs age, some of the RAS may be compacted and mixed with the surface layer (0- to 5- cm depth) of pre-STA soils and potentially underestimate the recently accreted materials.

Materials accreted in an EAV system are typically dominated by organic matter and most of it is internally generated as litter accumulation in the water column and in the floc layer (**Figure 43**). A portion of the litter is attached to live plant (standing dead litter) and, with time, the litter is detached from the plant and deposited into the water column. During all these stages, litter is undergoing decomposition through abiotic and biotic processes (Reddy and DeLaune 2008). Over time, the litter is partially decomposed and becomes unidentifiable as it is incorporated into the floc, residual undecomposed material is compacted, and develops into a new soil, as defined earlier as RAS (Bhomia et al. 2015). Floc and soils with high organic matter content exhibit low bulk densities, as noted in the Everglades peat soils and other organic rich peat soils (**Table 13**).

TP concentrations in the floc and RAS showed distinct horizontal and vertical gradients. Concentrations and storage were highest near the inflow and steadily decreased along the flow path to the outflow. This trend is consistent within other wetlands receiving defined inflow nutrient loads, such as constructed and natural wetlands (Bhomia and Reddy 2018, Kadlec and Wallace 2009, Reddy and DeLaune 2008, Newman et al. 2017).

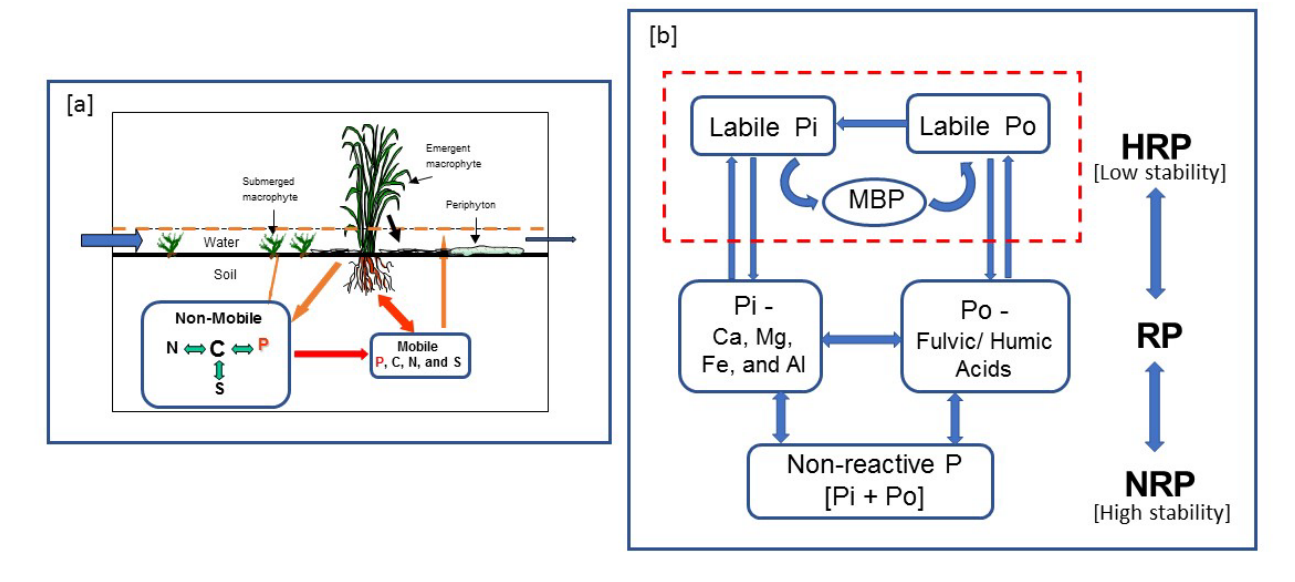


**Figure 43.** (a) Schematic showing mobile and non-mobile pools of macro-elements including P and (b) linkages between reactivity and stability of phosphorus pools in floc and soils.

Labile Pi of HRP includes porewater P and exchangeable P sorbed onto surfaces of metal oxides and recently precipitated amorphous P compounds. Labile Po includes labile organic P extracted with weak alkali (sodium bicarbonate at a pH of 8.5) and MBP. The organic pool primarily includes phosphodiesters (DNA and phospholipids) as identified by NMR. A significant relationship was noted between phosphodiesters and MBP (**Figures 44** and **45**).

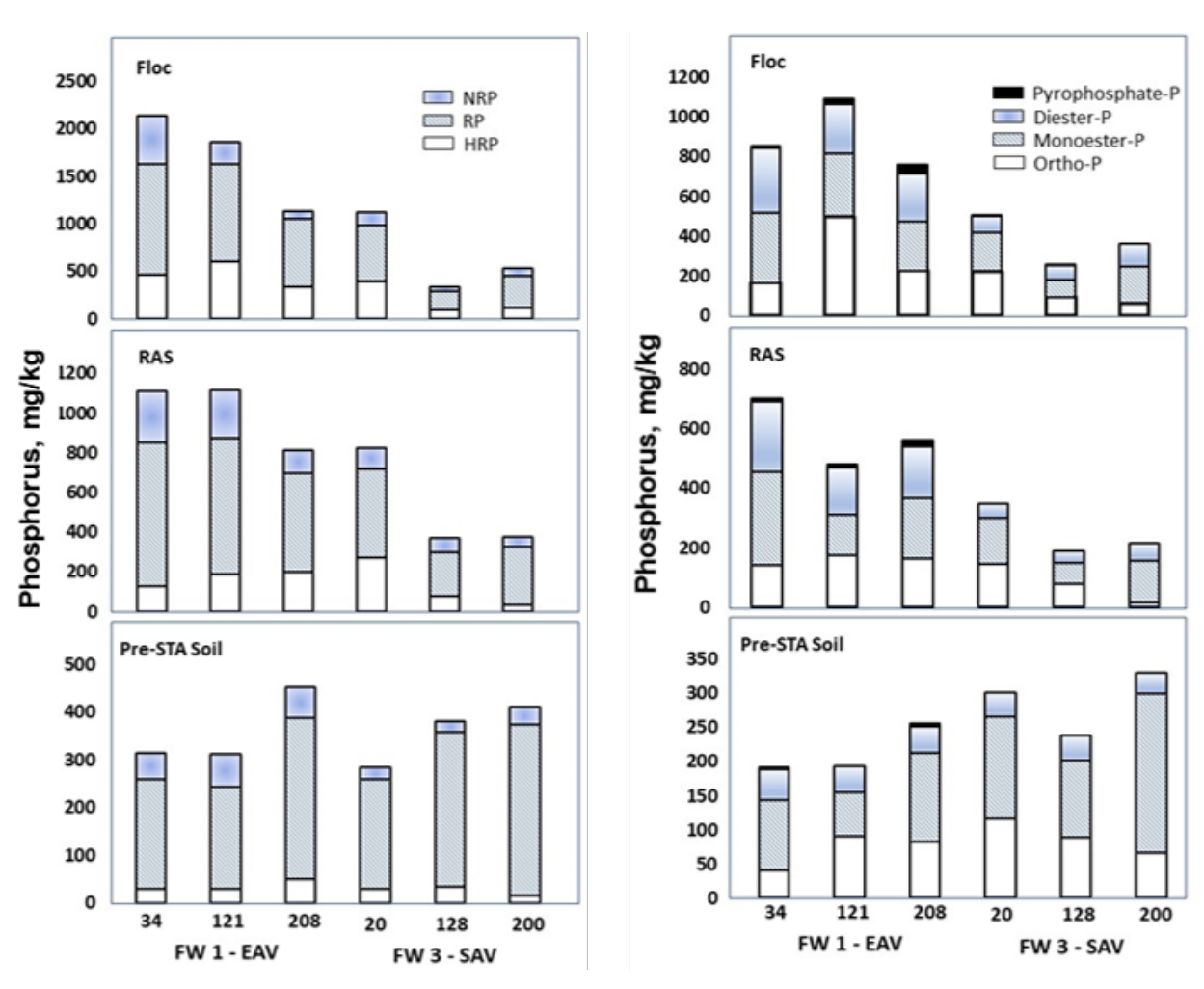
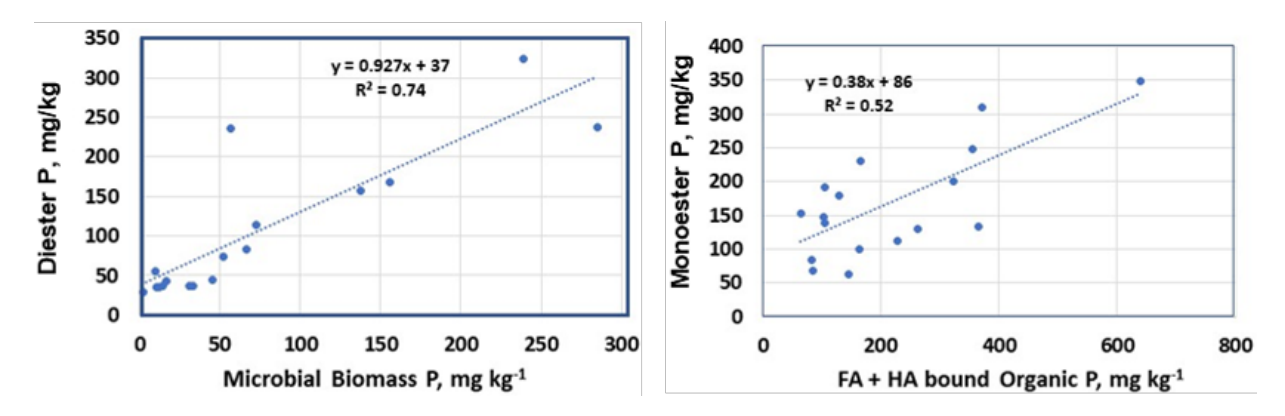


Figure 44. HRP, RP, and NRP estimated by conventional P fractionation method and <sup>31</sup>P-NMR method.



**Figure 45.** Relationship between MBP and phosphodiesters and organic P associated with fulvic and humic acids and phosphomonoesters.

HRP undergoes rapid transformations and interchange between inorganic and organic forms through a series of biotic and abiotic processes in soil layers including floc and RAS. In the EAV system, approximately 24% of the TP was stored in HRP pool as compared to 29% in the SAV system. Inorganic P added to the system is rapidly assimilated into microbial biomass and periphyton followed by uptake by vegetation. Organic P added to the system must first undergo enzymatic hydrolysis where ester linkages (oxygen-P bonds) and P is released into the soil porewater. Both EAV and SAV systems have received similar inorganic and organic P loads, resulting in substantial P enrichment in the plant tissue and in floc and RAS layers at locations in the first-half of the flow path (up to 2 km from inflow) as compared to the second half of the flow path. These results indicate that P assimilation by both microbial communities and vegetation reached saturation level and maintained low N:P ratios, suggesting the systems are shifting from P limitation to N limitation due to surplus P availability. In addition, inorganic P released during mineralization of organic P also maintains high porewater P levels and potentially results in upward P flux into the overlying water column.

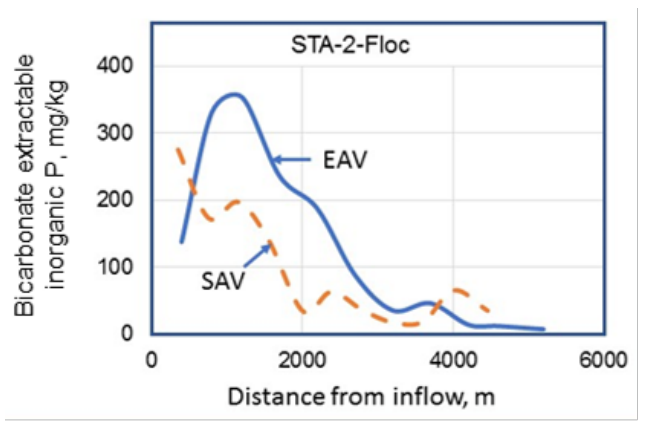
For the whole system, HRP pool P storage in STA-2 was higher (29% of the TP) in the SAV system compared to the EAV system (24% of the TP). The HRP pool can be a major source of internal P load to the water column, until this pool is stabilized.

Reactive inorganic P (referred to as reactive Pi, as extracted by 1 M HCl) can include P forms associated with Ca, Mg, Fe, Al, and reactive organic P (reactive Po) that are soluble in acid and alkali (1 M HCl and 0.5 M NaOH). The organic pool primarily includes phosphomonoesters such as inositol phosphates as identified by NMR. Although, phosphomonoesters are reactive, they are much more abundant in soils than phosphodiesters. Fate of the relatively stable pool is unknown in wetland soils, especially in STAs. A significant relationship was noted between phosphomonoesters and alkali extractable organic P associated with fulvic and humic acids (**Figures 44** and **45**).

On a whole system basis for STA-2, RP pool P storage in EAV and SAV were similar with 57 and 59% of the TP, respectively. The EAV system contained a higher proportion of TP (17 to 22% of the TP) stored in the NRP pool, as compared to 12 to 14% of TP in the SAV system.

During the period of record, the inflow flow-weighted mean TP concentration to STA-2 was 98 µg/L, while the period of record outflow flow-weighted mean TP concentration was 21 µg/L (Chimney 2017). Inflow water to STAs contains both organic and inorganic P forms and both forms go through coupled abiotic and biotic transformations in the water, floc, and soil layers of the STA. In the EAV system, inorganic P added to the water column is rapidly assimilated by the microbes (colonized on the litter and in the floc), periphyton, and vegetation. In addition to P uptake by biotic communities in the SAV system, some of the inorganic P may co-precipitate with calcium carbonate (CaCO<sub>3</sub>) in the water column and settle into the floc. The photosynthetic activity of the SAV creates environmental conditions (high pH driven by low carbon dioxide partial pressure) in the water column that are favorable to the precipitation of CaCO<sub>3</sub> (Farve et al. 2004). Inorganic P can be co-precipitated with the CaCO<sub>3</sub> during periods of high photosynthetic activity in SAV cells in STA-2 (Reddy and DeLaune 2008). Surface water Ca concentration in the overlying water column of both STAs studied ranged from 70 to 113 mg/L in the EAV system and 51 to 104 mg/L in the SAV system (Figure 46). Rapid loss of Ca from the SAV water column, especially in the downstream region of the transect stations, reflects potential CaCO<sub>3</sub> precipitation and accumulation in the floc and RAS layers (Figure 46). However, at stations closer to the inflow, Ca concentrations in the water column showed minimal change in both EAV and SAV systems.

Sources of labile Pi include porewater Pi that is in equilibrium with the Pi sorbed onto metal oxides and organic matter, and mineralization of organic P. This pool of P is readily available to microbes, periphyton, and macrophytes and serves to regulate the P concentration of the overlying water column (Reddy et al. 1998). High concentrations of labile Pi in P enriched areas in the upper portion of EAV and SAV cells suggest that floc and RAS maintain high porewater P concentrations, which can result in upward flux into the water column.



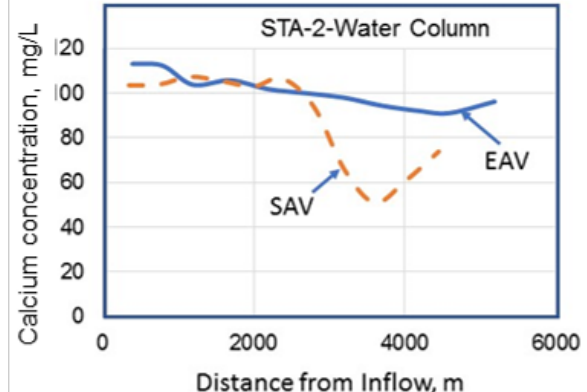


**Figure 46.** Floc-bicarbonate extractable inorganic P (Pi) and overlying water column total calcium concentration as function of distance from inflow in STA-2 FW 1 (EAV) and FW 3 (SAV).

Mineralization of organic P in the floc and RAS of the EAV system is the primary process producing labile Pi. In the EAV system, low N:P ratios and high MBC concentrations in the floc of the upper part of the treatment cell suggests luxury uptake of P by microbes. In the lower part of the treatment cell, much of the labile Pi and labile Po is tied-up in the microbial biomass. In RAS layers of the EAV system, labile Pi decreased, possibly due to microbial and plant uptake. Rapid turnover of microbial biomass results in release of labile Pi, which can potentially flux into the overlying water column. In the SAV system, labile Pi concentrations were high at sites of up to 1.5 km from the inflow of the treatment cell in both floc and RAS layers. It is likely that much of the labile Pi was probably occluded with the CaCO<sub>3</sub> matrix and incorporated into RAS, as indicated by the depletion of labile Pi and possible incorporation into slowly available Pi (HCl-Pi).

The reactive Pi extracted with 0.5 M HCl represents P bound to Ca, Mg, Fe, and Al. The fractionation scheme (**Figure 38**) used does not distinguish P bound to Al and Fe from P bound to Ca and Mg. A significant but weak correlation was observed between HCl extractable Ca and HCl-Pi in the EAV system and the relationship was not significant for the SAV system (data not shown). This suggests other metals may be involved in binding Pi. The relationship between HCl-Pi and HCl-Ca was masked by high concentrations of Ca in the form of CaCO<sub>3</sub>. For example, in STA-2, ratios of HCl-Ca to HCl-Pi ranged from 500 to 3,500 in SAV and 110 to 1,700 in EAV systems, respectively (**Figure 47**). The highest ratios in SAV were observed in areas with high underwater photosynthetic activity, which would bolster CaCO<sub>3</sub> formation and accumulation.

With the exception of two sites, 0.5 M HCl only extracted approximately 10 to 20% of total Fe and 20 to 50% of total Al in floc and RAS of the STA-2 EAV system. In the SAV system, HCl extracted approximately 6 to 17% of total Fe and 17 to 60% of total Al, respectively. Total Fe and total Al showed highly significant correlation with HCl-Pi, suggesting that both Fe and Al may be involved in binding P in these systems.

The acid extraction dissolved 99% of the total Ca and Mg present in the floc and RAS of both EAV and SAV systems, suggesting these metals are present mostly as amorphous and poorly crystalline forms and readily soluble in an acid medium. Previous studies have shown 98 to 100% of P associated with synthetic Ca phosphate was extracted using 0.5 M HCl (Hieltjes and Lijklema 1980, Olila et al. 1994). In the SAV floc and RAS, conditions are ideal for CaCO<sub>3</sub> formation and it is likely that Ca phosphate, Al phosphate, and iron phosphate are occluded with CaCO<sub>3</sub> and retained in the system (Reddy and DeLaune 2008). The role of Fe and Al needs further investigation to determine if these metals are involved in binding P in high Ca systems such as SAV.

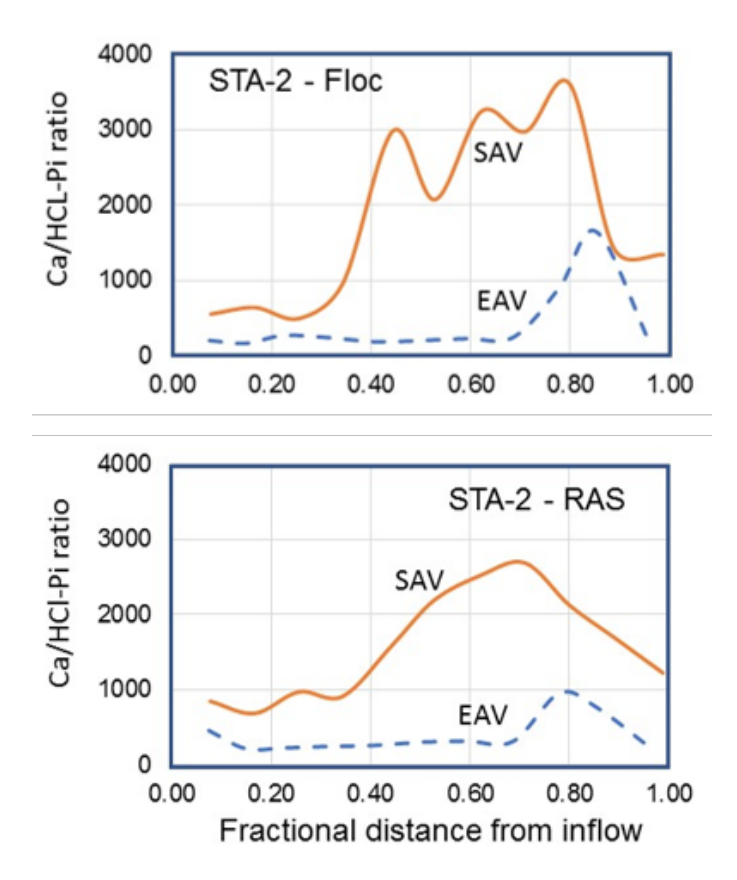


**Figure 47.** Ratio of HCl extractable Ca and Pi in the floc and RAS as a function of distance from inflow of FW 1 (EAV) and FW 3 (SAV) of STA-2.

The dominant inorganic component of RAS samples in FW 1 and FW 3 was  $CaCO_3$ , based on XRD. Calcite was the prevalent mineral, but aragonite (also  $CaCO_3$ ) was also detected in five of the six samples. Other minerals tentatively identified as trace constituents include quartz (SiO<sub>2</sub>), dolomite [CaMg(CO<sub>3</sub>)<sub>2</sub>], and palygorskite [(Mg, Al)<sub>5</sub>(Si, Al)<sub>8</sub>O<sub>20</sub>(OH)<sub>2</sub> ·8H<sub>2</sub>O]. All minerals identified or tentatively identified in the samples analyzed have been previously observed in the greater Everglades region (Das et al. 2012, Farve et al. 2004, Harris et al. 2007, Olila et al. 1994). There is an XRD trend of increasing background and development of an "amorphous hump" in progressing from sample 34 to 208 (i.e., from inflow to outflow) in FW 1. The trend is indicative of an increasing prevalence of noncrystalline materials, to include organic matter and possibly biogenic silica (e.g., diatom frustules and sponge spicules). Organic matter and other noncrystalline components that may be present in the sample constitute diluents that significantly diminish the efficacy of XRD as a tool to detect and identify minerals. It was anticipated that P minerals would be detected in samples with TP concentrations of > 1,000 mg/kg (samples 34 and 121 from FW 1). These concentrations are marginal with respect to prospects of detecting a phosphate mineral via XRD, and none was detected. However, that does not mean that no phosphate mineral is present.

Reactive organic P extracted with acid (HCl-Po) and alkali (FA-P and HA-P) is coupled to organic matter. P bonded to organic matter may include phospholipids, nucleic acids, inositol phosphates, glucose-6-phosphates, glycerophosphates, phosphoproteins, and polymeric organic P of high-molecular-weight compounds (Reddy and DeLaune 2008). Breakdown of organic matter and mineralization of organic P is regulated by several factors including nutrient load; physico-chemical environment of soil, floc, and water column; chemical composition of the litter, floc, and soils; redox conditions; and extreme events including drought, fire, and excessive rainfall. All these factors are pertinent to STAs in regulating biogeochemical processes and P mobility from high concentration zones to low concentration zones. NRP is insoluble in

both acid and alkali solutions and assumed to be in a stable pool. The NRP probably contains both organic and inorganic P forms. At present, the composition of NRP is unknown. It is likely that most of the NRP in the EAV system is dominated by organic forms, as the system is driven by accretion of organic matter and associated nutrients. The SAV is probably dominated by inorganic P associated with the accumulation of metals such Ca, Mg, Fe, and Al.

The ratio of total inorganic P (TPi) to total organic P (TPo) ranged from 0.3 to 1.1 for the EAV system and ratios generally decreased with distance from the inflow (**Figure 48**). These results suggest that the EAV system is primarily driven by biotic processes including the accretion of organic materials and associated elements. In the SAV system, the ratio of TPi to TPo ranged from 0.5 to 5.5, with high values observed in the upper part of the STA and decreased along the transect. High TPi accumulation is attributed to CaCO<sub>3</sub> formation associated with possible co-precipitation of P associated with Ca, Fe, and Al.

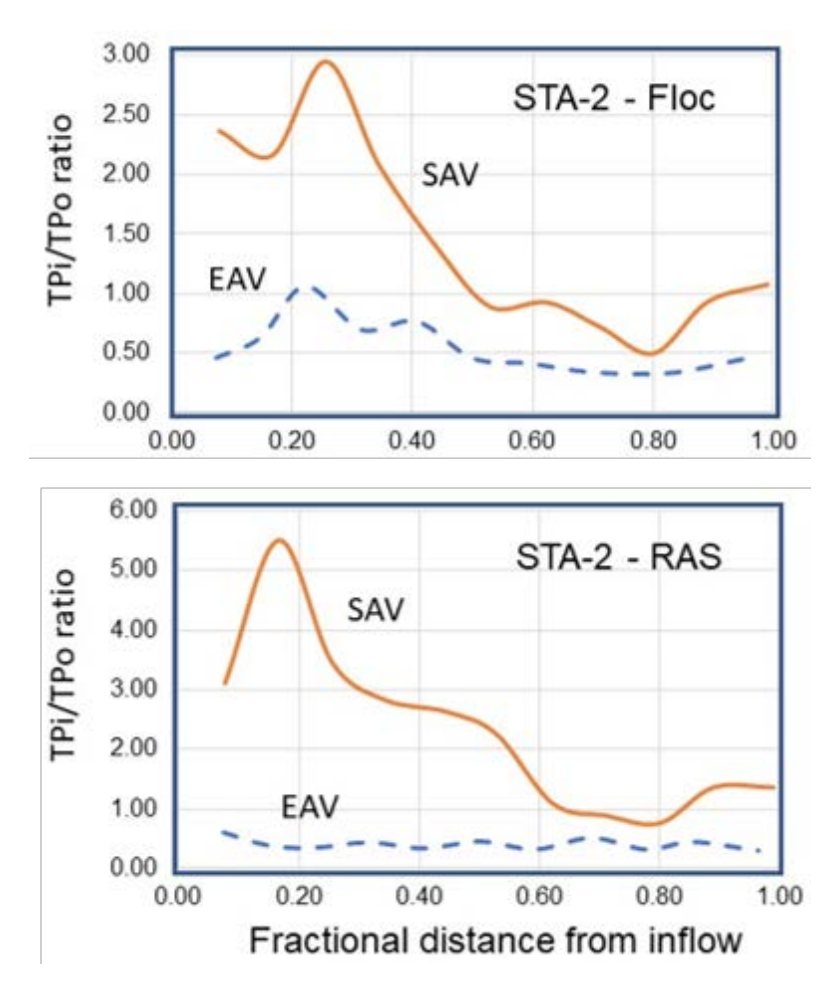


**Figure 48.** Ratio of TPi and TPo in the floc and RAS as a function of distance from inflow of FW 1 (EAV) and FW 3 (SAV) of STA-2.

## **CONCLUSIONS**

Steady loading of P into the STAs has increased the relative proportion of all forms of P in the floc and RAS, with the largest proportion stored in slowly available and refractory forms of organic P. Significant gradients were observed both as a function of distance from each inflow and with soil depth (floc, RAS, and pre-STA soils). P loading increased the proportion of P stored as inorganic P in SAV systems and as organic P in EAV systems. The average ratios (inflow to outflow) of TPi to TPo were 0.6 and 0.4 for floc

and RAS of the EAV system, respectively, decreasing with distance from inflow suggesting greater proportion of organic P accumulation than inorganic P. The average ratios (inflow to outflow) of TPi to TPo were 1.5 and 2.3 for floc and RAS of the SAV system, respectively, decreasing with distance from the inflow suggesting greater proportion of inorganic P accumulation than organic P.

Most of the P sequestered in EAV systems is present in organic forms. In treatment cells dominated by SAV, most of the P is sequestered in inorganic form. Steady nutrient loading to STAs resulted in accumulation of P in the upper portion of the treatment cell and reduction in the ratio of N to P in the floc and RAS. This resulted in a shift from P limitation to N limitation, which will alter the relative rates of biogeochemical processes. The system that originally adapted to high P use efficiency under P limiting conditions is now shifting to low P use efficiency. This results in surplus P that can be potentially transported downstream. Organic P is tightly coupled with organic C, N, and sulfur and cycles of these elements are mutually dependent on each other. For the past several years of STA operation, various organic and inorganic P compounds have substantially accumulated in soils and maintained the stoichiometry of these elements. For STAs to effectively meet the desired outflow TP concentrations, it is important to develop management strategies to keep them under P limiting conditions to avoid P leakage to the water column and downstream transport.

P accumulated in the floc and soils are in both organic and inorganic forms and can be divided into three groups based on their reactivity and stability. These groups are: HRP – highly reactive Pi and Po, RP – moderately reactive Pi and Po, and NRP – non-reactive P. In terms of stability, these P pools can be ranked as NRP > RP > HRP. Selection of vegetation and flow paths in operating STAs should focus on maximizing the rate of HRP conversion to stable P forms that can accrete in the soils of the systems. This information is critical in managing STAs for optimal P removal, because organic P sequestered in areas enriched with P may be remobilized and transported downstream, thus expanding P enrichment areas and export of P in the outflow. The stability of recently accreted P may, therefore, influence the long-term stability of STAs to function in a sustainable manner to maintain desired outflow P concentrations.

# **VEGETATION ASSESSMENTS**

Jill King, Jake Dombrowski, and Matt Powers

## INTRODUCTION

The role of aquatic vegetation is critical to understanding the removal of TP and other nutrients from the STAs. Vegetation communities in the STAs were surveyed and sampled with the overall objective of relating vegetation characteristics to water column P, floc, and soil P storage and stability, soil characteristics, soil accretion, and ultraviolet radiation/light penetration.

Currently, there is little information on vegetation biomass, species composition, and nutrient storage capacities in the STAs. The study builds on existing information and compares results from other project components in efforts to determine the level of influence of vegetation nutrient removal and storage. The study evaluates vegetation in STA-2 FW 1 and FW 3. FW 1 has predominantly EAV while FW 3 consists primarily of SAV. These FWs historically have had good performance and provide good comparisons of vegetation nutrient removal and storage.

### **METHODS**

Vegetation was sampled from STA-2 FW 1 and STA-2 FW3 in November 2015 and September 2016. An additional sampling event occurred in August 2017 for STA-2 FW3. These dates were selected opportunistically based on the limitations of staff resources and suitable field conditions that supported the harvesting of the vegetation (i.e. water depths). Sites were located at the inflow, midflow, and outflow regions of each FW (**Figure 50**) consistent with study sites for the other P Flux Study substudies, which measured water quality, soils, and microbial activity. In conjunction with the vegetation sampling, more frequent SAV surveys have been conducted in FW 3 on a quarterly basis, which provides more detailed information on biomass and species composition in the FW.



Figure 49. Location of vegetation sampling sites in STA-2 FWs 1 and 3.

STA-2 FW 1 vegetation has consisted almost entirely of cattail (*Typha domingensis*) with sawgrass (*Cladium jamaicense*) in lesser quantities with varying species of SAV underlying the water column. Other common vegetation species include water lettuce (*Pistia* sp.) and water lily (*Nymphaea odorata*)

STA-2 FW 3 vegetation species composition varies spatially and temporally. Since 2013 when SAV surveys were initiated in this FW, species have historically consisted of a mix of hydrilla (*Hydrilla* sp.), hornwart (*Ceratophyllum*), and common water nymph (*Najas guadalupensis*) at the inflow region, chara (*Chara* sp.) at the midflow region, and a mix of *Chara*, pondweed (*Potamogeton*), spiny naiad (*Najas marina*), and *Najas guadalupensis* at the outflow region.

Vegetation was harvested from random quadrats at the inflow, midflow, and outflow regions of each FW. For each sampling event, a 10-m x 10-m plot was demarcated with poly vinyl chloride (PVC) poles at each location, within which 0.25-square meter (m²) quadrats were randomly placed. The study used 4 quadrats per site for the first sampling event but was then revised to 8 quadrats per site for subsequent sampling events in an effort to obtain a more representative sample from each site. For SAV collections, 0.25m² box corers (**Figure 50**) were placed at randomly selected sites and using a hand-held jab saw, the material within the box corer was cut and carefully removed with a garden rake and placed into labeled resealable bags. Photos were taken at each site, and SAV species identification, SAV coverage by species, depth measurements, GPS coordinates, and any other relevant field conditions were recorded.





Figure 50. Harvest sites in STA-2 FWs 1 and 3 depicting the harvest equipment and field conditions.

For EAV collections, a 0.25-m² area was demarcated with PVC poles (**Figure 50**) and aboveground and belowground material was collected within this area. A hand-held jab saw was placed as far down as possible into the soil to cut and remove the vegetation material along the footprint of the PVC quadrat. The harvested material that included all plant components (roots, rhizomes, shootbases, etc.) were placed into large labeled burlap bags. Site photos were also taken, and the following information was recorded: time of harvest, species collected, coverages per species, water depth measurements, latitude/longitude, and any other relevant field conditions. Other important information, e.g. the number of live adults, dead adults, and juveniles and length measurement of the tallest leaf of all the plants within the quadrat, were also recorded.

The samples were transported to District facilities for cleaning. During cleaning, the EAV was separated into 5 plant parts: live leaves, dead leaves, roots, rhizomes, and shoot bases. All samples were placed in a drying oven at 60° Celsius.

Once the samples were sufficiently dried, the material was weighed and finely ground using a Wiley Mill. Samples were analyzed for TP, total nitrogen (TN), total carbon (TC), ash content, and total calcium (TCa; SAV only). P storages for SAV and EAV were calculated using biomass and tissue TP concentrations.

### **RESULTS**

### STA-2 Flow-Way 1

The predominant EAV found in STA-2 FW 1 was *Typha domingensis*. Other species were found and collected but not analyzed due to relatively small quantities. These included *Cladium jamaicense*, *Pistia* sp., and *Nymphae odorata*.

## EAV (Typha) Biomass and Nutrient Concentration

*Typha* biomass at all sites was consistently lower in 2016 than in 2015. The highest biomass was found at the inflow, while the lowest biomass was at the midflow site. The two-year average biomass was approximately 5, 2.5, and 4 kilograms per square meter ( $kg/m^2$ ) at the inflow, midflow, and outflow regions, respectively (**Figure 51**).

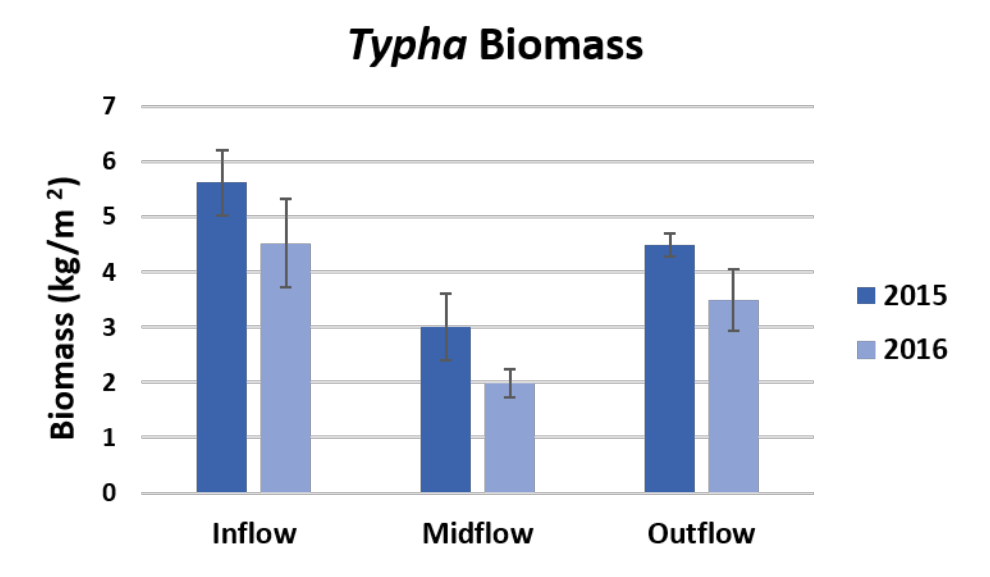


Figure 51. Typha biomass at the inflow, midflow, and outflow sites in 2015 and 2016.

Trends of TP concentrations in *Typha* were different between 2015 and 2016. For the 2015 event TP concentrations declined from inflow to outflow (**Figure 52**), however in 2016, concentrations were almost the same from inflow to outflow and then declined from the midflow to the outflow. The inflow to outflow gradient in TP concentration was evident in all the plant components, except for live leaves in 2016, which increased slightly from the inflow to the midflow site. Among the different *Typha* plant components, TP concentrations were highest in the shoot bases and rhizomes and lowest in dead leaves for both sampling events and at all stations (**Figure 53**).

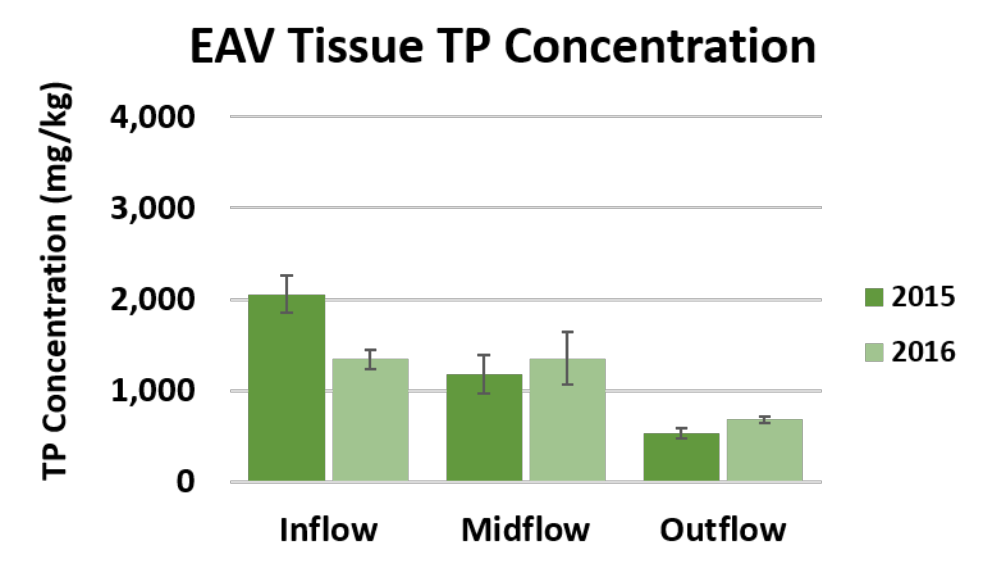
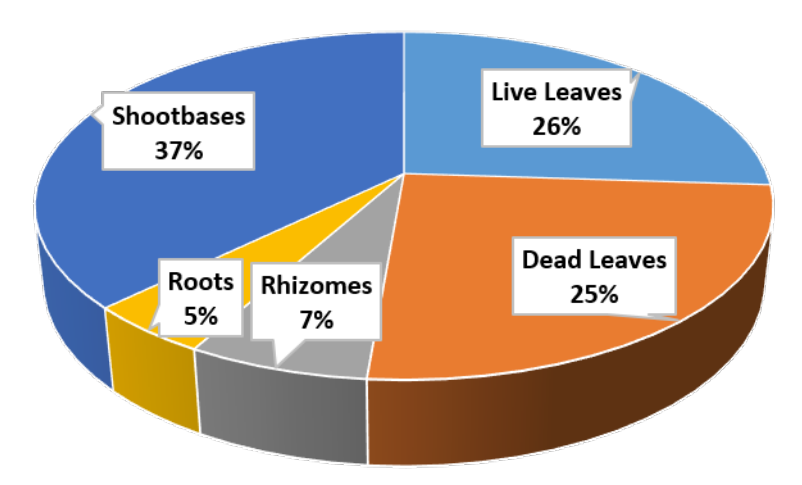


Figure 52. Average TP concentration in EAV in STA-2 FW 1 in 2015 and 2016.

# Typha TP Storage by component



**Figure 53.** Distribution of TP storage in each plant component in *Typha* sp. tissues from STA-2 FW 1 over two sampling events in 2015 and 2016. Percentages represent the average of TP storage in each plant component over the two sampling events.

The inflow to outflow gradient is also evident in TP storage in plant tissues (**Figure 54**), with 4.51, 1.93, and 1.07 g/m<sup>2</sup> at the inflow, midflow, and outflow, respectively, in 2015 and 5.09, 2.17, and 2.02 g/m<sup>2</sup> at the inflow, midflow and outflow, respectively in 2016. Among the different plant components, shoot bases had the highest TP storage (37% of the total plant TP storage), followed by live leaves (26%), and dead leaves (25%). Aboveground storage in live and dead leaves and belowground (shoot bases, roots, and rhizomes) were 51 and 49% of the total plant storage, respectively (**Figure 53**).

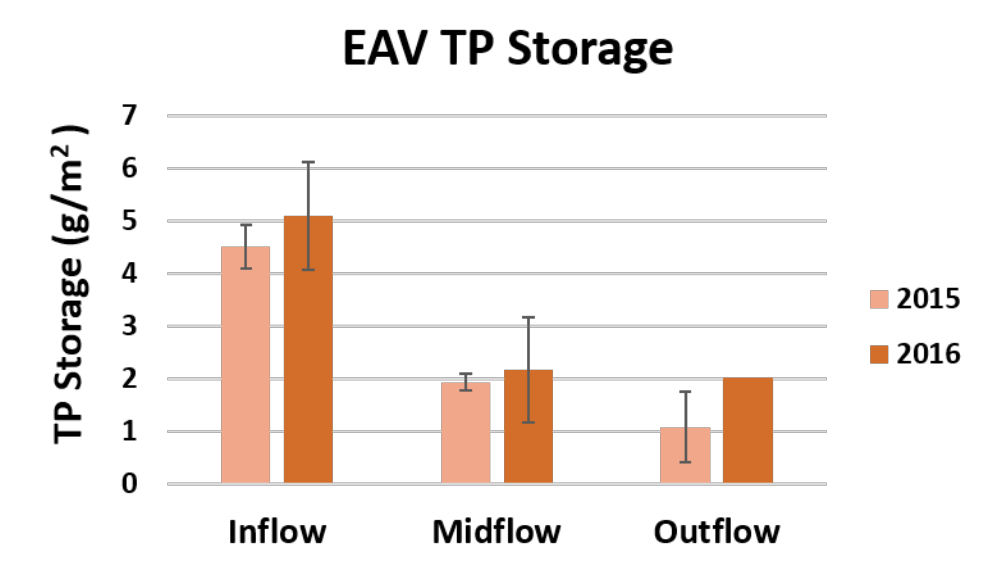
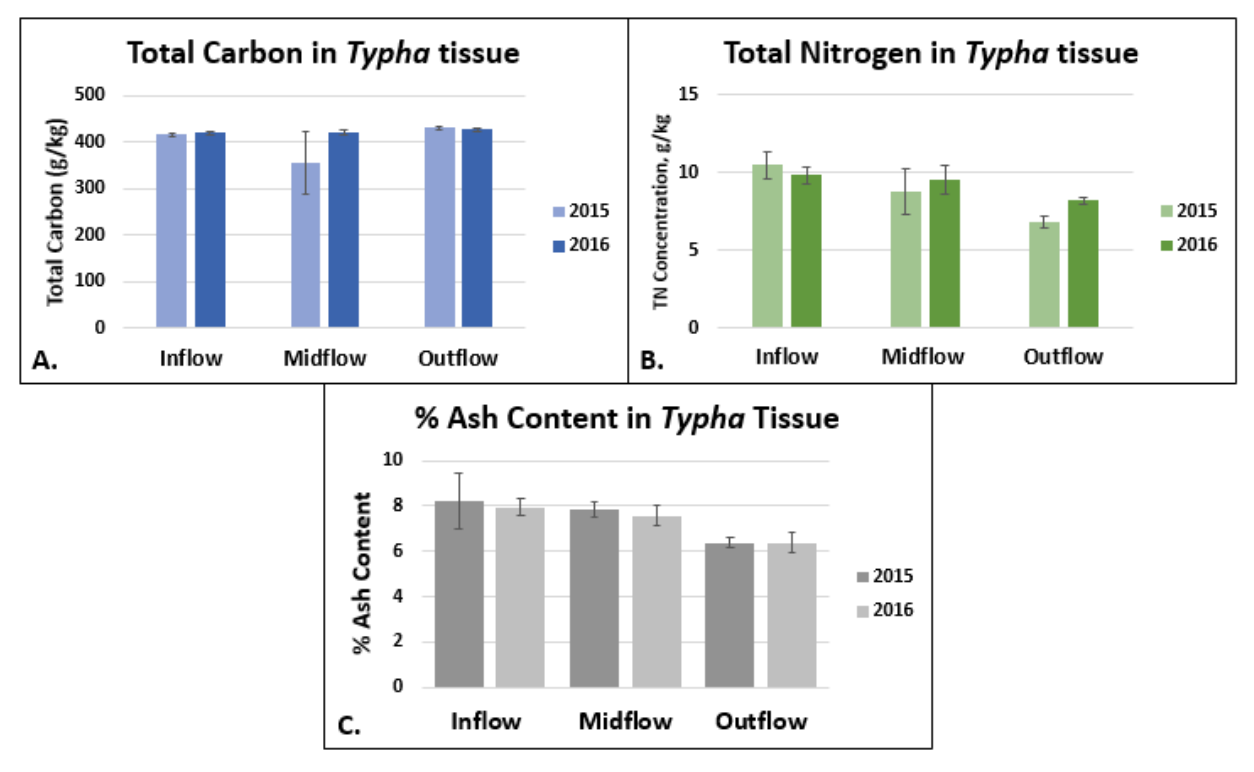


Figure 54. Average TP storage in EAV from STA-2 FW 1 in 2015 and 2016.

TC concentrations in *Typha* tissues in the first sampling event (2015) differed slightly along the FW, with concentrations of 416, 355, and 430 g/kg at the inflow, midflow, and outflow, respectively (**Figure 55**). In 2016, TC concentrations were similar spatially, at 419, 421, and 427 g/kg at the inflow, midflow, and outflow, respectively.



**Figure 55.** Average (A) TC and (B) TN concentrations, and (C) ash content in the *Typha* sp. tissues from STA-2 FW 1 at the inflow, midflow, and outflow locations in 2015 and 2016.

TN concentrations in *Typha* tissues declined slightly from inflow to outflow sites for both sampling events at 10, 9, and 7 g/kg at the inflow, midflow, and outflow for the 2015 sampling event, respectively, and 9.8, 9.5, and 8.2 g/kg at the inflow, midflow, and outflow for the 2016 sampling event, respectively (**Figure 56**). TN concentrations were similar at the inflow and midflow stations for both years but were higher at the outflow station in 2016.

Ash content in *Typha* tissues declined slightly from inflow to outflow for both sampling events. The results for the 2015 sampling event were 8.2, 7.9, and 6.4% at the inflow, midflow, and outflow, respectively. For the 2016 sampling event, ash content was 7.9, 7.6, and 7.8% at the inflow, midflow, and outflow, respectively (**Figure 56**).

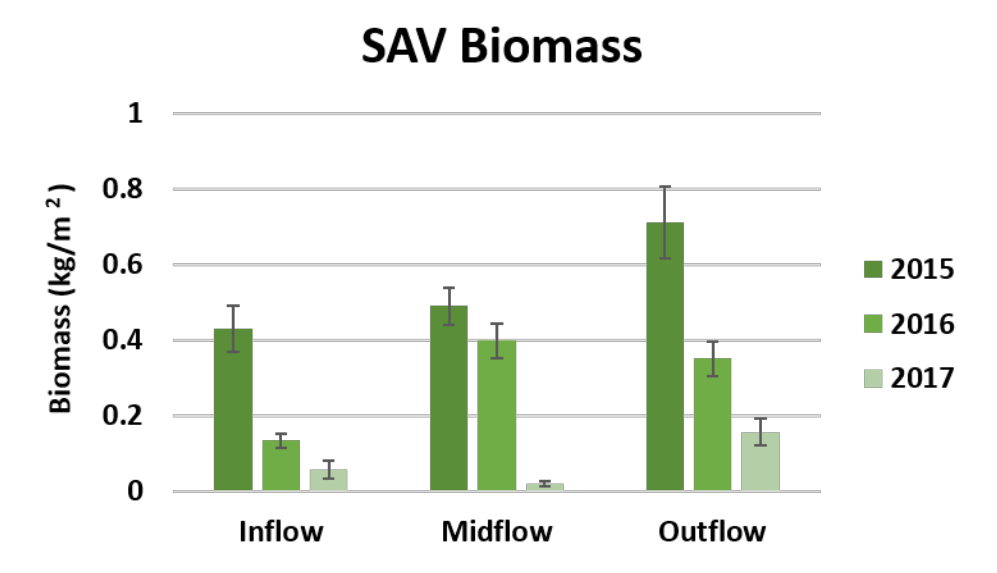


**Figure 56.** Comparison of SAV biomass at the inflow, midflow, and outflow sites in 2015, 2016, and 2017.

## STA-2 Flow-Way 3

### SAV Species Composition and Biomass

Species composition of SAV differed among sites within STA-2 FW 3. In the first sampling event, a mix of *Hydrilla* and *Ceratophyllum* was observed at the inflow region. The second sampling event in 2016 took place just after a significant bloom of water silk (*Spirogyra*), which seemed to choke out other SAV species. In the 2016 and 2017 sampling events, *Spirogyra* was the only species present at the inflow region, with substantially less biomass between the last two sampling events. The overall average biomass at the inflow declined from 0.43 to 0.05 kg/m² from 2015 to 2017 (**Figure 56**). This region of the FW received the highest loading (hydraulic and nutrient) and experienced the deepest water depths (60.5, 95.8, and 101.9 cm in 2015, 2016, and 2017, respectively) and highest turbidity during sampling events compared to the remainder of the flow-way.

At the midflow region, the vegetation consisted entirely of *Chara* during the three-year period. The region had dense *Chara* coverage in the first two sampling events with the vegetation topped out at the water surface and filling the water column often making the collection and placement of the box corer difficult. However, the region location experienced a substantial loss of biomass, as noted in the 2017 sampling event, with biomass decline from 0.49 kg/m² in 2015 to 0.02 kg/m² in 2017 (**Figure 56**). Water depths also increased in this region, from an average water depth of 61 cm in 2015, to 81 and 83 cm in 2016 and 2017, respectively.

The outflow region had the highest SAV species diversity with a mix of *Chara, Potamogeton, Najas marina*, and *Najas guadalupensis*. This region saw a decline in biomass from 0.71 to 0.16 kg/m² between 2015 and 2017 (**Figure 56**). Overall, the FW experienced a reduction of SAV biomass at the inflow, midflow, and outflow sites for the three sampling events, with the midflow experiencing the greatest loss of SAV biomass. Water depths at the outflow region remained relatively consistent across sampling events with average depths of 70.5, 74.9, and 75.9 cm in 2015, 2016, and 2017, respectively.

## **SAV Nutrient Composition**

Average SAV TP concentrations decreased from inflow to outflow locations for all three sampling events (**Figure 57**). Average TP concentration was highest at the inflow (2,981 mg/kg) and lowest at the outflow (590 mg/kg) despite the differences in SAV composition at each site. There were no clear trends for TP storage, however these results suggest a difference in storage capacities of the different SAV species (**Figure 58**).

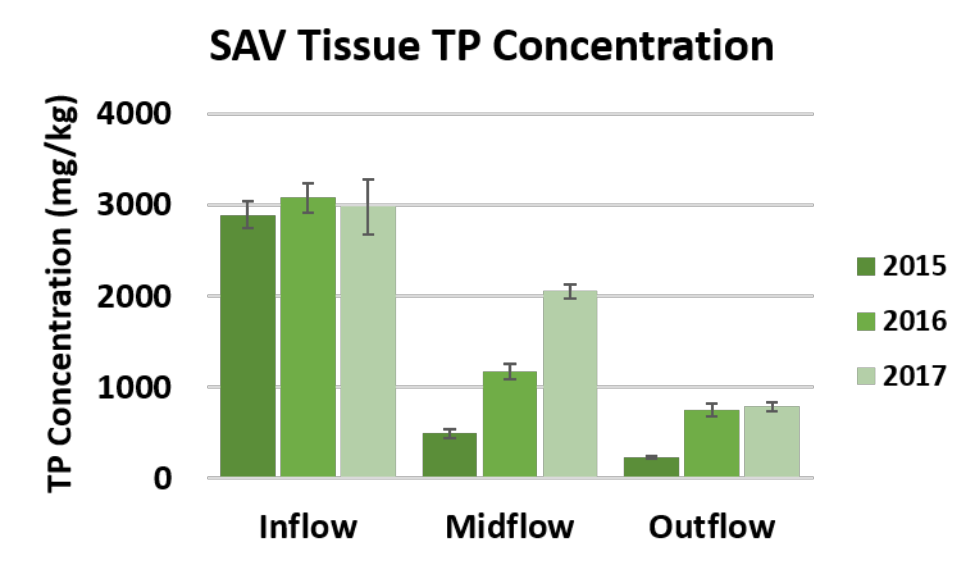


Figure 57. Average TP concentrations in SAV from STA-2 FW 3 in 2015, 2016, and 2017.

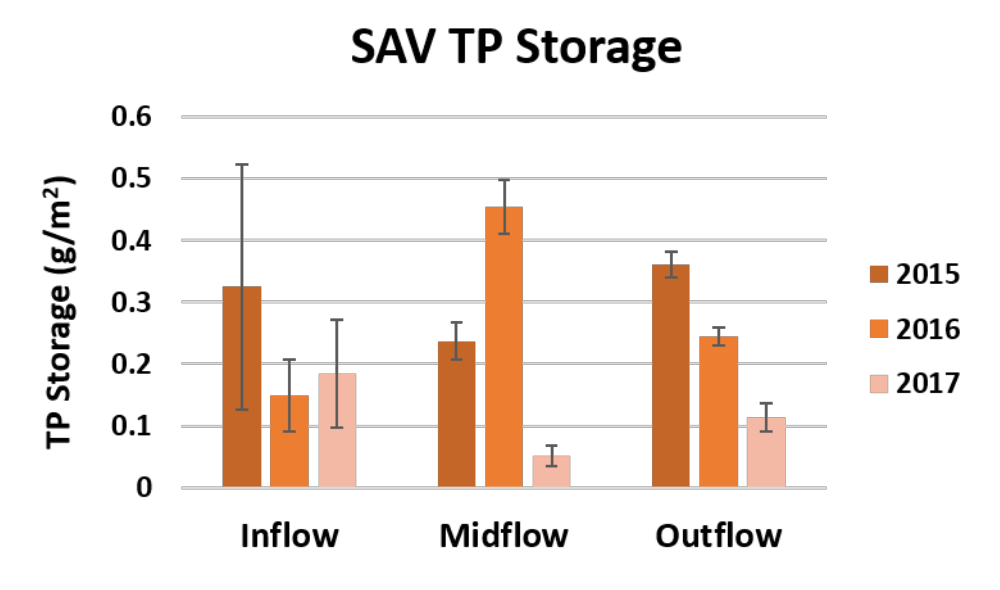
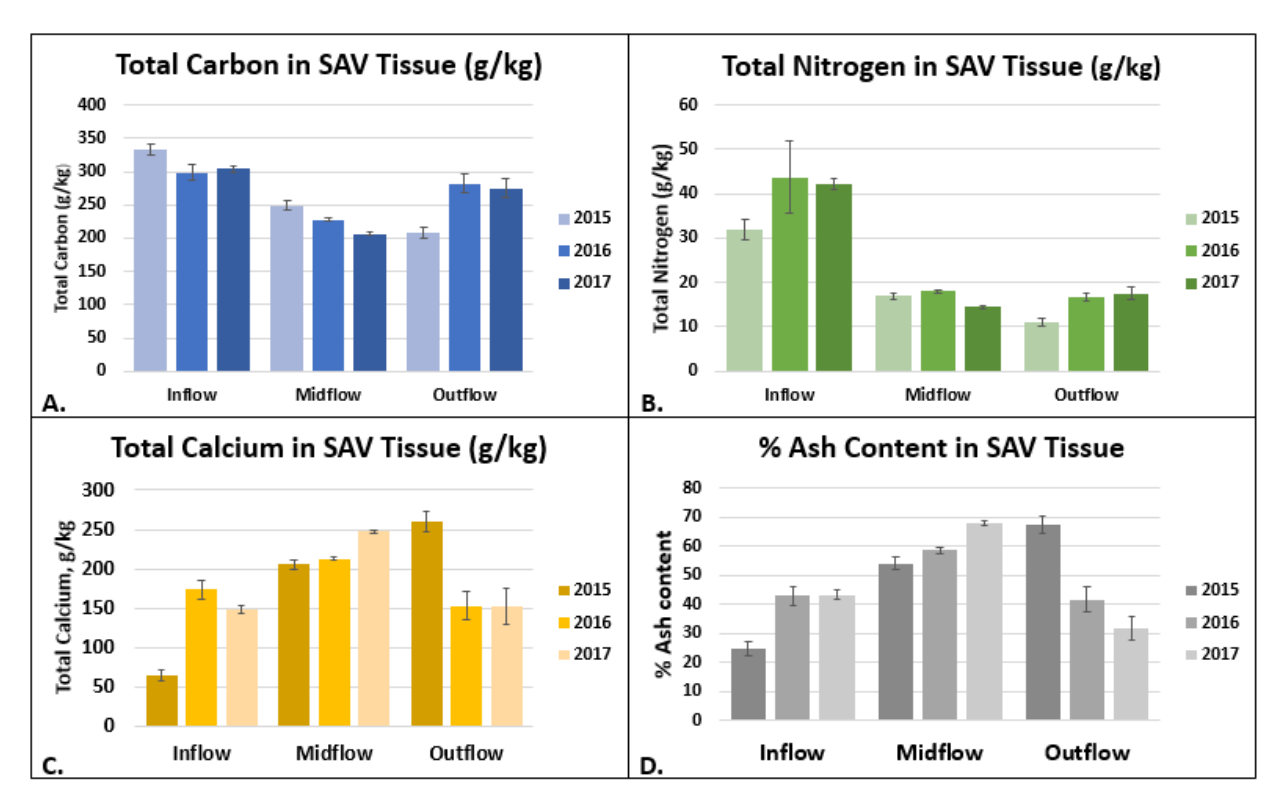


Figure 58. Average TP storage in SAV from STA-2 FW 3 in 2015, 2016, and 2017.



**Figure 59.** Average TC, TN, TCa concentrations, and ash content in the SAV at the inflow, midflow, and outflow regions of STA-2 FW 3 in 2015, 2016, and 2017.

For SAV, average TC concentrations were highest at the inflow region in all three sampling events (**Figure 59**). TC concentrations declined from the inflow to the outflow region in 2015 but increased between the midflow region and outflow region in 2016 and 2017 (average of 311, 228, and 255 g/kg at the inflow, midflow, and outflow, respectively. A declining temporal gradient was observed at the midflow site over the three sampling events. TC concentrations were consistently highest at the inflow region, despite the change in species composition and shift to the *Spirogyra* algae species.

TN concentrations in the SAV were highest at the inflow region for all three sampling events (**Figure 59**). TN concentrations decreased spatially in the first sampling event, however in the 2016 and 2017 sampling events, the concentrations at midflow and outflow regions were similar with averages of 39, 16, and 15 g/kg at the inflow, midflow, and outflow, respectively). Despite the changes in biomass at all the sites, the TN concentrations remained fairly constant spatially at the midflow and outflow sites.

No clear trends were observed for the TCa concentrations (**Figure 59**). At the inflow site, TCa concentrations increased over time between the first two events, but then decreased from the second to the third event, possibly with the change in species composition at the site. TCa concentrations increased at the midflow site over the three events. There was a substantial decline in concentrations at the outflow region between the first and second year. Ca concentrations averaged 129, 222, and 189 g/kg at the inflow, midflow, and outflow sites, respectively (**Figure 59**).

Ash content increased from inflow to outflow in 2015 (**Figure 59**). However, in 2016 and 2017, ash content increased from inflow to midflow regions followed by a sharp decline at the outflow region. Ash content at the inflow and midflow regions increased over the three years while ash content at the outflow region declined. Ash content averaged 37, 60, and 47% at the inflow, midflow, and outflow, respectively (**Figure 59** and **Table 15**). The overall mean biomass and nutrient content for the sites in both FWs over all sampling events are shown in **Table 15**.

**STA-2 FW 1 (EAV)** STA-2 FW 3 (SAV) **Parameter** Units Inflow Midflow Outflow Inflow Midflow Outflow **Dry Biomass**  $5.07 \pm 0.78$  $2.50 \pm 0.73$  $3.99 \pm 0.71$  $0.21 \pm 0.20$  $0.30 \pm 0.25$  $0.41 \pm 0.28$ kg/m<sup>2</sup> **Total Phosphorus**  $7.22 \pm 1.06$  $5.48 \pm 0.07$  $2.59 \pm 0.55$  $2.98 \pm 0.09$  $1.24 \pm 0.78$  $0.59 \pm 0.31$ g/kg **Total Carbon**  $417 \pm 2.4$  $388 \pm 46.2$  $249 \pm 2.2$  $260 \pm 104$  $226 \pm 32$  $245 \pm 52$ g/kg  $37.8 \pm 8.5$ Total Nitrogen g/kg  $10.1 \pm 0.45$  $9.1 \pm 0.51$  $7.5 \pm 0.96$  $17.5 \pm 0.73$  $13.9 \pm 3.9$ **Total Calcium** NA 129 ± 57  $222 \pm 22$  $189 \pm 62$ g/kg NA NA Ash Content  $8.08 \pm 0.2$  $7.72 \pm 0.22$  $7.08 \pm 0.99$  $36.9 \pm 10.5$  $60.1 \pm 7$  $46.9 \pm 18.4$ %

**Table 15.** Mean biomass and nutrient content (± 1 standard deviation) for EAV and SAV vegetation in STA-2 FW 1 and STA-2 FW 3. Values represent the mean of all sampling events per FW.

### **SUMMARY**

Two biomass sampling events were conducted in STA-2 FW 1 (EAV [*Typha* sp.]) and three events in STA-2 FW 3 (SAV) between 2015 and 2017. Overall, both EAV and SAV total plant biomass declined at each of the sites over all of the sampling events. In FW 3, SAV communities steadily declined from July 2015 onward, but the most substantial loss occurred over the last two years, coinciding with extreme weather and flow events. A complete loss of SAV was noted in FW 3 during the February 2018 survey. High loading, high water levels for extended periods of time, herbivory, and recent major storms are all potential factors resulting in the SAV biomass loss. FW 3 has historically been one of the most utilized FW of all the STAs in terms of flows and loads. STA-2 received the largest TP load of all the STAs in WY2018, with an inflow TP load of 87 t and an HLR of about 2.4 centimeters per day (cm/d) (Chimney, 2019).

EAV biomass was highest at the inflow region while SAV biomass was highest at the outflow region. The observed gradient in the EAV biomass is an indication of overall productivity as a nutrient gradient in the water column, floc, and soil. The observed spatial trend in SAV biomass is likely due to this plant type's preference for lower nutrient concentration and the species differences (i.e. predominantly *Spirogyra* species in the front region and predominantly a mix of *Chara*, *Potamogeton*, *Najas marina*, and *Najas guadalupensis* in the outflow region). These factors will continue to be analyzed through the remainder of the study.

Over the three years, SAV species composition at the inflow of FW3 transitioned from *Hydrilla* and *Ceratophyllum* to *Spirogyra*. While the actual cause of this species transition is still being investigated, observations and data indicates the inflow region is generally deeper than the rest of the FW and has large open compartments with little to no emergent vegetation to provide some buffer from wind and wave action. Turbidity is typically higher in this part of the FW, which may result in less than ideal light conditions for more favorable SAV species to thrive. High nutrient loading directly into the SAV area is also likely a major factor. The midflow site was consistently *Chara* but experienced the most substantial SAV loss of the three sites over the three years of the study. The vegetation species in the outflow region remained consistent among the species observed, however the region also experienced a significant loss in biomass over the three years.

The TP concentration gradient from inflow to outflow was observed for all events and both vegetation types. TP concentrations in *Typha* were comparable between 2015 and 2016, with highest TP concentrations at the inflow and declining toward the outflow region. This trend was observed in all the plant components, except for the live leaves in 2016, which increased slightly in TP concentration from the inflow to midflow site. Shoot bases had the highest TP concentrations and TP storage at all sites. The distribution of TP storage in above and belowground components were similar, with live and dead leaves accounting for 51% of the P mass storage and the belowground (shoot bases, roots, and rhizomes) accounting for 49% of the P mass storage.

TP storage was much higher in EAV than SAV for all sites, indicating higher productivity in large macrophyte communities. TP storage in SAV remained relatively constant spatially and temporally whereas storage in EAV was more than twice as high at the inflow than the midflow and outflow sites. It is evident from these results that the vegetation difference between the two cells influence the mode and trend in P reduction and storage in these FWs.

Concentrations of TC in *Typha* tissues remained nearly the same at each of the sites between 2015 and 2016 while no obvious spatial or temporal trends in TC were observed for SAV. Concentrations of TN in *Typha* were generally consistent between 2015 and 2016 with a slight gradient from inflow to outflow sites. For SAV, TN remained relatively consistent during the three years (2015–2017) and a gradient from inflow to outflow was not observed for the first two years. The third event saw a significant shift in biomass at the midflow. Ash content in *Typha* declined slightly from inflow to outflow in 2015, but in 2016 increased from midflow to outflow. For SAV, ash content increased in 2015, then decreased from midflow to outflow in 2016 and 2017. The ash content at the midflow region increased from 2015 to 2017 despite the substantial loss of SAV at this region.

Another sampling event was conducted in STA-2 FW 1 in March 2018 (dry season), but data was not available for analysis at the time of the development of this appendix. This sampling will provide some comparisons seasonally as this event was conducted in the dry season. The next harvesting events took place in April and May 2018 in STA-3/4 Cell 3A (EAV-dominated cell) and Cell 3B (SAV-dominated cell) and are currently being processed. These sites in STA-3/4 will continue to be sampled and will provide valuable comparisons amongst these FWs.

# LITERATURE CITED

- Bhomia, R.K., P.W. Inglett and K.R. Reddy. 2015. Soil and phosphorus accretion rates in sub-tropical wetlands: Everglades Stormwater Treatment Areas as a case example. *Science of the Total Environment* 533:297-306.
- Bhomia, R.K. and K.R. Reddy. 2018. Influence of vegetation on long-term phosphorus sequestration in subtropical treatment wetlands. *Journal of Environmental Quality*, doi: 10.2134/jeq2017.07.0272.
- Bostic, E.M., J.R. White, R. Corstanje and K.R. Reddy. 2010. Redistribution of wetland soil phosphorus ten years after the conclusion of nutrient loading. *Soil Science Society of America Journal* 74:1808-1815.
- Boudreau, B.P. 1996. The diffusive tortuosity of fine-grained unlithified sediments. *Geochimica et Cosmochimica Acta* 60:3139-3142.
- Cade-Menun, B. and C.W. Liu. 2013. Solution Phosphorus-31 Nuclear Magnetic Resonance Spectroscopy of Soils from 2005 to 2013: A Review of Sample Preparation and Experimental Parameters. *Soil Science Society of America Journal* 78:19-37.
- Carignan, R. 1984. Interstitial water sampling by dialysis: Methodological notes. *Limnology and Oceanography* 29:667-670.
- Cheesman, A.W., B.L. Turner and K.R. Reddy.2012. Soil phosphorus forms along a strong nutrient gradient in a tropical ombrotrophic wetland. *Soil Science Society of America Journal* 76:1496-1506.
- Chen, H., D. Ivanoff and K. Pietro. 2015. Long-term phosphorus removal in the Everglades stormwater treatment areas of South Florida in the United States. *Ecological Engineering* 79:158-168.
- Chimney, M.J. 2017. Chapter 5B: Performance and Operation of the Everglades Stormwater Treatment Areas, *South Florida Environmental Report Volume I.* South Florida Water Management District, West Palm Beach, FL.

- Chimney, M.J. 2019. Chapter 5B: Performance and Operation of the Everglades Stormwater Treatment Areas, *South Florida Environmental Report Volume I.* South Florida Water Management District, West Palm Beach, FL.
- Corstanje, R., D.R. Grafius, J. Zawadska, J.M. Barradas, G. Vince, D. Ivanoff and K. Pietro. 2016. A datamining approach to identifying spatial patterns of phosphorus forms in the stormwater treatment areas in the Everglades, USA. *Ecological Engineering* 97:567-576.
- Das, J., S.H. Daroub, J.H. Bhadha, T.A. Lang, O.A. Diaz and W.G. Harris. 2012. Physicochemical assessment and phosphorus storage of canal sediments within the Everglades Agricultural Area, Florida. *Journal of Soils and Sediments* 12:952-965.
- DBE. 2017. Field and Supplemental Laboratory Support for Evaluating Phosphorus Sources, Flux, and Transformation Processes in the Stormwater Treatment Areas Annual Report. Prepared by DB Environmental, Inc. under Agreement 4600003029-WO01 for South Florida Water Management District, West Palm Beach, FL. Submitted June 2, 2017.
- Dickhudt, P.J., C.T. Friedrichs, L.C. Schaffner, and L.P. Sanford. 2009. Spatial and temporal variation in cohesive sediment erodibility in the York River Estuary, eastern USA: A biologically influenced equilibrium modified by seasonal deposition, *Marine Geology* 267:128-140.
- Dickhudt, P.J., C.T. Friedrichs and L.P. Sanford. 2011. Mud matrix solids fraction and bed erodibility in the York River Estuary, USA, and other muddy environments. *Continental Shelf Research* 31:S3-S13.
- Dierberg, F.E., T.A. DeBusk, S.D. Jackson, M.J. Chimney and K.C. Pietro. 2002. Submerged aquatic vegetation-based treatment wetlands for removing phosphorus from agricultural runoff: Response to hydraulic and nutrient loading. *Water Research* 36:1409-1422.
- Dierberg, F.E., T.A. DeBusk, J.L. Henry, S.D. Jackson, S. Galloway and M.C. Gabriel.2012. Temporal and spatial patterns of internal phosphorus recycling in a South Florida (USA) stormwater treatment area. *Journal of Environmental Quality* 41:1661-73.
- Farve, M, W.G. Harris, F. Dierberg and K. Portier. 2004. Association between phosphorus and suspended solids in an Everglades treatment wetland dominated by submersed aquatic vegetation. *Wetlands Ecology and Management* 12:365-375.
- Ferre, B., C.R. Sherwood and P.L. Wibergb. 2010. Sediment transport on the Palos Verdes Shelf, California. *Continental Shelf Research* 30:761-780.
- Fisher, M.M. and K.R. Reddy.2001. Phosphorus flux from wetland soils affected by long-term nutrient loading. *Journal of Environmental Quality* 30:261-271.
- Gust, G. and V. Mueller. 1997. Interfacial hydrodynamics and entrainment functions of currently used erosion devices. Pages 149–174 in Cohesive Sediments, Burt, Parker and Watts, Wallingford, UK.
- Harris, W.G. and G.N. White. 2008. X-ray diffraction techniques for soil mineral identification. Pages 81–115 in: A. Ulery and R. Drees (eds.), Methods of Soil Analysis: Part 5 Mineralogical Methods. Soil Science Society of America, Madison, WI.
- Harris, W.G., M.M. Fisher, X. Cao, T. Osborne and L. Ellis.2007. Magnesium-rich minerals in sediment and suspended particulates of South Florida water bodies: Implications for turbidity. *Journal of Environmental Quality* 36:1670-1677.
- Hesslein, R.H. 1976. An in-situ sampler for close interval pore water studies. *Limnology and Oceanography* 21:912-914.
- Hieltjes, A.H.M. and L. Lijklema. 1980.Fractionation of inorganic phosphorus in calcareous sediments. *Journal of Environmental Quality* 9:405-407.

- Inglett, P.W. and K.S. Inglett. 2013. Biogeochemical changes during early development of restored calcareous wetland soils. *Geoderma* 192:132-141.
- Ivanoff, D.B., K.R. Reddy and J.S. Robinson. 1998. Chemical fractionation of organic P in selected Histosols. *Soil Science* 163:36-45.
- Jerauld, M., J. Juston and T.A. DeBusk. 2018. Appendix 5C-1: Evaluation of Phosphorus Sources, Forms, Flux, and Transformation Processes in the Stormwater Treatment Areas, *South Florida Environmental Report Volume I.* South Florida Water Management District, West Palm Beach, FL.
- Joint Committee on Powder Diffraction Standards. 1980. *Mineral Powder Diffraction File*. International Center for Diffraction Data, Swarthmore, PA.
- Julian, P. and S. Hill. 2012. A.R.M. Loxahatchee National Wildlife Refuge Total Phosphorus Outlier Analysis and Proposed Alternative Screening Criterion: Distribution Independent Outlier Analysis. Presented to the Everglades Technical Oversight Committee on May 30, 2012. Available from the South Florida Water Management District, West Palm Beach, FL.
- Juston, J.M. and T.A. DeBusk. 2011. Evidence and implications of the background phosphorus concentration of submerged aquatic vegetation wetlands in stormwater treatment areas for Everglades restoration. *Water Resources Research* 47:W01511.
- Juston, J.M., R.H. Kadlec, W.F. DeBusk, M.J. Jerauld and T.A. DeBusk. 2015. Persistence of legacy soil P and elevated background water P concentrations in Water Conservation Area 2A, a northern Everglades wetland. *Water Resources Research* 51:9746-9762.
- Kadlec, R.H. 2001. Phosphorus dynamics in event driven wetlands. Pages 365–391 in: *Transformations of Nutrients in Natural and Constructed Wetlands*, Backhuys Publishers, Leiden, The Netherlands.
- Kadlec, R.H. 2006. Free surface wetlands for phosphorus removal: The position of the Everglades Nutrient Removal Project. *Ecological Engineering* 27:361-379.
- Kadlec, R.H. and S.D. Wallace. 2009. Treatment Wetlands, 2nd Edition. CRC Press, Boca Raton, FL.
- Kim, S.-C., C.T. Friedrichs, J.P.-Y. Maa and L.D. Wright. 2000. Estimating bottom stress in tidal boundary layer from acoustic Doppler velocimeter data. *Journal of Hydraulic Engineering* 126:399-406.
- Knight, R., B. Gu, R.A. Clark and J.M. Newman. 2003.Long-term phosphorus removal in Florida aquatic systems dominated by submerged aquatic vegetation. *Ecological Engineering* 20:45-63.
- Kozerski, H.P., H. Behrendt and J. Kohler. 1999. The N and P budget of the shallow, flushed lake Muggelsee retention, external and internal load. *Hydrobiologia* 408/409:159-166.
- Kozerski, H.P. and K. Leuschner. 2000. A plate sediment trap: Design and first experiences. *Verhandlungen des Internationalen Verein Limnologie* 27:242-245.
- Kozerski, H.P. 2003. More about plate sediment trap measurements. Reply to comment of Sukhodolov et al. *Water Research* 37:2796–2801.
- Kröger, R., M.M. Holland, M.T. Moore and C.M Cooper. 2007. Plant senescence: A mechanism for nutrient release in temperate agricultural wetlands. *Environmental Pollution* 146(1):114-119.
- Kuczera, G. and E. Parent. 1998. Monte Carlo assessment of parameter uncertainty in conceptual catchment models: The Metropolis algorithm. *Journal of Hydrology* 211:69-85.
- Li, Y.-H. and S. Gregory. 1974. Diffusion of ions in sea water and in deep-sea sediments. *Geochimica et Cosmochimica Acta* 38:703-714.
- Liao, X., P.W. Inglett and K.S. Inglett. 2014. Vegetation and microbial indicators of nutrient status: Testing their consistency and sufficiency in restored calcareous wetlands. *Ecological Indicators* 46:358-366.

- McNeil, J., C. Taylor, and W. Lick. 1996. Measurements of erosion of undisturbed bottom sediments with depth. *Journal of Hydraulic Engineering* 122(6):316-324.
- Moisander, P.H., J.L. Hench, K. Kononen and H.W. Paerl. 2002. Small-scale shear effects on heterocystous cyanobacteria. *Limnology and Oceanography* 47(1):108-119.
- Newman, S. and K. Pietro. 2001. Phosphorus storage and release in response to flooding: Implications for Everglades stormwater treatment areas. *Ecological Engineering* 18:23–38.
- Newman, S, T.Z. Osborne, S.E. Hagerthey, C. Saunders, K. Rutchey, T. Schall and K.R. Reddy. 2017. Drivers of landscape evolution: Multiple regimes and their influence on carbon sequestration in a subtropical peatland. *Ecological Monographs*. Accepted manuscript online: 29 JUN 2017 02:35AM EST | DOI: 10.1002/ecm.1269.
- Olila, O., K.R. Reddy and W.G. Harris. 1994. Forms and distribution of inorganic phosphorus in sediments of two shallow eutrophic lakes in Florida. *Hydrobiologia* 302:147-161.
- Pant, H.K. and K.R. Reddy. 2003. Potential internal loading of phosphorus in a wetland constructed in agricultural land. *Water Research* 37:965-972.
- Reddy, K.R., Y. Wang, W.F. DeBusk, M.M. Fisher and S. Newman. 1998. Forms of soil phosphorus in selected hydrologic units of the Florida Everglades. *Soil Science Society of America Journal* 62:1134-1147.
- Reddy, K.R. and R. DeLaune. 2008. *Biogeochemistry of Wetlands: Science and Applications*. CRC Press Boca Raton, FL.
- Reddy, K.R., T. Chua and C.J. Richardson. 2013. Chapter 35: Organic Phosphorus Mineralization in Wetland Soils. Page 683-700. In: R.D. DeLaune, K.R. Reddy, C.J. Richardson and P.J. Megonigal (eds.), *Methods in Biogeochemistry of Wetlands*, Book Series Number 10, Soil Science Society of America, Madison, WI.
- Sanford, L.P. and J.P. Maa. 2001. A unified erosion formulation for fine sediments. *Marine Geology* 179:9-23.
- SAS Institute Inc. 2016. Using JMP® 13. SAS Institute Inc., Cary, NC, USA.
- Scinto, L.J., W.T. Anderson and D.N. Johnson. 2011. Soil characterization in selected stormwater treatment areas: STA 5. Final Report to the South Florida Water Management District, West Palm Beach, FL.
- SFWMD. 2012. *Restoration Strategies Regional Water Quality Plan*. South Florida Water Management District, West Palm Beach, FL. April 27, 2012. Available on line at <a href="https://www.sfwmd.gov/sites/default/files/documents/rs">https://www.sfwmd.gov/sites/default/files/documents/rs</a> waterquality plan 042712 final.pdf.
- SFWMD. 2013. Science Plan for the Everglades Stormwater Treatment Areas. South Florida Water Management District, West Palm Beach, FL. June 2013. Available online at <a href="https://www.sfwmd.gov/sites/default/files/documents/rs\_scienceplan\_060713\_final.pdf">https://www.sfwmd.gov/sites/default/files/documents/rs\_scienceplan\_060713\_final.pdf</a>.
- University of Florida. 2016. Evaluation of Soil Biogeochemical Properties Influencing Phosphorus Flux in the Everglades Stormwater Treatment Areas (STAs), Quarterly Report 4, June 2016. Submitted to South Florida Water Management District, West Palm Beach, FL.
- University of Florida. 2017. Evaluation of Soil Biogeochemical Properties Influencing Phosphorus Flux in the Everglades Stormwater Treatment Areas (STAs), Year 2 Annual Report, July 2016—June 2017. Submitted to South Florida Water Management District, West Palm Beach, FL.
- Villapando, O. and J. King. 2018. Appendix 5C-3: Evaluation of Phosphorus Sources, Forms, Flux, and Transformation Processes in the Stormwater Treatment Areas. In: 2018 *South Florida Environmental Report Volume I*, West Palm Beach, FL.

- Wang, P., H. Shen and P. Xie. 2012. Can Hydrodynamics Change Phosphorus Strategies of Diatoms? Nutrient Levels and Diatom Blooms in Lotic and Lentic Ecosystems. *Microbial Ecology* 63:369-382.
- Zhao, H. 2018. Everglades Stormwater Treatment Areas Performance Update. A presentation given at the 15<sup>Th</sup> Annual Public Meeting on the Long-Term Plan for Achieving Water Quality Goals for Everglades Protection Area Tributary Basins, February 23, 2018, West Palm Beach, FL.